CAPTURE AND RECOVERY OF ORGANIC GASES WITH ELECTROTHERMAL SWING ADSORPTION AND POST-DESORPTION TREATMENT

BY

KAITLIN ENGLE MALLOUK

DISSERTATION

Submitted in partial fulfillment of the requirements
for the degree of Doctor of Philosophy in Environmental Engineering in Civil Engineering
in the Graduate College of the
University of Illinois at Urbana-Champaign, 2016

Urbana, Illinois

Doctoral Committee:

Professor Mark J. Rood, Chair and Director of Research
Professor Tami C. Bond
Professor Yuanhui Zhang
Dr. Sotiria Koloustou-Vakakis

ABSTRACT

Several industrial processes, including foam packaging manufacturing, use liquefied organic gases (boiling points (T_b) < 20°C) as inert feedstocks. These processes produce low concentration (e.g., 2,000 ppm_v) organic gas streams that must be treated to prevent emissions of the organic gases to the atmosphere. The organic gases are typically not reused in the process and are instead thermally oxidized. The ability to selectively capture, concentrate, and reuse the effluent organic gases is expected to increase the opportunities to manufacture materials in a more sustainable manner and improve the economics of industrial processes that emit organic gases to the atmosphere.

Activated carbon fiber cloth (ACFC) with electrothermal swing adsorption (ACFC-ESA) has been shown to be an effective means of capturing and recovering organic vapors (T_b > 50°C). However, additional gas treatment needs to be coupled downstream of the ACFC-ESA system to extend this technology to capture and recover organic gases. To this end, a new bench-scale ACFC-ESA gas recovery system (GRS) with post-desorption condensation was developed and tested with four organic gases and under a select range of process conditions to assess its effectiveness for capturing and recovering organic gases.

The GRS was tested to determine the mass collection efficiency and energy requirements for recovering liquid adsorbate from a carrier gas containing select concentrations of each adsorbate. The four adsorbates tested were: isobutane, R134A, n-butane, and dichloromethane. The inlet relative pressure of the adsorbates ranged from 8.3×10^{-5} to 3.4×10^{-3}. The GRS successfully captured and recovered all relative pressures and adsorbates of interest except dichloromethane, which was chemically incompatible with components of the GRS. Of the remaining adsorbates (i.e., isobutane, R134A, and n-butane), each was captured and recovered with greater than 99% mass collection efficiency, which meets existing emission reduction requirements for packaging manufacturing. The heating and compression energy

required to capture and liquefy the gases ranged from 1,200 to 52,000 kJ/mol liquefied depending on the relative pressure of the inlet adsorbate. This energy consumption is 0.87 – 138 times that to recover vapors with boiling points ranging from 56.5 - 101°C using the Vapor Phase Removal and Recovery System (VaPRRS), which is similar to the GRS, but does not include compression and cooling and thus cannot liquefy low boiling point organic gases.

The GRS system was also modified to capture isobutane from a carrier gas with select relative humidities that ranged from 5-80% while maintaining the water vapor concentration of the carrier gas. During this testing, the clean, humid adsorption carrier gas and the N_2 used to inert the system during desorption were recirculated for the first time, which resulted in a reduction in the amount of water vapor and N_2 required to operate the system once it reached steady state. In an industrial setting, this new ability to recycle the carrier gas stream is expected to improve system sustainability and reduce operating costs because it eliminates the need for re-humidification, decreases the demand for N_2 production to inert the adsorption vessels during desorption, and reduces energy requirements. The energy required to capture and recover isobutane (relative pressure = 6.7×10^{-4}) with relative humidities ranging from 5 to 80% ranged from 2910 – 5750 kJ/mol liquefied. Experiments with recirculating carrier gas showed that the energy requirements to capture and recover liquid isobutane from a high relative humidity adsorption stream were significantly lower at the 95% confidence level than in experiments without carrier gas recirculation. Based on these results, implementing ACFC-ESA with carrier gas recirculation, particularly for humid adsorption gas streams, reduces the humidification energy requirements by 60%, the energy to supply N_2 by 25 to 60%, and the total energy to capture and recover liquid isobutane (heating, compression, water and N_2 energy) by 38%, while also reusing resources such as N_2 and water.

This research is a significant advancement over previous research accomplishments because the GRS expands the applicability of ACFC-ESA to compounds with boiling points

below 20°C. Additionally, characterization of the GRS using mass and energy balances has shown that it can be used for compounds with boiling points ranging from -26.5°C to -0.5°C so long as those compounds have a reasonable, reversible affinity for ACFC. Finally, demonstrating that operation of this technology with humidified gas streams and carrier gas recirculation reduces the water vapor, N_2, and overall energy requirements makes the technology more likely to be adopted by industries that generate low concentration organic gas streams.

To the Engle-Mallouk-Watts clan, who continue to love and support me daily.

ACKNOWLEDGEMENTS

A Ph.D. is a hard-won degree and its completion would not be possible without support on many fronts. First and foremost, I am grateful for my husband Seth who started this journey with me and was my cheerleader and confidant throughout. I would not have made it through without him.

I acknowledge my advisor, Dr. Mark Rood, who guided my research, supported my love of teaching, and taught me a great deal about how to work in the academy. In addition, my doctoral committee Tami C. Bond, Yuanhui Zhang, and Sotiria Koloustou-Vakakis offered constructive feedback on my work throughout my studies and supported me by providing career advice and letters of recommendation. My success was enhanced because of them.

My peers were, of course, a major part of my ability to complete this work. The Air Quality Engineering and Science group provided constructive feedback on papers and presentations, offered help in the lab, and often brought a smile to my face. In particular, I am grateful for the friendship and technical support of John Atkinson, Dave Johnsen, Andy Nelson, and Beni Brem.

I owe a debt of gratitude to my lawyer, Ms. Heather Herrington. Heather gave me the courage to continue fighting for my hard-earned degree. I will always cherish the support and friendship she provided during this challenging time in my life and career.

I am also extremely appreciative of the funding I benefitted from during my time at the University of Illinois. The Graduate Assistance in Areas of National Need Fellowship (GAANN) and the Support for Under-Represented Groups in Engineering Fellowship (SURGE) were deciding factors in my decision to enroll at University of Illinois. Once on campus, funding from the National Science Foundation Graduate Research Fellowship and grant #1236203, Pregis Corporation Inc, the Milton Feldstein Memorial Scholarship from the Air & Waste Management Association (A&WMA), the Mavis Future Faculty Fellowship, and the Department of Civil and

Environmental Engineering Alumni Graduate Assistantship for Teaching Excellence and Engelbrecht Fellowhsip were honors to receive and were critical to my success. I would also like to acknowledge financial support for travel to professional conferences provided by the Lake Michigan States Sections of the A&WMA and the University of Illinois Department of Civil and Environmental Engineering.

Lastly, I would like to say this to my children, Sebastian and Aurora: you both entered my life as the process of completing my PhD was coming to an end. I hope that one day, when I tell you the story of earning my doctorate, you will be inspired by the dedication and perseverance it took for me to finally become Dr. Kaitlin Engle Mallouk, PhD.

TABLE OF CONTENTS

1. Introduction and Literature Review

1.1. Organic Gas Emissions / Motivation for This Research

Organic gases are organic compounds with boiling points (T_b) below 20°C with a range of structures including simple alkanes and aldehydes. Select organic gases are considered greenhouse gases and they can act as precursors to O_3 formation (*1*). Additionally, select organic gases have harmful health effects and are thus regulated via the toxic release inventory (e.g., acetaldehyde, T_b = 20.2°C) (*2*) and others (e.g., isobutane, n-butane) must be controlled to comply with other regulations (e.g., *3*). The total yearly emissions of organic gases are not specifically quantified on a national or international scale, however the 2014 United States Greenhouse Gas Emission Report developed by the United States Environmental Protection Agency (USEPA) estimates that in 2012 a total of 10,971 Gg/yr of non-methane volatile organic compounds (VOCs) were emitted to the atmosphere from the United States with 1,538 Gg/yr coming from industrial sources (*4*). VOCs are defined by the United States Code of Federal Regulations (CFR) as any compound of carbon that participates in photochemical reactions with the exceptions of CO, CO_2, carbonic acid, dichloromethane, 1,1,1,2-tetrafluoroethane, and others as described in the CFR (*5*).

Several industrial processes use liquefied organic gases as inert feedstocks in their facilities resulting in the production of low concentration (e.g., $\leq$ 2,000 ppm_v) organic gas streams in air. According to the USEPA's AP-42, 7.7 – 9.8 g of uncontrolled organic gas per kg of expandable polystyrene foam is emitted by the packaging industry during production operations (*6*). Based on the polystyrene production by major US manufacturers of 2,074 Gg in 2012 (*7*), the total emission of organic gases from polystyrene production is 16 to 20.3 Gg per year in the United States. To reduce the amount of these emissions, treatment of the low concentration organic gas stream is necessary (*8*).

The industrial process of particular interest in this research involves production of packaging materials. Isobutane and other “blowing agents” are used to create low-density polystyrene foam. The resulting gas stream that requires treatment includes air and low concentration organic gas, and has 30-50% relative humidity (RH) at a temperature around 40°C. The humidity and organic gas have to be continually resupplied to the process due to the use of thermal oxidation to treat the resulting gas stream.

Typically, thermal oxidation or adsorption is used to reduce the amount of organic gas emissions to the atmosphere (*8*). Thermal oxidation works by combusting the compound to form CO_2, H_2O and other combustion byproducts (*9*). However the CO_2 produced during the thermal oxidation process is a greenhouse gas that contributes to increased climate forcing in the atmosphere. In addition, thermal oxidation results in the loss of the properly conditioned (i.e., temperature, water vapor concentration, and nitrogen (N_2) concentration when appropriate) carrier gas, which then must be generated again with heat exchangers, humidifiers, and a N_2 supply as part of the facility operation. A potentially more sustainable emissions reduction technique is to capture the organic gases from the industrial carrier gas stream while maintaining the condition of the carrier gas and then recover the organic gas in a reusable (e.g., liquid) form so that it could be recycled.

The primary goal of this research is to develop a new technology to capture and recover organic gases for reuse to improve the sustainability of using organic compounds until alternative manufacturing processes are developed that do not generate these organic gases. In addition, maintaining the carrier gas condition is expected to lower the operating costs and environmental impact of the facility because the carrier gas will not have to be humidified or treated with N_2 once steady-state conditions are achieved (*10*). This would allow valuable resources, such as water, N_2, and energy, to be conserved.

The gases of interest in this research include 1,1,1,2-tetrafluoroethane (R134A), isobutane, n-butane, and dichloromethane (DCM). The characteristics of these compounds are detailed in section 1.3.2 and Table 1.3.

1.2. Organic Gas Control Methods

Generally there are two classes of organic gas pollution prevention: process modification and ancillary control. Process modification is the preferred alternative for emissions reductions because it reduces the amount of emissions produced. Process modification could involve feedstock substitution, where a less harmful chemical replaces the organic gas used in the process; operational changes that reduce the formation or volatilization of organic gas; or equipment modification that prevents the organic gases from escaping (*11*). If process modifications are not possible or do not result in acceptable reduction of organic gas emissions, then ancillary control of organic gas emissions is necessary.

There are two common classes of ancillary control methods to reduce the amount of organic compounds emitted to the atmosphere: destruction-based and recovery-based. Destructive methods include incineration and biological treatment, which remove organic compounds from gas streams by converting them to CO_2, H_2O, and/or biomass. The use of a destructive method means that the organic compound cannot be recovered for reuse in its original form. If recovery for reuse is desired, there are several methods available for gas treatment: absorption, condensation, membrane separation, and adsorption. These methods are appropriate over different concentration ranges as shown in Figure 1.1

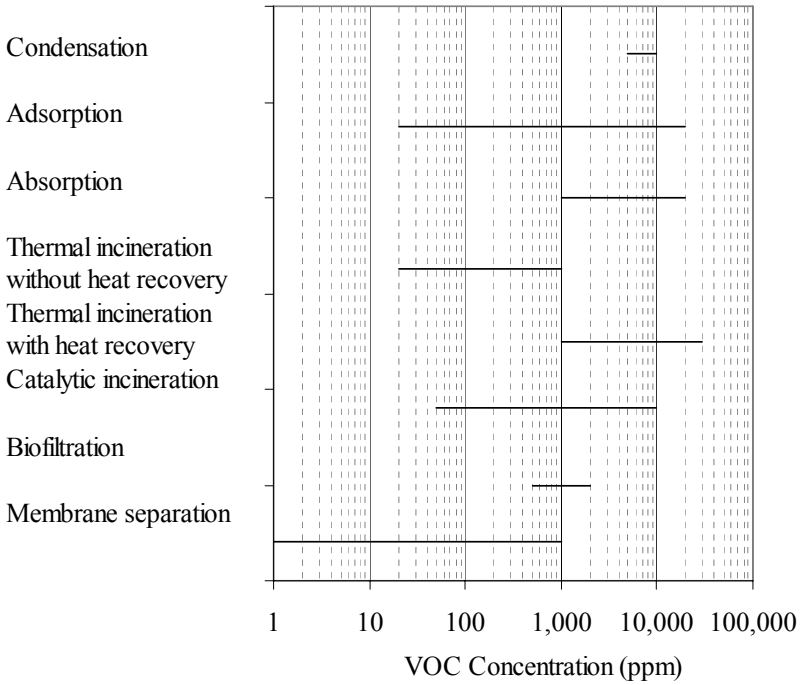

Figure 1.1 Range of concentrations for various VOC treatment technologies. Adapted from (*12*), Copyright 2000, with permission from Wiley.

1.2.1. Absorption

Capture of organic compounds using absorption involves the transfer of the organics from the gaseous stream to a liquid stream. Absorption is based on the "preferential solubility of a gaseous component in the liquid" (*9*). Although absorption can process a wide range of carrier gas flow rates (*13*), it is generally not suitable for the recovery of organic gases for several reasons. First, many organic gases are insoluble in water (*14*), which would require the use of an absorbent other than water. Additionally, absorption requires post-capture treatment of the liquid absorbent stream, which requires handling of large volumes of liquids adding cost to the control system.

1.2.2. Condensation

Condensation involves cooling and/or compression of a gas stream to lower the organic compound's partial pressure below its saturation point. For pure organic gases at standard

pressure, this requires the gas stream to be cooled below the organic gas' boiling point (e.g., to -11.7°C for isobutane). For a low concentration organic gas stream, the cooling requirement is even greater. This type of cooling is not possible using the commonly used cooling mediums, such as water (*15*), due to freezing of the coolant. In general, condensation requires high organic compound concentrations (> 5,000 ppm_v) and is often energy intensive for compounds with normal boiling points below 33˚C because large amounts of coolant at a temperature below the organic compound's boiling point or compression to high pressures is required to achieve condensation (*15,16*). Additionally, if water vapor is present in the carrier gas, this water could condense or freeze during the condensation operation, which will require subsequent treatment of the condensed liquids and defrosting of the heat exchanger (*17,18*).

1.2.3. Membrane Separation

Membrane separation is based on the principle of relative permeability through a membrane interface: the higher the permeability of the organic compound relative to the permeability of the carrier gas, the better the achievable separation. Membrane separation reported in the literature often focuses on organic compound concentrations greater than 10,000 ppm_v, which is higher than the organic gas concentrations being considered here (i.e., 2,000 ppm_v) (*19, 20, 21*). One paper did report the selective capture and recovery of a low concentration (i.e., 3,000 ppm_v) ethyl acetate stream using a polydimethylsiloxane membrane and showed that the ethyl acetate could be recovered at concentrations up to 20% by volume (*22*). Additionally, membranes are expensive, are susceptible to fouling, and must be replaced frequently (*16, 18*).

1.2.4. Adsorption

Adsorption occurs when a compound (adsorbate) adheres to an interface (adsorbent). For this application, the adsorbate is the organic gas in a carrier gas and the adsorbent is the surface of a solid carbon material. This adherence can be either a chemical or a physical

process. Chemical adsorption, or chemisorption, occurs when a covalent bond is formed between the adsorbate and the adsorbent. Chemisorption is not easily reversible and therefore it is not ideal for the recovery of the adsorbate or reuse of the adsorbent (*9, 15*). Physical adsorption, or physisorption, is achieved through van der Waals interactions between the adsorbate and the adsorbent. Physisorption is reversible by application of heat, vacuum, purge gas stripping, or displacement desorption (*27*), making it ideal for recovery of the adsorbate (*9*) and reuse of the adsorbent. Additionally, adsorption can achieve greater than 90% removal efficiency for inlet VOC concentrations greater than 500 ppm_v and can be effective for removing VOCs with molecular weights greater than 45 g/mol (*15*). These characteristics make adsorption a good option for capture of low concentration organic gases.

1.2.5. Adsorption with Condensation for Capture and Recovery of Organic Gases

An ideal technique for capture and recovery of organic gases would result in the organic gas being recovered as a liquid for compact storage and ease of reuse. As mentioned in section 1.2.2, condensation of low concentration organic compounds can require cooling and/or compression. Additionally, the annual operating costs of a condensation system are sensitive to the total flow rate entering the system: up to $4.24/LPM without upstream activated carbon adsorption compared to $1.24/LPM (neither standard nor actual conditions were specified) with upstream activated carbon adsorption (*18*). Coupling an adsorption system to capture low concentration organic compounds and recover them at high concentration with a condensation system to liquefy the organic compound could reduce the flow rate into the condensation system by two orders of magnitude resulting in a much smaller condenser, thus lowering the capital and operating costs of the system.

The following sections provide relevant background information and justification for the technology developed as part of this research: a bench-scale adsorption system that uses

activated carbon fiber cloth (ACFC), electrothermal swing adsorption (ESA), and post-desorption treatment.

1.3. Adsorption

1.3.1. Adsorbents

There are many adsorbents currently used to remove adsorbates from carrier gases. The most industrially relevant adsorbents are activated alumina, silica gel, zeolites, and activated carbon (*23*) (Table 1.1). Activated alumina and silica gel have polar surfaces and are typically used to remove water vapor and other polar compounds from carrier gases and can also be used for inorganic compounds. Zeolites are inorganic materials with a well-defined crystalline pore structure (*18*). Zeolites can be tailored to a specific application by controlling the pore structure and silica to aluminum ratio of the zeolite (*27*). While zeolites can be tailored to have some advantages over activated carbon, such as tolerance to high relative humidities, high thermal stability, and low flammability, they are still expensive and are generally not used industrially for capture of organic compounds (*18*).

Table 1.1. Physical properties of typical adsorbents (*24*).

Adsorbent	**Shape**[a]	**Surface Area (m^2/g)**	**Pore Width (Å)**	**Porosity (-)**	**Bulk Density (g/cm^3)**	**Polarity**
Activated alumina	G, S, T	90-400	70-272	0.25-0.6	0.75-0.8	Polar
Silica gel	G, S, P	300-900	40-144	0.3-0.5	0.43-0.83	Polar
Zeolites	C, S, P	600-800	6-12	0.3-0.55	0.5-0.88	Non Polar
GAC[b]	G	500-1600	10-130	0.4-0.8	0.3-0.56	Largely Non Polar
ACF[c] (*25*)	F	700-1800	6.1-14.4	0.72-0.95	0.6-1.2	Largely Non Polar

[a] G = granular, S = spherical beads, T = tablets, P = powder, C = cylindrical pellets, F = fiber.
[b] GAC = granular activated carbon
[c] ACF = activated carbon fiber
Note that activated carbon can also be in the form of S, P, C, F, and monolith (*26*).

1.3.1.1. Activated Carbon

There are several forms of activated carbon including granular activated carbon (GAC) and activated carbon fibers (ACFs). GAC is commonly used to remove organic compounds from gas streams and its physical properties give it a high adsorption capacity for most relevant organic compounds (*15*, *27*). ACFs, a nano-engineered material, have been shown to also have high adsorption capacities for organic compounds over a wide range of concentrations (*28*). Additionally, ACFs have several advantages over GAC: no ash content, high micropore volume (*29*), rapid heat and mass transfer properties (*29*, *30, 31*), shapeability (*31*), and electrical resistance (*29, 30, 31, 32*), which allows adsorbate desorption through electrothermal desorption (Joule heating).

ACFs can be made into several forms including felt and cloth. Activated carbon fiber cloth (ACFC) is manufactured from one of several precursors including polyacrylonitrile, pitch, Novoloid, and Rayon (*25*). The ACFC used in this research is made from phenolic-Novolac™ resin and was manufactured by Nippon Kynol, Inc[1]. Nippon Kynol ACFC is available in four degrees of activation with ACFC-10 being the least activated and ACFC-25 being the most activated (*25*). Several characteristics can be used to describe ACFC including surface area, micropore surface area, total pore volume, micropore volume, and microporosity (micropore volume as a percentage of total pore volume). The surface area, micropore surface area, and total pore volume increase, while microporosity decreases, with levels of increasing activation (Table 1.2). These properties were determined using N_2 adsorption at 77 K.

[1] Other manufacturers of ACFC include Calgon Carbon Corporation (http://www.calgoncarbon.com/), Jacobi Carbons (formerly PICA, http://www.jacobi.net/), and Nantong Yongtong Environmental Technology Company (http://www.ytacf.com/en/).

Table 1.2. Typical properties of ACFC adsorbents (Adapted from ref *25*).

ACFC Type	Total Surface Area (m^2/g)	Micropore Surface Area (m^2/g)	Total Pore Volume (cm^3/g)	Micropore Volume (cm^3/g)	Mean Pore Width (Å)	Micro-porosity (%)
ACFC-10	810	790	0.40	0.38	6.1	95.6
ACFC-15	1,322	1,279	0.66	0.62	7.0	94.4
ACFC-20	1,604	1,540	0.80	0.75	7.4	92.9
ACFC-25	1,864	1,786	0.93	0.86	8.9	92.2

ACFC-15, in particular, was chosen for this research because it had been previously shown to have a higher adsorption capacity for several compounds (n-butane, benzene, and acetone) at low concentrations (< 3,000 ppm_v) than the other Nippon-Kynol ACFCs (*33*). The intermediate degree of activation of ACFC-15 also allows for a high degree of microporosity while maintaining mechanical integrity at an intermediate cost when compared to the other degrees of activation (*25*).

1.3.2. Adsorbates

The adsorbates that will be tested in this research include 1,1,1,2 tetrafluoroethane (R134A), isobutane, n-butane, and methylene chloride (dichloromethane, DCM). The physical properties of these adsorbates are shown in Table 1.3.

Table 1.3. Physical properties of adsorbates of interest.

Characteristic	1,1,1,2 tetrafluoroethane (R134A)	Isobutane	n-butane	Dichloro-methane
Class	Haloalkane	Alkane	Alkane	Haloalkane
Molecular Formula	CH_2FCF_3	i-C_4H_{10}	n-C_4H_{10}	CH_2Cl_2
Molecular Weight (g/mol)	102.03	58.12	58.12	84.93
Boiling Point (˚C) (*34*)	-26.5	-11.7	-0.5	39.8-40 (*35*)
Bulk Liquid Density at (T) (kg/m^3)	1,206 (25˚C) *(34)*	548 (27˚C) (*36*)	582 (22˚C) (*37*)	1,336 (20˚C) (*14*)
Saturation Vapor Pressure at 20˚C (kPa)[a]	570	302	207	47
$^1\chi^v$ (molecular connectivity index)[b]	3.01 (if F treated as Cl)	1.73	1.91	1.6
Effective Molecular Diameter (Å)	6.4[c] (*38*)	6.35(*39*)	4.15 (*39*)	3.3 (*40*)
Effective Molecular Length (Å)	NA	6.35 (*39*)	8.24 (*39*)	NA
Water Solubility (kg/kg) (*14*)	NA	Insoluble	Insoluble	0.02

NA= not available; [a]based on (*14*); [b] calculated from (*41*); [c] based on predicted molar volume

Isobutane was chosen for initial testing because of its relevance to the packaging industry as an inert gas used to manufacture packaging material. Isobutane has the potential to be recovered and recycled to reduce reliance on raw material inputs. R134A is a common refrigerant that is regulated by the Clean Air Act Amendment 40CFR. Its boiling point is 14.6˚C lower than isobutane, which will help assess the operating range of the gas recovery system (GRS). Testing with R134A expands the range of boiling points being tested to 50°C. n-butane was selected because it is isomeric to isobutane but has a higher boiling point. Based on this boiling point difference, ACFC should theoretically have a higher adsorption capacity for n-butane than isobutane, which will reduce the energy requirements for capture and recovery.

DCM was chosen because it appears on the USEPA toxic release inventory and it was difficult to capture and recover with the Vapor Phase Removal and Recovery System (VaPRRS) (*42*), which is the predecessor to the GRS studied here. DCM has a higher boiling point (39.8°C) than both iso- and n-butane and is considered a haloalkane rather than an alkane because it contains chlorine atoms. In addition, these compounds have a range of molecular sizes, which is known to affect adsorption behavior (*43*). Note that the effective molecular diameters are less than the mean pore width of ACFC-15 and the effective molecular lengths of the adsorbates (when available) are similar to the mean pore width of ACFC-15 (6.35 Å to 8.24 Å for isobutane and n-butane, respectively, when compared to 7.0 Å for ACFC-15).

1.3.2.1. Competitive Adsorption with Water Vapor

The ability to selectively capture an organic adsorbate from a humid airstream is desirable for several reasons. Organic compounds have been shown to interact with water vapor during adsorption on activated carbon and this interaction is a function of the hydrophobicity and volatility of the organic compound (*44*, *45*). Specifically, hydrophobic, light organic compounds compete with water vapor for adsorption sites, lowering the adsorbent's effective capacity for the organic compound and increasing the required amount of adsorbent for treating a given waste stream (*44*, *46, 47*). Figure 1.2 shows an example of how water vapor can be a competitive adsorbate. Note how the adsorption of benzene (a water-insoluble compound) decreases as adsorption of water increases at 45% RH. The competitive adsorption not only affects the adsorbent's capacity for the organic compound, but also reduces the adsorbent's capacity for water vapor. In Figure 1.2, the adsorption capacity of ACFC-20 for water vapor at 90% RH is 350 mg water / g ACFC, however the equilibrium adsorption capacity of ACFC-20 for water vapor at 90% RH has been shown to be nearly 1.5 times that amount (*48*). Being able to capture and recover organic compounds from a humid carrier gas would be beneficial because water vapor is often present in industrial carrier gases. In addition, if the

production process requires the maintenance of the water vapor concentration of the organic compound laden carrier gas, selectively capturing the organic compound while maintaining the water vapor concentration in the carrier gas would provide energy savings because the carrier air would not have to be re-humidified.

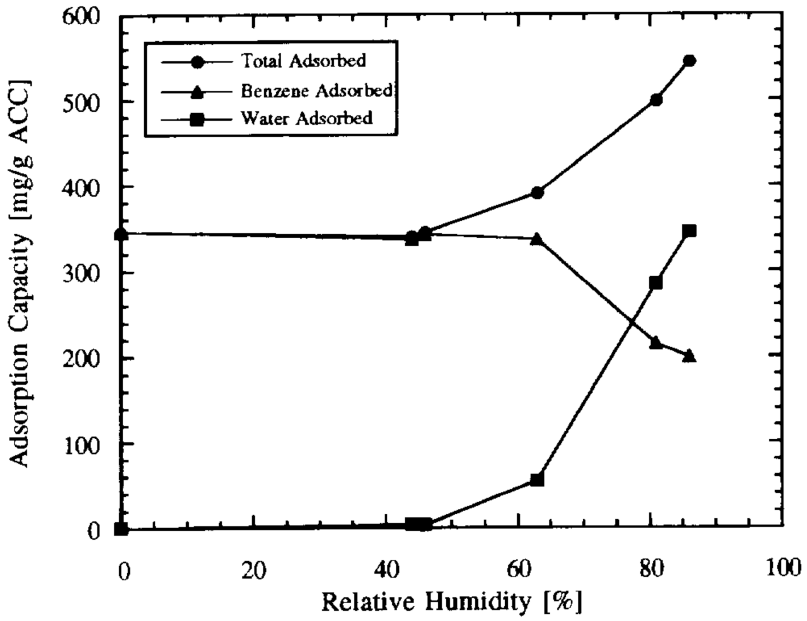

Figure 1.2 Adsorption capacities of 500 ppm_v benzene on ACFC-20 at several relative humidities. Reprinted from (*46*), Copyright 1996, with permission from Elsevier.

1.3.3. Equilibrium Adsorption Isotherm

Adsorption capacity for a given adsorbate is an important characteristic for determining the quality of the adsorbent-adsorbate pair. Adsorption capacity is the mass of adsorbate that is adsorbed per unit mass of adsorbent at equilibrium. Characteristics of the adsorbent that affect its equilibrium adsorption capacity include surface area, pore volume, and surface functional groups (*24*). Additionally, for a given adsorbent-adsorbate pair, the equilibrium adsorption capacity is dependent on the system's total pressure and temperature.

An equilibrium adsorption isotherm describes the equilibrium adsorption capacity of an adsorbent-adsorbate pair as a function of the relative pressure of the adsorbate at a fixed

temperature and pressure. Adsorption isotherms are classified as one of five types based on their shape. The system of five isotherm types, known as the Brunauer classification, is shown in Figure 1.3 (*49*). Type I isotherms are characteristic of a monolayer adsorption and describe the adsorption of organic compounds on microporous activated carbon (*50*). Type II isotherms are typical of gases adsorbing on to nonporous solids. Type III and Type IV isotherms are characteristic of multilayer formation of the adsorbate on the adsorbent, with Type IV representing monolayer formation followed by the formation of additional layers of adsorbate on the adsorbent. A Type V isotherm is typical of water vapor adsorbing on activated carbon. For this research, Type I and Type V isotherms are the most relevant because they characterize the adsorption of organic compounds and water vapor on activated carbon, respectively.

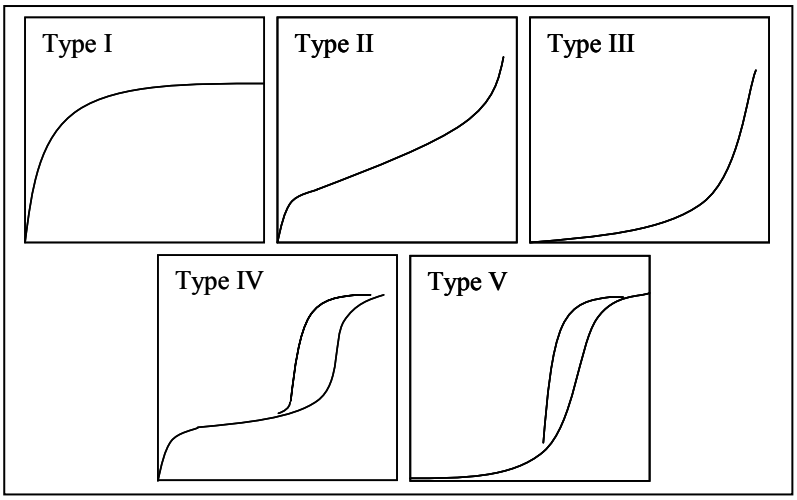

Figure 1.3. Typical adsorption isotherm shapes. The x-axes are concentration or relative pressure of the adsorbate and the y-axes are relative amount of adsorbate adsorbed. Reprinted from (*51*) with permission from David Ramirez.

As an example, Foster, *et al.* measured the adsorption isotherm for n-butane on ACFC, which shows Type I behavior (*33*). When plotted on a semi-log scale, the rapid change in adsorption capacity at low relative pressures is more easily observed (Figure 1.4).

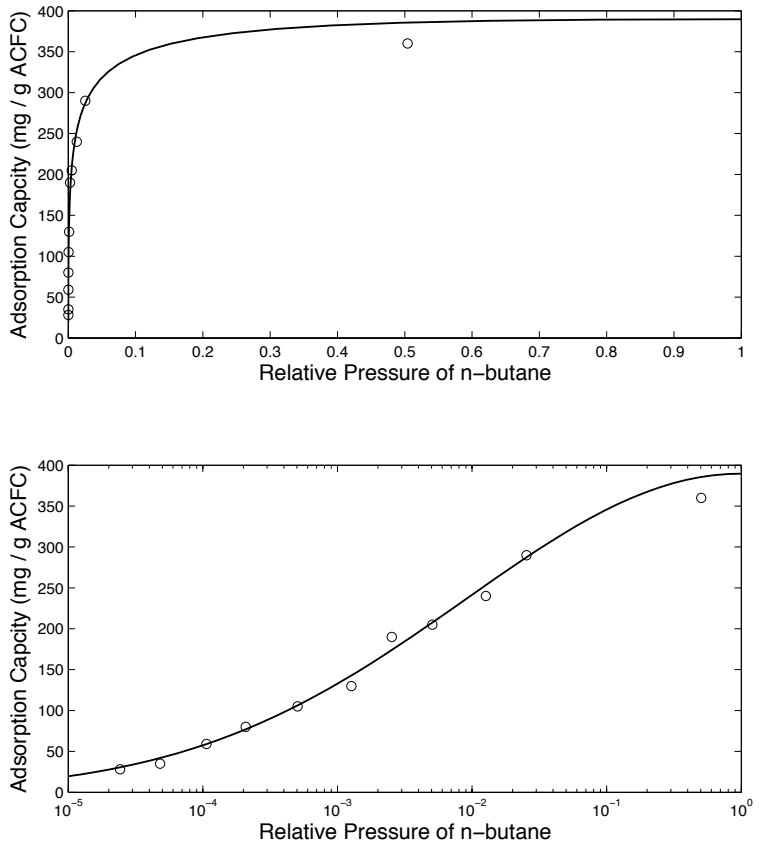

Figure 1.4. Adsorption isotherm for n-butane on ACFC-20 measured and reported by Foster, *et al.* (*33*). Note that the ACFC-20 used by Foster is most similar to the ACFC-15 used throughout the research reported here.

1.3.4. Mathematical Models of Equilibrium Adsorption Isotherms for Organic Compounds on ACFC

The various isotherm types can be modeled using mathematical relationships. These mathematical relationships can be used in models of adsorption systems to characterize mass and energy distributions during operation. The isotherm models also allow for prediction of adsorption capacity under different operating conditions (inlet concentration, temperature). Some common isotherm models for describing the adsorption of organic compounds on activated carbon are the Freundlich, Toth, Yaws, Dubinin Radushkevich (DR), and Direct Quantitative Structure–Activity Relationship (DQSAR) equations. Utilization of these adsorption isotherm models to describe the adsorption of the compounds of interest on ACFC will allow

quantification of the distribution of adsorbate mass during an electrothermal swing adsorption process and prediction of the process performance.

1.3.4.1. The Freundlich Equation

The Freundlich equation (**Eq 1.1**) describes the adsorption capacity as a function of adsorbate partial pressure (*27*). It is widely used to describe the adsorption of organic compounds on activated carbon, however it is not valid at the high and low end of the adsorbate's partial pressure range (*52*).

$$q = k_f P_i^{1/n} \qquad \text{Eq 1.1}$$

where q = equilibrium adsorption capacity of the adsorbate on the adsorbent having units consistent with the rest of the equation, P_i is the equilibrium gas-phase partial pressure of the adsorbate, and k_f and n are constants determined by equation fitting. In the case where n = 1, the isotherm is linear and in the case when n is greater than 10, the isotherm approaches an "irreversible isotherm," indicating that the equilibrium partial pressure must decrease substantially for desorption to occur (*53*).

1.3.4.2. The Toth Equation

The Toth equation (**Eq 1.2**) is another empirical relationship that, unlike the Freundlich equation, is valid over the entire partial pressure range of the adsorbate. Due to this validity, Do recommends that the Toth equation be the "first choice… for fitting data" for hydrocarbons and other adsorbates on activated carbon (*52*). Others have successfully used the Toth equation to describe the adsorption of light alkanes on nanoporous activated carbon (*54*).

$$q = q_s \frac{bP_i}{\left[1+\left(bP_i\right)^t\right]^{1/t}} \qquad \text{Eq 1.2}$$

where q_s is the saturation adsorbed phase concentration, b is the Langmuir affinity constant (kPa^{-1}), and t is a parameter that is usually less than 1. Both b and t are specific to the

adsorbate/adsorbent pair and the model can be fitted to experimental data to determine their values. The parameter *t* is a measure of system heterogeneity: as the value of *t* deviates from 1 the system heterogeneity increases (*52*).

1.3.4.3. The Yaws Equation

The Yaws Equation (**Eq 1.3**) is a correlation isotherm that was developed for adsorption of VOCs on activated carbon (*55*). It is a useful equation due to its simplicity and its reliance solely on the concentration of the adsorbate. It uses three fitting coefficients to improve the fit of the equation with experimental data. In addition, "results from the equation are applicable for conditions commonly encountered in air pollution control techniques" (*56*)

$$\log_{10} q = A + B\log_{10} y + C\left(\log_{10} c\right)^2 \qquad \text{Eq 1.3}$$

where q has units of g adsorbate per 100 g of adsorbent; A, B, and C are correlation constants; and c is the concentration of adsorbate in the gas phase in ppm_v.

1.3.4.4. The DR Equation

The DR isotherm (**Eq 1.4**) is based on Polanyi theory and was developed to describe the Type I isotherms generated when organic compounds adsorb on microporous adsorbents (*57*).

$$W = W_0 \exp\left[-\left(\frac{RT\ln\left(\frac{P_{i,s}}{P_i}\right)}{E}\right)^2\right] \qquad \text{Eq 1.4}$$

where W = volume of adsorbate per mass of adsorbent, W_0 = limiting micropore volume per unit mass of adsorbent, R = ideal gas constant, T = absolute temperature, $P_{i,s}$ = saturation partial pressure of the adsorbate, and E = characteristic adsorption energy of the adsorbate. The DR equation assumes that the vapors adsorbed in micropores can form liquids (*52*).

1.3.4.5. The DQSAR Equation

The DQSAR equation (**Eq 1.5**) is a semi-predictive model based on the Polanyi-Radushkevich theory of adsorption potential (*58, 59)*. Theoretically, the DQSAR equation can be used to predict the adsorption capacity of an adsorbate/adsorbent pair with knowledge of the adsorbent's micropore volume (often provided by the vendor) and the adsorbate's molecular connectivity index (a function of molecular structure) (*50*). This is an advantage of the DQSAR equation, since it does not require the development of experimental adsorption isotherm data to obtain fitting parameters. Ramirez, *et al*. used this technique to predict the adsorption of several organic compounds on ACFC-20 with relative errors from 4 to 14% and coefficient of determination, R^2, values between 0.888 and 0.987 (*50*). However, Ramirez observed that when isotherms were measured above the adsorbate's boiling point (125 or 175°C for methyl ethyl ketone (T_b = 80°C)), the DQSAR model had much higher average absolute relative difference (15 and 90%, respectively) (*50*).

$$q = W_0 \rho \exp\left[-k \left(RT \ln\left(\frac{P_{i,s}}{P_i} \right) \right)^2 \right] \qquad \text{Eq 1.5}$$

where ρ = density of the adsorbed material (assumed to be the bulk liquid density (***Error! Bookmark not defined.***), and k = parameter that depends only on the adsorbate. Nirmalakhandan and Speece developed a correlation (**Eq 1.6**) for the calculation of k based on the modified, first-order molecular connectivity index, ${}^1\chi^{\upsilon}$ (*58*). ${}^1\chi^{\upsilon}$ can be calculated as outlined by Prakash, *et al.* (*41*) and is listed in Table 1.3 for the four adsorbates being considered in this work.

$$\log k = 1.585 - 0.442\,{}^1\chi^{\upsilon} \qquad \text{Eq 1.6}$$

The saturation pressure of the adsorbate can be determined using one of several available relationships. For this research, the Antoine equation was used:

$$P_{i,s} = \exp\left(A_1 + \frac{A_2}{T} + A_3 \ln(T) + A_4 T^{A_5} \right) \qquad \text{Eq 1.7}$$

where the pressure is in Pascal and A_n = constants for Antoine's equation (*14*).

1.3.5. Mathematical Models of Equilibrium Adsorption Isotherms for Water Vapor on ACFC

Several studies have shown that untreated ACFC exhibits a Type V isotherm (Figure 1.5) when adsorbing water vapor with significant adsorption of water occurring at relative humidities greater than 30-40% for ACFC-15 (*45*, *48*). This indicates that if the inlet RH is below 30-40%, the competitive adsorption mentioned above is inhibited (*46, 60*). Previous researchers have lowered the RH of the gas stream within the adsorption vessel while maintaining the water vapor's dew-point temperature by warming the ACFC above the temperature of the inlet gas stream (10°C increase) during the adsorption cycle (*61*). Assuming the gas stream rapidly warms to the temperature of the ACFC as it passes through the ACFC, the RH is effectively lowered due to the increased dry bulb temperature. For example, if the inlet carrier gas is at 20°C and 75% RH, heating the air to 30°C lowers the RH to 41% and heating to 40°C lowers the RH to 24%, which is below the threshold for water vapor adsorption of 30%-40% RH.

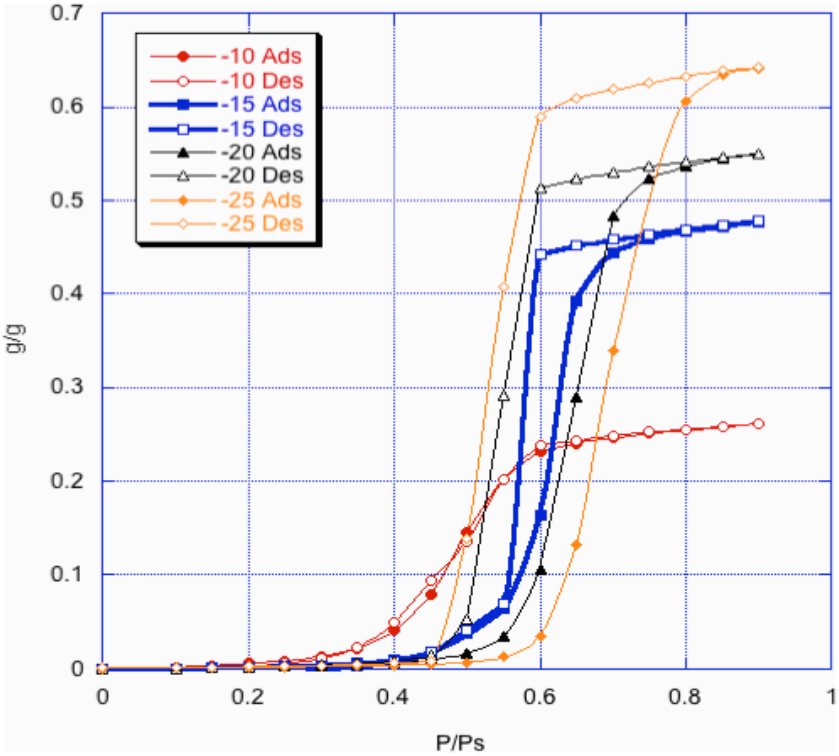

Figure 1.5. Water vapor adsorption isotherms on ACFCs. The numbers associated with each line in the plot refer to the type of ACFC (e.g., "-10" refers to ACFC-10). Reprinted with permission from (*48*), copyright 2007 Springer.

Equilibrium adsorption isotherms for water adsorption on ACFC have been determined by Cal, *et al*. and Qi, *et al*. who used the DS-4 (**Eq 1.8**) and QHR (**Eq 1.9**) equations, respectively to fit the isotherm data (*45, 62*).

$$\frac{P_i}{P_{i,s}} = \frac{a}{ca_0 + ca\left[1 - \exp\left(-k_{DS-4}^2\left(a - a_c\right)^2\right)\right]} \qquad \text{Eq 1.8}$$

where a is the amount of water vapor adsorbed at the corresponding relative pressure of water vapor, and a_0, c, k_{DS-4}, and a_c are fitting parameters.

Eq 1.9

where P_{50} is an isotherm constant and $P = P_{50}$ when $q = q_{50}$, the amount adsorbed when the outlet adsorbate concentration is 50% of the inlet adsorbate concentration during a

breakthrough curve, and k_{QHR} is a proportionality constant. The values of the parameters for the isotherm equations determined by Cal, *et al.* and Qi, *et al*. are shown in Table 1.4.

Table 1.4. Model parameters for the DS-4 equation (*45*) and the QHR (*60*) equation for water vapor adsorption on ACFC. (Note: Data for ACFC-10 is not available).

Adsorbent	a_c	a_0	C	k_{DS-4}	k_{QHR}	P/P_{50}	q_0 (g/g)
ACFC-15	25.6	0.935	2.03	0.154	20.0	0.451	0.351
ACFC-20	47.9	0.228	1.93	0.0639	27.9	0.542	0.571
ACFC-25	81.9	0.390	1.62	0.0292	23.3	0.650	0.788

1.3.6. Heat of Adsorption

To fully model the adsorption/desorption system additional information about the different energy components of the process is required. In particular, adsorption is exothermic (releases heat) and desorption is endothermic (consumes heat). The thermodynamic quantity used to describe the energy released or consumed is the isosteric heat of adsorption (ΔH_s). ΔH_s represents the minimum amount of energy necessary to desorb an adsorbate, assuming the adsorption process is completely reversible and no other system components are involved in the heat transfer (*42*). Knowledge of ΔH_s for a given adsorbate-adsorbent system allows an energy balance to be conducted on the adsorption/desorption process. Dombrowski, *et al*. demonstrated that for organic vapors ΔH_s represents 3-10% of the total energy required to recover the adsorbate in liquid form with the VaPRRS (*42*).

Although the isosteric heat of adsorption is an important thermodynamic quantity in adsorption systems, the literature is limited in ΔH_s values for adsorbate/adsorbent systems. Chakraborty, *et al*. showed that ΔH_s for methane on silicate was 21 kJ/mol (*63*). Sircar determined that the ΔH_s for ethane on NaX zeolite was 32 kJ/mol and has determined values for

N_2, O_2, and CO_2 on various adsorbents (*64*, *65*). Ramirez, *et al*. determined that ΔH_s values for acetone and benzene on ACFC-20 were 40-60 kJ/mol and 60-70 kJ/mol, respectively (*66*).

The method for determining the isosteric heat of adsorption for an adsorbate/adsorbent pair is described by Ramirez, *et al*. (*66*) who used the Clausius-Clapeyron equation coupled with the Polanyi adsorption potential and the DR equation to derive an equation for ΔH_s (**Eq 1.10**). By determining adsorption isotherms at several temperatures and using **Eq 1.10**, the isosteric heat of adsorption can be calculated for a given adsorbate/adsorbent pair and subsequently used in system energy balances.

$$\Delta H_s = \frac{RT^2}{P_{i,s}}\frac{dP_{i,s}}{dT} + E\left(\ln\left(\frac{q_0}{q}\right)\right)^{0.5} + \frac{\alpha TE}{2}\left(\ln\left(\frac{q_0}{q}\right)\right)^{-0.5} \qquad \text{Eq 1.10}$$

where α is the thermal coefficient of limiting adsorption:

$$\alpha = \frac{1}{T_c - T_b}\ln\left(\frac{\rho_b}{\rho_c}\right) \qquad \text{Eq 1.11}$$

where ρ_b and ρ_c are the gas densities at the boiling temperature (T_b) and the critical temperature (T_c), respectively. In equations **Eq 1.10** and Eq 1.11, the variables R, T, T_c, T_b ρ_b and ρ_c are all well known from the literature. $P_{i,s}$ is determined from the Antoine equation, which is an accepted correlation for determining saturation pressure. E, q_0, and q are all experimentally determined using gravimetric adsorption isotherms and best-fit algorithms in Excel (Excel for Mac 2011) or MATLAB (2013a).

1.4. Regeneration

Regeneration is the process by which an adsorbed compound is desorbed from an adsorbent allowing for the adsorbent to be reused and the adsorbate to be recovered. Generally this is done in one of several ways: pressure swing, purge gas stripping, displacement, and/or thermal swing desorption (*27*). Pressure swing operation reduces the total system pressure at

nearly constant temperature, which results in a lowering of the equilibrium adsorption capacity of the adsorbent causing the adsorbate to desorb. This is equivalent to moving to the left on an adsorption equilibrium curve like those shown in Figure 1.3. Purge gas stripping works by lowering the partial pressure of the adsorbate in the carrier gas, thus causing the adsorbate to desorb to maintain equilibrium. Purge gas stripping is effective for weakly adsorbed species and results in very low adsorbate concentrations in the desorption gas stream. Displacement desorption works by introducing a competitive adsorbate into the system, thus causing the adsorbate of interest to be displaced/desorbed as a result of the competitive adsorption. Thermal swing operation increases the adsorbent and adsorbate temperatures to lower the equilibrium adsorption capacity causing the adsorbed species to desorb. Thermal swing is thought to be the most common method of regeneration and usually uses a hot gas to heat the adsorbate (*27*). Steam is also used as the hot medium, in which case the desorption process becomes a combination of temperature swing and displacement desorption (*27*).

Other methods for heating the adsorbent for thermal swing desorption include microwave heating, inductive heating, and electrothermal heating (*67*). These techniques have increased energy efficiency over steam regeneration because they heat the adsorbent directly (*68*). Electrothermal regeneration or Joule heating involves passing an electrical current through the adsorbent, which acts as a resistor and causes an increase in temperature. Electrothermal regeneration is advantageous because it results in rapid and efficient heating of the ACFC, the power and carrier gas flow rate are controlled independently during desorption allowing for efficient use of resources, and it does not require additional utilities, like steam, that are necessary in traditional regeneration techniques (*69*). However, electrothermal regeneration has a few disadvantages: it requires electricity as the source of energy for regeneration of the adsorbent and the atmosphere surrounding the adsorbent must be made inert prior to regeneration if the adsorbate is flammable.

This research combines the use of adsorption on activated carbon fiber cloth with electrothermal heating to capture and recover low concentration organic gases from carrier gases. The technology is referred to as activated carbon fiber cloth with electrothermal swing adsorption (ACFC-ESA).

1.5. Existing Adsorption Systems Using ACFC and Electrothermal Regeneration

Previous research has developed a recovery system for capture and reuse of low concentration organic vapors (e.g., toluene with T_b = 111°C) from carrier gases using ACFC-ESA (*69*, *70*). This system, known as the VaPRRS is capable of capturing 73-1,000 ppm_v ($P/P_{i,s}$ = 0.002-0.01) organic vapor and recovering it as a liquid for reuse or more efficient disposal (*69, 70*). Extensive characterization of this system has been conducted including material and energy balances (*70*) and cost estimates (*69*). Systems using this technique currently exist on the bench and pilot scales (50 to 1,700 standard liters per minute (SLPM, T = 273 K, P = 1 atm)) (*71*). While the VaPRRS is effective at capturing and recovering high boiling point organic vapors (T_b = 55 - 116°C), it is not capable of recovering organic gases as liquids because it does not have a post-desorption treatment system to increase the partial pressure of the organic gases above their saturation vapor pressure. Dombrowski, *et al.* showed that for lower boiling point organic vapors (e.g., dicholormethane, T_b = 39.8 °C), the VaPRRS could not efficiently recover the adsorbate as a liquid (*42*). The development of an ACFC-ESA system that can handle low boiling point compounds would be a significant advancement over the VaPRRS technology.

Additional research has leveraged adsorption on ACFC and electrothermal desorption as a pre-treatment process for low concentration organic gas streams being treated with biofilters or thermal oxidizers. The steady-state tracking (SST) process captures variable concentration VOC in carrier gases that are typically generated by processes such as coating operations and produces a steady concentration VOC and carrier gas with VOC concentrations ranging from

250 ppm_v to 5,000 ppm_v. The steady concentration stream at a flow rate 10-20% of the flow rate during the adsorption cycle can then be sent to a biofilter or to a thermal oxidizer where the VOC is converted to biomass or CO_2 and H_2O, respectively (*72*).

1.6. Mass and Energy Balances to Describe ACFC-ESA

Several researchers have analyzed ACFC-ESA systems using mass and energy balances to predict the amount of condensate captured and quantify the energy use distribution in the system to identify potential areas for energy efficiency improvement (*70, 72*). For example, Sullivan, *et al.* used a combined mass and energy balance, **Eq 1.12**, to determine the ACFC temperature as a function of electrical energy input (*70*).

$$V_{RMS}I_{RMS} = m_s\Delta H_s\frac{dq}{dt} + \sum m_f c_{pf}\frac{dT}{dt} + m_s\left(c_{ps} + qc_{pi} + \left(q_0 - q\right)c_{pv}\right)\frac{dT}{dt} + \rho_g Q_g c_{pg}\frac{dT}{dt} + hA_{conv}\left(T - T_\infty\right) + \varepsilon\sigma A_{rad}\left(T^4 - T_\infty^4\right) + \frac{kA_{cond}}{L}\left(T - T_\infty\right) \quad \text{Eq 1.12}$$

where V_{RMS} and I_{RMS} are the root mean square (RMS) voltage and current, respectively; m_s is the mass of the solid adsorbent; $q = \rho_l W$ where ρ_l is the density of the adsorbate in liquid form; m_f is the mass of the adsorption vessel's components in direct contact with the adsorbent; c_p values are the mass-specific heat capacities for the adsorber's components (c_{pf}), the adsorbent (c_{ps}), the liquid adsorbate (c_{pl}), the gas-phase adsorbate (c_{pv}), and the carrier gas (c_{pg}); ρ_g is the density of the carrier gas; Q_g is the volumetric flow rate of the gas; h is the convective heat transfer coefficient at the ACFC interface; ε is the emissivity of the ACFC; σ is the Stefan-Boltzmann constant; A_{conv}, A_{rad}, and A_{cond} are the effective surface areas for convection, radiation, and conduction, respectively; L is the length of the conductive heat transfer, k is the conductive heat transfer coefficient, and T_∞ is the ambient temperature.

The mass balance used by Sullivan, *et al.* to predict the amount of condensate collected is described by equation **Eq 1.13** and Figure 1.6. This mass balance assumes that liquid adsorbate is formed on the inside of the vessel walls and that the vapor phase concentration of

adsorbate is in equilibrium with this condensed phase, which is accurate for adsorbates with boiling points above 50°C. This temperature limitation makes **Eq 1.13** applicable to the VaPRRS, but not applicable to the ACFC-ESA system explored in this research, which handles adsorbates with boiling points < 20°C.

$$\frac{dm_l}{dt} = \rho_l m_s \frac{dW}{dt} - \frac{P_{tot} V M_w}{RT} \frac{dy}{dt} - \frac{Q_g t P M_w y_i}{RT} \qquad \text{Eq 1.13}$$

where dm_l is the change in condensate mass in the control volume, P_{tot} is the total pressure in the vessel, P is the pressure of the gas leaving the vessel, V is the volume of the vessel, M_W is the molecular weight of the adsorbate, y_i is the mole fraction of the adsorbate in the gas, and t is time.

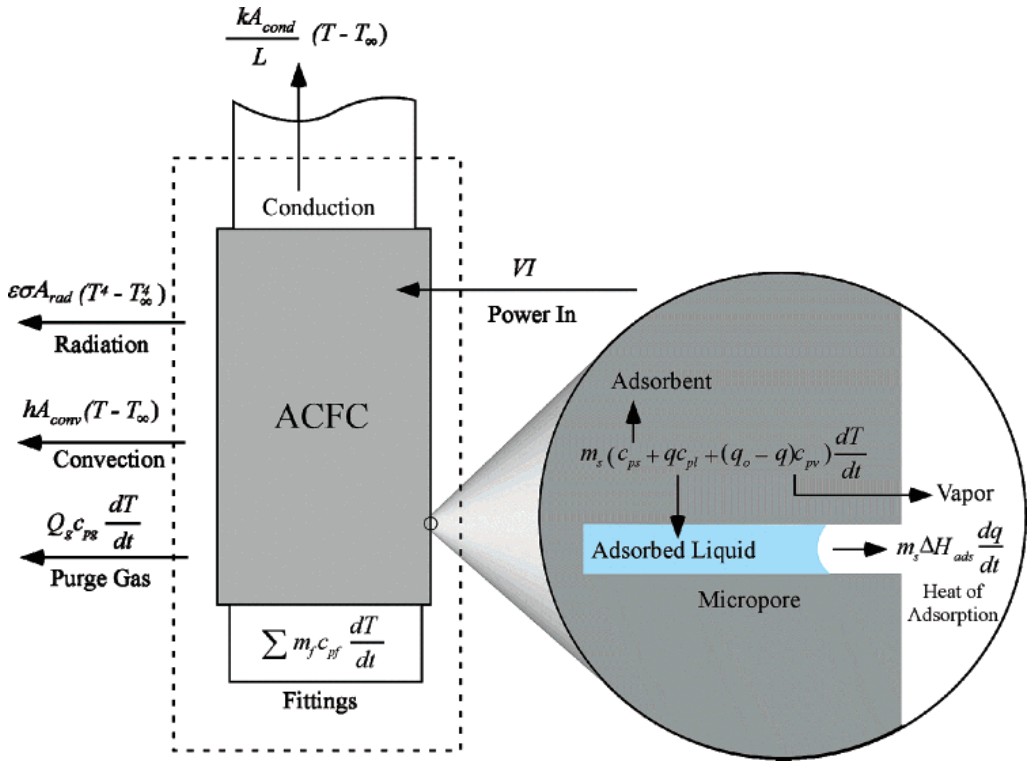

Figure 1.6. Diagram describing the energy balance for the ACFC-ESA system. Reprinted with permission from (*70*). Copyright 2004 American Chemical Society.

The mole fraction of the adsorbate in the gas phase was determined by Sullivan, *et al.* with **Eq 1.14**, which combines the DR equation (**Eq 1.4**) with the Wagner equation. The Wagner equation predicts saturation vapor pressure as function of temperature and is similar to the Antoine equation (Eq 1.7).

$$y_i = \frac{P_c \exp\left[\left(\frac{VP_A + VP_B x^{1.5} + VP_c x^3 + VP_D x^6}{1-x}\right)\right]}{P_{tot} \exp\left[E\sqrt{-\ln\left(W/W_0\right)}\Big/RT\right]} \qquad \text{Eq 1.14}$$

where P_c is the critical pressure of the adsorbate, VP_A, VP_B, VP_C, VP_D are Wagner constants for the adsorbate, and $x = 1-(T/T_c)$.

When the modeled and measured results were compared for methyl ethyl ketone (T_b = 79.6 °C), methyl propyl ketone (T_b = 101°C), and acetone (T_b = 56.5°C), the modeled condensate recovery results agreed with the measured values with mean absolute errors less than 6.7% (*70*). However, Sullivan, *et al*. also indicated that the assumptions used in their model are less valid as the saturation vapor pressure of the adsorbate increases (i.e., as the boiling point decreases) and that auxiliary cooling of the desorption effluent "may be needed for compounds with saturation vapor pressures greater than 0.2 atm at 20°C" (*70).*

1.7. Post-Desorption Condensation

The organic compounds of interest in this research have boiling points below 40°C, which, as noted above, precludes the use of the VaPRRS for their recovery as liquids. In order to extend the applicability of the VaPRRS and capture and recover low boiling point compounds using ACFC-ESA, post-desorption condensation is required. This can be achieved with a combination of pressurization and cooling, assuming the concentration of the desorbed organic gas is sufficiently high.

To define the threshold concentration for effective liquefaction, the organic compound's concentration must exceed its saturation concentration. The relationship between temperature, pressure, and concentration can be determined using Antoine's equation (**Eq 1.7**). Dalton's law (**Eq 1.15**) can be used to determine the partial pressure of the adsorbate in the system. The gas stream that is generated during desorption cycles is assumed to be a binary mixture of organic compound and N_2 that obeys the ideal gas law.

$$P_i = y_i P_{tot} \qquad \text{Eq 1.15}$$

This analysis was conducted for isobutane by Mallouk, *et al.* assuming a total pressure of 10.3 bar gauge (1.03×10^6 kPa gauge) and resulted in **Figure 1.7** (*73*). The crosses marked A and B indicate the minimum threshold concentrations to achieve condensation if the compression/cooling system could achieve 20 and 30°C, respectively. A reduction in temperature in the cooling module would also reduce the minimum threshold concentration needed to achieve condensation.

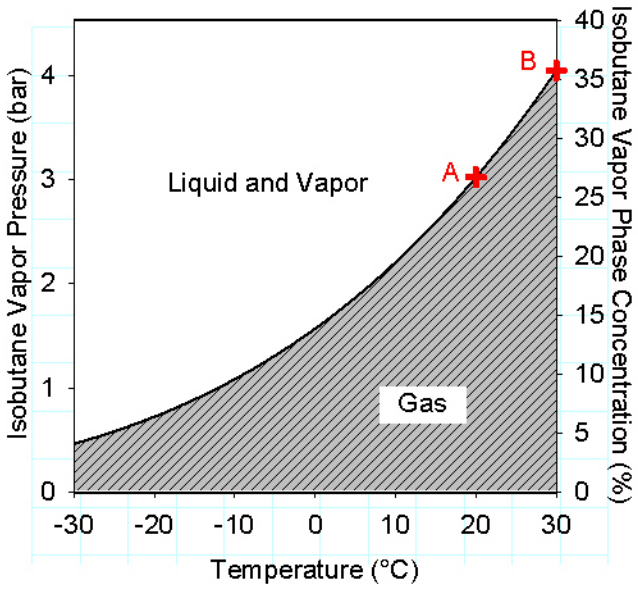

Figure 1.7. Isobutane saturation vapor pressure and required concentration for condensation as a function of temperature assuming a total pressure of 10.3 bar gauge. Reprinted with permission from (*73*). Copyright 2010 American Chemical Society.

If the conditions indicated in **Figure 1.7** are achieved downstream of the desorption module, then liquefaction of the captured isobutane is achieved. A similar analysis can be conducted for other compounds so that the compression and cooling conditions can be tailored to compounds with boiling points different from isobutane. Again, post-desorption condensation using a combination of compression and cooling extends the applicability of the VaPRRS to low boiling point compounds that were previously not recoverable using ACFC-ESA.

1.8. Research Objectives and Significance

This research had three major objectives surrounding the development and characterization of a bench-scale adsorption system that combines an ACFC-ESA and post-desorption treatment for capturing and recovering low boiling point organic compounds.

1.8.1. Develop and Test a Bench-Scale ACFC-ESA System with Post-desorption Treatment

The first objective of this research was to develop and test an ACFC-ESA system with post-desorption treatment to capture low boiling point organic compounds and recover them as

liquids. The bench-scale system was first tested with isobutane as a model compound and characterized with mass and energy balances. The necessary operating conditions for recovering the isobutane as a liquid were determined with thermodynamic analysis. This is a significant advancement over previous technology because it expands the range of compounds that can be captured and recovered with ACFC-ESA to those with boiling points below 40°C.

1.8.2. Evaluate and Characterize ACFC-ESA System with Post-desorption Treatment

The second objective of this research was to evaluate the bench-scale ACFC-ESA system with post-desorption treatment using mass and energy balances for several organic compounds that span a range of boiling points (-26.5 to 39.8°C) and have different functional groups (e.g., alkanes, fluorocarbons). The compounds of interest in addition to isobutane were n-butane, dichloromethane, and R134A, which have boiling points that span 50°C. The performance of the system, defined by capture efficiency and energy efficiency, was assessed, analyzed as function of adsorbate relative pressure, and compared to existing technologies to determine the system's relative performance.

The experimental results generated with the bench-scale system were also compared to modeled results based on gravimetric adsorption isotherms and the isosteric heats of adsorption. These comparisons can then be used to make estimations regarding the performance of the bench-scale system with other organic gases and the performance of larger, industrially-relevant, scale systems. This contribution is important to complete to more fully evaluate the general applicability of this new technology and benchmark its performance with existing technologies.

1.8.3. Conduct Multicomponent Adsorption with Carrier Gas Recirculation for Improved System Sustainability

The final objective of this research was to use the bench-scale ACFC-ESA system to capture isobutane from a carrier gas with relative humidities ranging from 5-80% while

maintaining the water vapor concentration of the carrier gas. In addition, the clean, humid adsorption carrier gas and the N_2 used to inert the system during desorption was recirculated during operation, which resulted in a reduction in the amount of water vapor and N_2 required to operate the system once it reaches steady state. In an industrial setting, this new ability to recycle the carrier gas stream will represent an improvement in system sustainability and a reduction in operating costs because it reduces the need for re-humidification and decreases the demand for N_2 production to inert the adsorption vessels during desorption, which has been shown to account for greater than 50% of the total energy usage in the pilot-scale VaPRRS system (*71*). The operation of the ACFC-ESA system with humid air was characterized by mass and energy balances. This component of the research is vital because many of the industrially relevant treatable gas streams have relative humidities in the range that could affect ACFC's adsorption capacity for the compounds of interest. Understanding how a treatment system could be engineered to process humidified gas streams and conserve N_2 consumption will make the technology more commercially relevant.

2. METHODS

To achieve the research objectives discussed in the previous section, the following equipment and experimental procedures were used.

2.1. Adsorption Isotherm Measurement and Modeling

2.1.1. Experimental Apparatus: Cahn 2000 Microbalance

To measure gravimetric adsorption isotherms for adsorbate/adsorbent pairs a Cahn 2000 microbalance was used (Figure 2.1). The microbalance measures changes in mass of the adsorbent as it is exposed to select concentrations of the adsorbate.

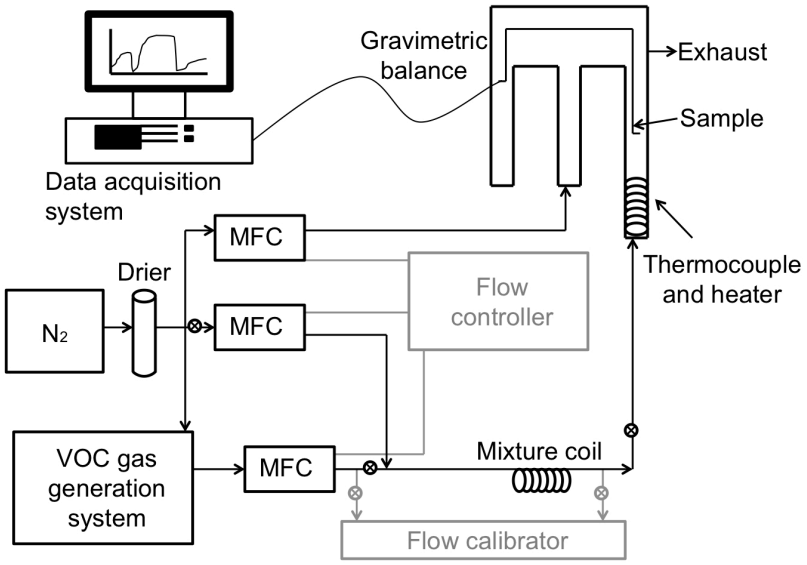

Key: MFC – Mass Flow Controller; VOC – Volatile Organic Compound

Figure 2.1 Diagram of the Cahn 2000 microbalance used for measuring adsorption isotherms.

The specifics of the operating of the Cahn 2000 microbalance have been previously described (*50*), but are summarized here for clarity: The microbalance was operated in a controlled temperature and RH room (24°C, 65% RH). The carrier gas for the system was N_2 at a flow rate of 300 or 500 sccm that was dried and purified using a Dririte filter. Select concentrations of the adsorbate of interest were added to the dried and purified N_2 stream. The

gaseous flows were controlled with mass flow controllers (Tylan) and the liquid dichloromethane flow was controlled with a syringe pump (kdScientific, model 100). Before each experiment, the balance was zeroed and calibrated. The adsorbent sample of interest was then placed on the balance pan and heated to 70°C until its mass was changing less than 10 µg over 30 min. The sample was then cooled to ambient temperature and its mass was recorded.

Once exposure to a given adsorbate concentration was underway, the adsorbent was monitored for changes in mass. Once the mass was changing less than 10 µg over 30 min, its value was recorded and the next adsorbate concentration was supplied.

Isotherm experiments were conducted with adsorbate concentrations ranging from 20 to 500,000 ppm_v. All experiments were conducted at 24°C, except for a series of measurements conducted for isobutane and R134A on ACFC-15 that occurred at temperatures of 24, 31.5, 40, and 50°C, which were used to determine the isosteric heat of adsorption for isobutane and R134A on ACFC-15. The elevated temperatures were achieved with heating tape wrapped around the glass vessel containing the sample.

2.1.2. Modeling of Measured Adsorption Isotherms

The isotherm data generated using the Cahn 2000 microbalance was fit to five adsorption models: Freundlich, Toth, Yaws, DR, and DQSAR, which are described in detail in section 1.3.4. MATLAB's (version R2013a) least squares nonlinear regression function and Microsoft Excel's (version 2010) Goal Seek function were used to find the model parameters that best fit the data based on the average absolute relative difference between the data and the model.

2.1.3. Isosteric Heat of Adsorption Determination

The isotherms for isobutane and R134A on ACFC-15 were measured at four temperatures (25, 31.5, 40, and 50°C) prior to the analysis to determine ΔH_s (**Eq 1.10**). Each of these isotherms was fit to a model using the DR equation (**Eq 1.4**). The isotherm data were then

used to determine ΔH_s using the DR parameters for the 31.5°C isotherm. The 31.5°C isotherm was chosen because it falls in the middle of the explored temperature range (25 to 50°C).

2.1.4. In-Pore Liquefaction

To determine if adsorbate liquefaction is occurring in the pores of the adsorbent, the volume of adsorbate adsorbed at high relative pressures was determined from the isotherm data fitting. Using the saturated adsorbed phase mass determined from the DR model fitting of the measured data and the bulk liquid density of the adsorbates (Table 1.3), the maximum volume of each adsorbate that would adsorb at saturation was determined. This volume was assumed to be equivalent to the adsorbent's available pore volume for that adsorbate (Table 1.2). Liquefaction was considered likely if the pore volume available for adsorption determined for a given adsorbate/adsorbent pair was within 10% of the measured total pore volume determined by N_2 adsorption at 77 K.

2.2. Gas Recovery System Setup and General Operation

An experimental system was developed to complete proof-of-concept tests that demonstrated that it is possible to capture and recover organic gases as liquids using ACFC-ESA. The Gas Recovery System (GRS), which uses ACFC-ESA consists of a gas generation system, two ACFC adsorption vessels with electrothermal regeneration capability, a post-desorption temperature and pressure control module, and a data acquisition and control system (*73*). Two ACFC adsorption vessels were used so that the system could operate continuously: while one vessel is adsorbing, the other is regenerating. The post-desorption temperature and pressure control module were implemented so that the desorbed gas stream could be cooled and pressurized to reach the condensation requirements detailed in section 1.7. The determination of operating conditions for this system are described in section 2.5, below.

2.2.1. First Generation Gas Recovery System

Initial tests of the GRS were conducted using first generation GRS with isobutane as the sole adsorbate. This system consisted of two large adsorption vessels with two ACFC cartridges per vessel and a primitive pressure and temperature control system, as described below. Each adsorption/desorption vessel provided 3.5 L of empty internal volume and held two vertical annular cartridges, each with 91.3 grams of ACFC (Kynol ACC5092-15) (**Figure 2.2**).

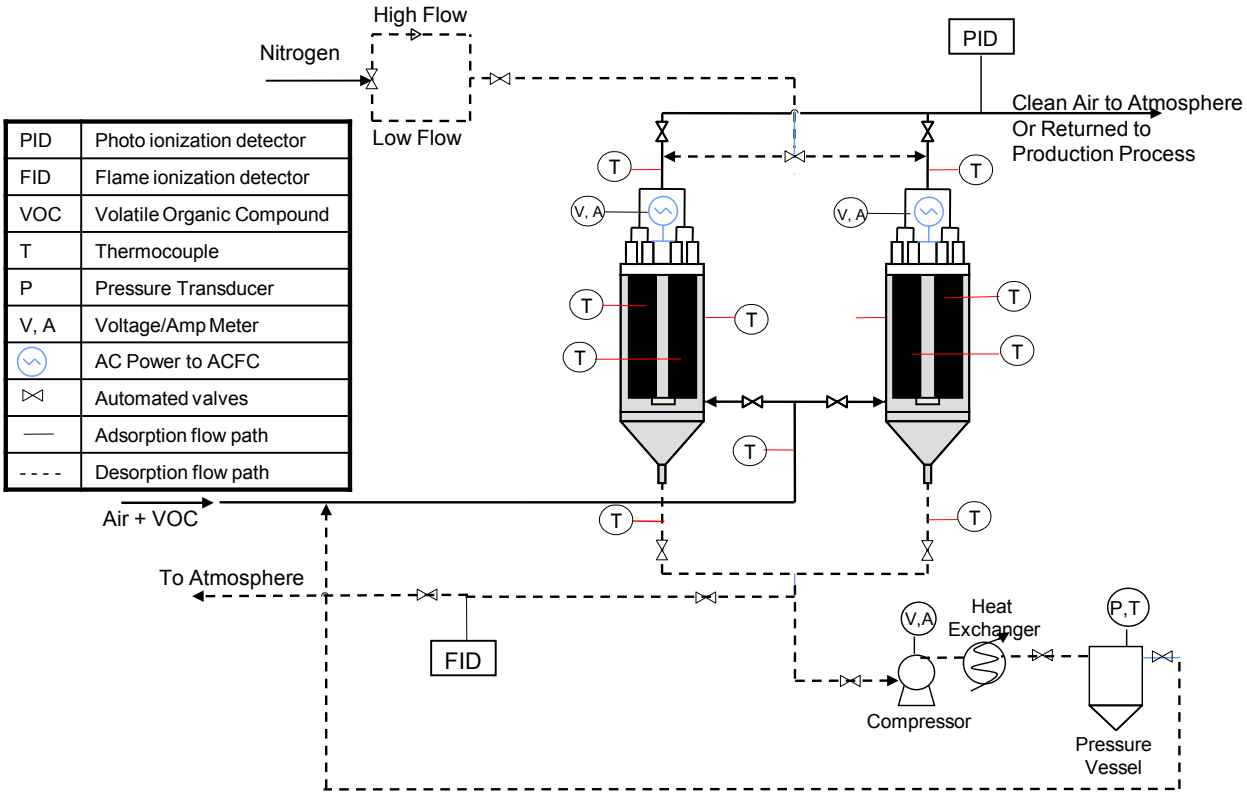

PID	Photo ionization detector
FID	Flame ionization detector
VOC	Volatile Organic Compound
T	Thermocouple
P	Pressure Transducer
V, A	Voltage/Amp Meter
	AC Power to ACFC
	Automated valves
——	Adsorption flow path
- - - -	Desorption flow path

Figure 2.2 First generation experimental apparatus with 3.5L adsorption vessels each containing two annual ACFC cartridges. Reprinted with permission from (*73*). Copyright 2010 American Chemical Society.

The ACFC-15 studied here has an N_2-BET surface area of 1,335 m^2/g, as determined with adsorption isotherms for N_2 at 77 K (Micromeritics ASAP 2010). The arithmetic mean pore width for ACFC-15 is 0.76 nm, and 96.6% of the pore volume is microporous (*48*). Temperature of the ACFC was measured using 0.081 cm diameter Type K thermocouples (Omega, Inc.).

During the adsorption cycle, pressurized air flowing at 50 – 100 SLPM passed through a high efficiency particulate air filter (HEPA) filter and silica gel to remove particulate matter and water vapor, respectively. The air was then combined with the organic gas, which was obtained from a pressurized cylinder (Aeropres Corp., 97.8% isobutane, vapor withdrawal) at a controlled flow rate. The resulting isobutane relative pressure was $6.7x10^{-4}$. All gas flow rates were controlled with mass flow controllers (air: Aalborg, model GFC571S; N_2 and isobutane: Tylan Inc.). The isobutane and carrier gas entered the bottom of one vessel and passed through the ACFC cartridges in parallel. The organic gas concentration was monitored downstream of the adsorption vessel with a photo-ionization detector (PID, RAE Systems, Inc., PDM-10A). The PID was calibrated with select concentrations of isobutane in dry air from 0 to 2,500 ppm_v.

The desorption cycle of the second vessel occurred concurrently with the adsorption cycle of the first vessel. N_2 entered the top of the vessel experiencing desorption and then passed through the ACFC. N_2 is used to create a chemically inert atmosphere so that combustion cannot take place during regeneration when electricity, flammable concentrations of organic gases, and high temperatures are all present. ACFC heating required control of the voltage applied to the cloth with a silicon controlled rectifier (SCR, Robicon, Model 440 102.10). The ACFC was heated until it reached 200°C, at which point heating was discontinued. Isobutane concentration in the desorption gas stream was measured with a flame ionization detector (FID, MSA Inc., Series 8800). The FID was calibrated using mixtures of isobutane (0 – 100% by volume) and N_2. After the isobutane was desorbed from the ACFC it entered a compression module consisting of a compressor (Air Dimensions Inc., R272-BT-EA1) capable of producing pressures up to 13.1 bar gauge (190 psig), a custom copper tubing heat exchanger (outer diameter 1.59 cm, inner diameter 1.38 cm, length 3.4 m), and a polycarbonate pressure vessel (1 L, > 10 bar gauge pressure rating). Pressure was monitored with a pressure

transducer (Dwyer, IS626-12-GH-P1-E1-S1). Gases exiting the pressure vessel were exhausted to the hood and not recycled back into the adsorption system.

2.2.2. Second Generation Gas Recovery System

Changes were made to the first generation GRS to minimize the internal volume of the adsorption vessels and improve the temperature and pressure control system for the desorption gas stream. These changes would maximize the concentration of the desorbed organic gas and shift the system equilibrium towards a higher liquid fraction. Experiments were conducted with isobutane to determine the most cost effective heating temperature during desorption. The updated adsorption/desorption vessels (Figure 2.3) each consisted of a custom Pyrex® cylinder (height = 38 cm) and conical base (height = 7 cm) with a Teflon® top plate (height = 1.9 cm).

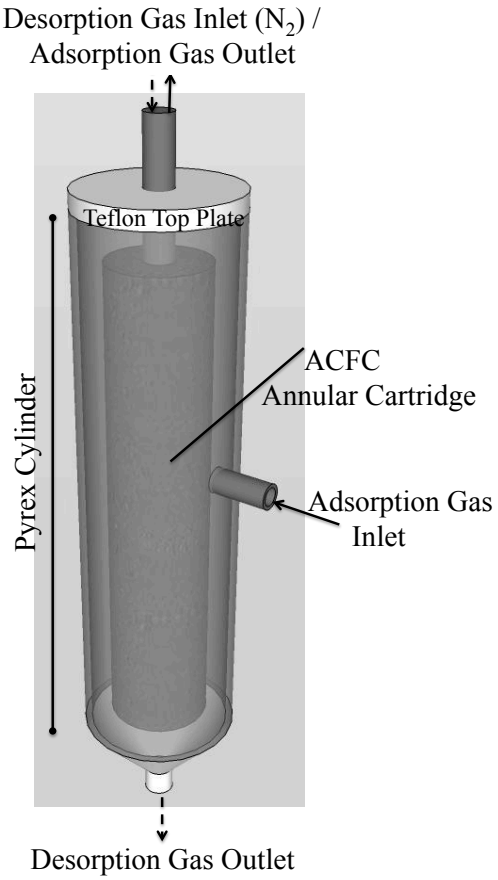

Figure 2.3 Adsorption/desorption vessel with one annular ACFC cartridge. Solid and dashed arrows represent the flow path for adsorption and desorption cycles, respectively.

Each vessel provided 1.43 L of empty internal volume, which represents a 40% reduction in empty internal volume compared to the first generation adsorption vessels. Each second generation adsorption vessel held a vertical annular cartridge with 115 g of ACFC (Kynol ACC5092-15). Each ACFC cartridge had 20 layers of ACFC and was 25 cm from top to bottom with a 5 cm outer diameter and 2 cm inner diameter. Temperature of the ACFC was measured using 0.16 cm (0.062 in) diameter Type K thermocouples (Omega, Inc.). To aid in heat removal from the adsorption vessels, small electric fans (23 cm diameter) were aimed at the vertical midpoint of each adsorption vessel and ran on high for the duration of the experiments.

The desorption gas entered the same pressurization system as in the first generation system, however now the pressure vessel was contained in a polycarbonate vessel that contained 16 L of a 70/30 glycol/water mixture that maintained the internal temperature of the pressure vessel at ≤ 0°C. The gases exiting the pressure vessel were recycled back to the adsorption stream, resulting in only one outlet for isobutane (liquefaction) (**Figure 2.4**).

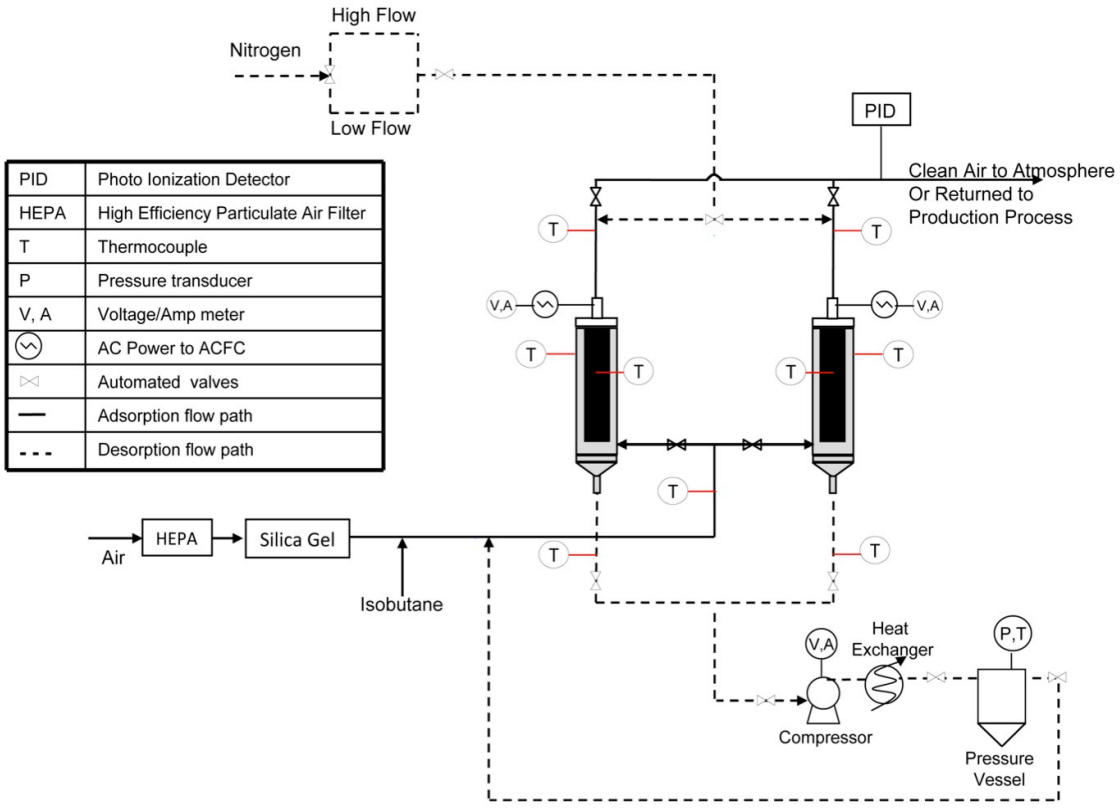

Figure 2.4 Second generation experimental apparatus with smaller adsorption vessels and recycling of the gases exiting the desorption system. Arrangement of the ACFC within the vessel can be viewed in Figure 2.3. Reprinted with permission from (*75*). Copyright 2013 American Chemical Society.

Experimental conditions were the same as those in the first generation GRS with the modification that the temperature of the ACFC during desorption was controlled to 150, 175, or 200°C.

2.2.3. Third Generation Gas Recovery System

Further modifications were made to the GRS to improve the performance of the post-desorption pressure and temperature control system through a series of controlled experiments that varied the ACFC heating and desorbed gas compression time of the system. These experiments were conducted on this updated system using isobutane, n-butane, R134A, and dichloromethane (DCM). However, the experiments with DCM were discontinued after it was discovered that the DCM was destroying valve seals and other components of the GRS. During the adsorption cycle, pressurized house-air passed through a pretreatment system that consisted of a HEPA filter, silica gel, and ACFC to remove particulate matter, water vapor, and organic compounds, respectively. The air flow rate ranged from 10 – 50 SLPM depending on the adsorbate and was controlled with a mass flow controller (Aalborg, model GFC571S). This is equivalent to a gas velocity through the outer cross section of the cartridge of 4.2×10^{-3} – 2.1×10^{-2} m/s at actual conditions. The air was then combined with the organic gas, which was obtained from a pressurized cylinder (purities as follows: n-butane: 95%[2] (*74*), isobutane: 98.3%, R134A: 99.5%) at a controlled flow rate. All gas flow rates were controlled with mass flow controllers (n-butane/isobutane/R134A: Alicat Scientific, MC-200SCCM- D5/M; N_2: Tylan Inc., FC-280). The organic gas concentration was set to a given relative pressure (see section 2.6). The organic gas and carrier gas entered the side of one vessel and passed through the ACFC cartridge from the outside to the inside of the cartridge. The empty bed contact time determined from the envelope volume of the ACFC and the actual gas flow rate ranged from 0.15-0.78 s. The organic gas concentration was monitored downstream of the adsorption vessel with either a PID (RAE Systems, Inc., PDM-10A) or FID (MSA/Baseline Inc., series 8800). The PID and FID were

[2] This particular blend of n-butane was used because it represented the n-butane being used by the project sponsor.

calibrated using multi-point calibration with the relevant compounds used to characterize the GRS. The gas streams used in the PID and FID calibrations were generated from the same gas cylinders used during GRS operation and the flow rates were controlled using mass flow controllers.

The desorption cycle of one vessel occurred concurrently with the adsorption cycle of the other vessel and consisted of six steps, with duration of each cycle provided after the description of each cycle:

1. N_2 entered the top of the vessel experiencing desorption and then passed through the ACFC from the inside to the outside of the cartridge flowing at 3.5 SLPM (gas velocity through inner cross sectional area of the cartridge = $3.9x10^{-3}$ m/s at actual conditions). This was done to clear oxygen from the vessel prior to heating. The flow rate was chosen to clear greater than 2 column volumes in one minute, which earlier tests showed resulted in a 90% reduction in oxygen concentration in the vessel. Note that the limiting oxygen concentration (LOC, concentration of oxygen below which combustion is not possible, independent of the concentration of fuel) is 12% (*14*), which would require a 42% reduction in atmospheric oxygen concentration. The 90% reduction in oxygen concentration allows for a safety factor to prevent explosions in the system. (1 min)
2. The N_2 flow rate was reduced to 0.5 SLPM (gas velocity through inner cross sectional area of the cartridge = $5.3x10^{-4}$ m/s) to minimize the amount of carrier gas being used during desorption. This change allows for high concentrations of organic gas to be generated during desorption. The ACFC began heating to a set point of 150°C. The value of 150°C was chosen based on previous experiments that examined the energy used by the system at 150, 175, and 200 °C. An ACFC temperature of 150°C was able to regenerate the carbon sufficiently for the lowest energy cost (*75*). ACFC heating

required controlling the voltage applied to the cloth with an SCR (Robicon, Model 440 102.10). As the organic gas was desorbed from the ACFC in this step, it was recycled to the adsorbing vessel. (1 min)

3. ACFC heating continued and the desorbing organic gas entered a compression module consisting of a compressor (Air Dimensions, Inc., R272-BT-EA1) capable of producing pressures up to 13.1 bar gauge (190 psig) and a custom glass pressure vessel (0.5 L for isobutane at a relative pressure of $6.7x10^{-4}$ and 0.1 L for n-butane, R134A, and higher relative pressures of isobutane). The pressure vessel was contained in a polycarbonate vessel that contained 16 L of a 70/30 glycol/water mixture that maintained the internal temperature of the pressure vessel at ≤ 0°C. Pressure in the pressure vessel was controlled at 10.3 bar gauge (150 psig), with exhaust from the pressure vessel being returned to the adsorbing vessel. This pressure was chosen to maintain consistency with experiments using the first generation GRS (*73*). Total pressure was monitored with a pressure transducer (Dwyer, IS626-12-GH-P1-E1-S1) and temperature was measured with a 0.16 cm (0.062 in) diameter type K thermocouple (Omega, Inc.). (2 – 7 min)
4. The N_2 flow rate was increased to 3.5 SLPM and the ACFC heating continued with the desorbed gas being recycled to the adsorbing vessel. This step cleared the ACFC of desorbing organic gas prior to turning off the voltage applied to the ACFC (0.5 min)
5. Heating was stopped and the vessel was exposed to 3.5 SLPM of N_2. This was done to clear any remaining gas-phase organic compound out of the desorbing vessel. (2 min)
6. The N_2 flow rate was reduced to 0.5 SLPM and once the temperature of the ACFC reached 60°C, N_2 flow to that vessel was discontinued. Earlier experiments showed

that if the desorbing vessel was switched to adsorption before reaching 60°C, the initial adsorption of adsorbate would be inferior due to premature breakthrough.

The desorption process time (steps 1-5) ranged from 6.5 to 11.5 min depending on the experiment. During step 3 when the compression module was used, the pressure in the desorption system was maintained at 1.05 bar absolute (15.2 psia) by controlling the flow through the compressor via a variable area solenoid valve (AscoValve, SD8202G013V). This pressure maintenance was done to ensure that the desorbing vessel was slightly pressurized to prevent atmospheric oxygen from entering the system. The amount of liquid organic compound collected was determined by visually noting the liquid level in the pressure vessel.

2.2.4. Fourth Generation Gas Recovery System

Several modifications were made to the third generation GRS to allow for RH control and recycling of the carrier gas stream during operation. These modifications allowed testing with humid carrier gas streams and helped exhibit proof of concept for the carrier gas recycling. Figure 2.5 below, shows the flow schematic for the fourth generation GRS. Major additions include two additional pressure sensors (Dwyer IS626-00-GH-P1-E1-S1 and Omega PX309-030AI), two RH sensors (Vaisala HUMICAP HMT363), an oxygen sensor (Alpha Omega Instruments, 2000-B115BTX), an FID (MSA/Baseline Inc. series 8800), a recirculation blower (Air Dimensions H302-FT-AA1), and a custom humidification system. The humidification system consisted of an annular humidifier which controls the flow of water vapor through a 19.05 mm ID tubular Gore Tex® membrane (*76*). An annular stainless steel mesh supported the Gore Tex® membrane on the carrier gas flow side. The RH is controlled with a PID controller (Watlow, 955A), which modulates the current supply to heating tape surrounding the humidifier. The more current flowing through the heating tape, the more heat is transferred to water circulating around the membrane, which leads to more water diffusion through the membrane and a higher RH in the carrier gas. Due to the addition of heat to the carrier gas from the humidification system and

an increase in water vapor in the desorption gas stream due to the humidity in the carrier gas, a cooling system was employed to control the temperature of the carrier gas and collect desorbed water vapor. The cooling system consisted of polypropylene tubing wrapped around the adsorption vessels and a glass Erlenmeyer flask water collection vessel. The tubing had a 70/30 glycol/water mixture flowing through it that was chilled using a water bath/circulator (Thermo Neslab RTE-110). This cooling system allowed for separation of water vapor and the desorption gas stream and prevented 99% of adsorbed water vapor from entering the compressor.

Another modification for the carrier gas recirculation was to implement an outlet for system pressure maintenance ("purge") and a makeup supply of house air to ensure that the system had 40 SLPM air flowing during adsorption. The total makeup air supplied to the system was 2.65 SLPM to make up the air lost in the purge and through the O_2 sensor and FID.

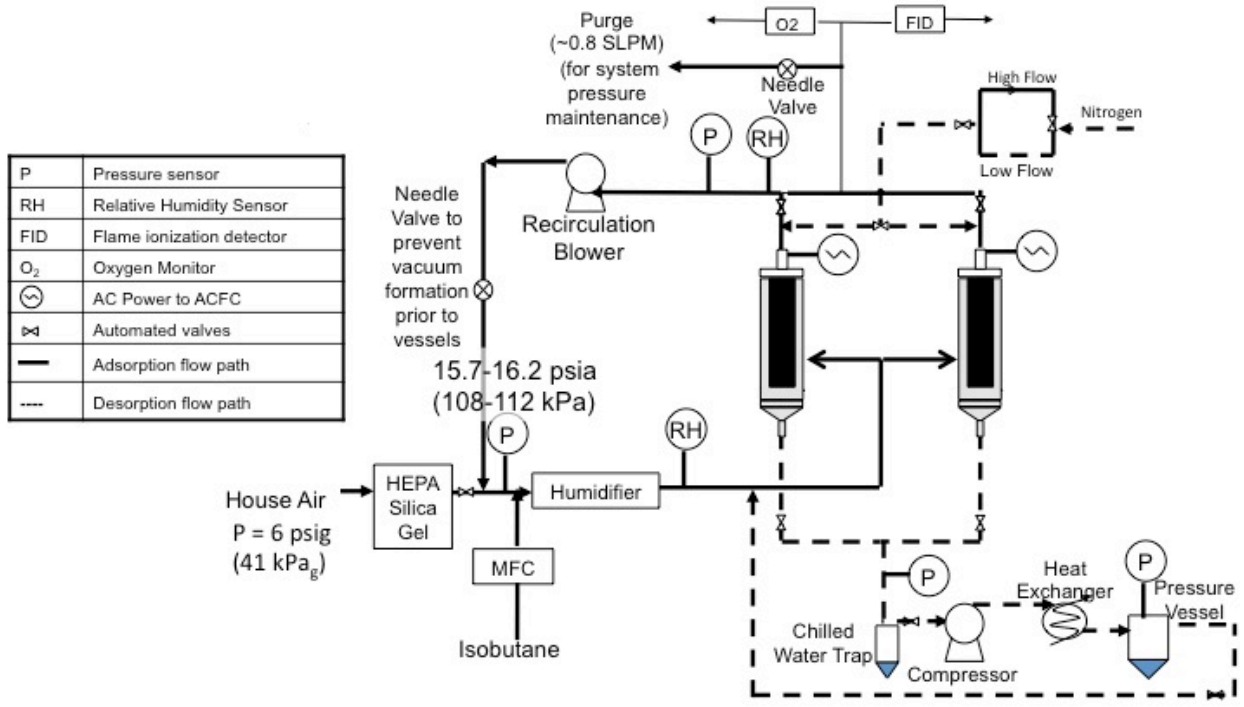

Figure 2.5 Fourth generation experimental apparatus with modifications for RH control and recycle of carrier gas stream. Solid and dashed lines represent the flow path for adsorption and desorption cycles, respectively.

The general operation of the fourth generation GRS is similar to that of the third generation GRS with isobutane being the primary adsorbate of interest (with water being a competitive adsorbate) and the time for Step 3, above, being 4 min for a total regeneration time (Steps 1-5) of 6.5 min.

2.2.5. Automation Software and Desorption Gas Handling

All generations of the GRS were fully automated (no human intervention required when system was operating once startup is complete). The control system consisted of National Instruments Fieldpoint™ hardware connected to a personal computer with LabView™ 6.1 software (*77*). The control system monitored and recorded values for gas concentrations and temperatures, ACFC temperatures, pressure, RMS voltage, and RMS current. The LabView™ program maintained a user-defined ACFC temperature during desorption by controlling the power applied to the ACFC with a proportional-integral-derivative (P-I-D) delayed feedback controller (*77*). For these experiments, the P-I-D constants, which are user-tunable, were: P = 10, I = 10^{-5}, D = 0.01. The LabView™ program also determined when the ACFC that was undergoing an adsorption cycle was saturated based on user-defined parameters and automatically switched that vessel to a desorption cycle while simultaneously beginning the reciprocal adsorption cycle. This ensured that the organic gas/carrier gas was treated continuously by adsorption. Additionally, for the second through fourth generation GRSs, the program was designed to ensure that all gas streams were recycled back to the adsorbing vessel except for the treated carrier gas. The recycled streams included the fractions of the desorption stream that were not compressed/cooled and the gas stream generated at the outlet of the temperature and pressure control module as the pressure vessel's pressure was maintained. As is described above in section 2.2.3, not all of the desorbed gas was compressed/cooled because when the ACFC is first heated, the concentration of adsorbate that

was produced was low (average of less than 10% by volume based on modeling results) and would negatively impact the energy and mass collection efficiencies of the liquefaction. A total of 1.5 min (Steps 2 and 4) of the 3.5-9.5 min heating time involved desorbed gas bypassing the compression/cooling system.

2.2.6. Risks Associated with GRS Operation

There are several risks associated with operating the GRS, particularly when combustible compounds are involved. For example, there are times during desorption when the isobutane concentration is within its flammability limits (1.8 – 8.5% by volume) (*34*). If air were present during these times, due to leaks or lack of N_2 supply, a fire could ignite or the ACFC could burn. ACFC burning appears to be one cause of adsorption capacity degradation. An additional possible source of ACFC burning, besides the ignition of isobutane during desorption, is when the ACFC itself experiences elevated temperatures in the presence of O_2. Other researchers have found that ACFC degradation occurs due to thermal decomposition of adsorbates at elevated temperatures (> 288°C) even in the presence of N_2 (*78*). Other risks include high-pressure operations in select parts of the GRS, which could be dangerous if fittings were not secured properly, and the presence of high voltage and current during regeneration operations for pilot-scale and full-scale operations. These risks can be minimized with proper personnel training and system controls to prevent leaks, over-pressurization, and exposure to high voltage and current.

2.2.7. Engineering Challenges Related to GRS Development

Many engineering challenges were overcome in the development of the GRS from the starting point of the VaPRRS. These challenges included achieving the required conditions for condensation downstream of the desorption process and controlling the pressure with the adsorption vessels to prevent air infiltration among others.

In particular, designing the compression, cooling, and storage system for the desorbed gas stream required several iterations and constant adjustments. As discussed above, the initial system consisted of over 1.5 L of internal volume between the tubing leading out of the compressor and the pressure vessel. Considering that the N_2 flow through the system during desorption was only 0.5 LPM and the total volume of liquid isobutane that could be recovered was 12 mL per desorption cycle, this initial volume was much larger than appropriate. Subsequently, a new copper tubing heat exchanger and pressure vessel were designed and implemented which reduced the volume of the components downstream of the desorption process to 0.55 L. This modification ensured that a larger fraction of the desorbed gas made it into the chilled pressure vessel and also made it easier for the operator to read the isobutane liquid level within the pressure vessel. Due to the high pressure conditions experienced by the compression and cooling system, leaks were a common occurrence and the system needed to be checked for pressure maintenance regularly. In addition, the back-flow prevention valve that was integrated into the compressor failed and required the implementation of an external back-flow prevention valve, which also had a tendency to fail and needed to be replaced regularly.

As with the high pressure maintenance in the compression and cooling system, the temperature within the pressure vessel also had to be carefully monitored. In order to minimize the temperature, a custom acrylic container was built to allow the pressure vessel and surrounding tubing to be submerged in a glycol/water mixture that was continuously stirred with a magnetic stir bar. The glycol/water mixture was chilled to between -10 and 0°C using a FTS Systems FC100 Immersion Cooler. When the immersion cooler was non-operational, dry ice was used to chill the glycol/water mixture.

Another major modification to the GRS that was implemented to improve performance was a pressure maintenance system for the adsorption vessels during desorption. Several years after the start of this research, it was discovered that that ACFC was burning during some

desorption cycles. This was a result of the adsorption vessels experiencing vacuum during desorption due to the operation of the compressor downstream of the desorption process. The vessels had begun failing to prevent air infiltration under vacuum conditions, so air was infiltrating the vessels during desorption and causing the ACFC to burn. The solution to this problem was several-fold. First, gaskets and other sealants were added to the adsorption vessels to seal them as tightly as possible against vacuum. Next, a variable-area solenoid valve was added to the inlet of the compressor so that the flow of gas into the compressor could be controlled based on the pressure in the desorbing vessel. Experiments were conducted to determine what set-point pressure to use for the compressor flow control, and 15.2 psia was found to be a reasonable pressure. After the implementation of this pressure maintenance system, the ACFC stopped degrading.

2.3. Performance Metrics for the Gas Recovery System

Several performance metrics were used to compare different operating conditions, adsorbates, and system configurations for the GRS. These include capture efficiency, energy usage, effective adsorption capacity, and mass distribution in the GRS.

2.3.1. Capture Efficiency

Figure 2.6 represents the boundaries set for determining material balances for the GRS.

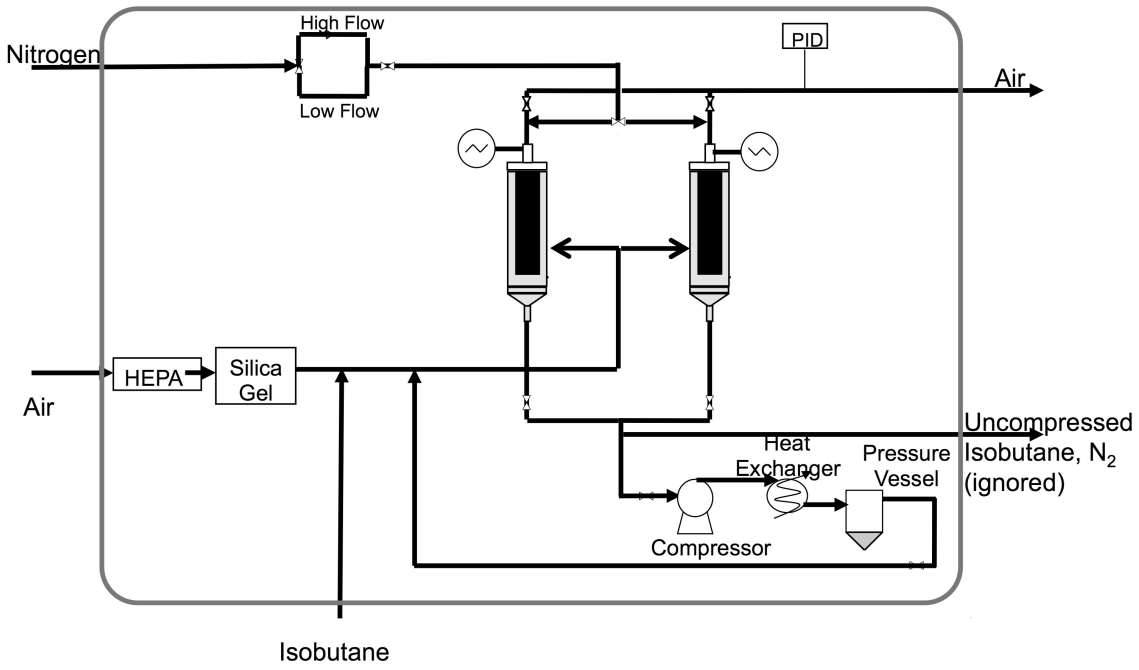

Figure 2.6 Experimental apparatus (2nd generation). The grey rounded border represents the system boundaries for mass balances for the GRS.

Capture efficiency describes the amount of captured adsorbate relative to the amount supplied to the vessel for a particular adsorption cycle (Eq. 2.1). To determine the capture efficiency, the total mass adsorbed by the GRS is required. The mass of any adsorbate adsorbed at any time, t_i, during adsorption is M_{ti} (Eq 2.2) (*70*), where the subscript i represents the percent of the inlet adsorbate concentration reached by the outlet concentration (e.g., t_5 is the time at which the outlet concentration has reached 5% of the inlet concentration). Once the amount of adsorbate adsorbed is determined, it is compared to the amount of adsorbate that was supplied to the GRS to find the capture efficiency of the system. Breakthrough time and mass of adsorbed adsorbate were determined when the organic gas concentration at the vessel's outlet reached 5% of the inlet concentration, corresponding to t_5 and M_{t5}, respectively.

$$\text{Capture Efficiency} = \frac{M_{t,ads}}{\left(M_w Q_g y_{in} t_{ads}\right)/RT} x100\% \qquad \text{Eq 2.1}$$

where $M_{t,ads}$ = mass adsorbed when $t_i = t_{ads}$ (Eq 2.2), t_{ads} = duration of adsorption cycle, M_W = molecular weight of the adsorbate, Q_g = total volumetric flow rate of the gas, R = ideal gas law constant, T = absolute temperature, y_{in} = concentration of the adsorbate in the inlet gas stream (mole fraction).

$$M_{ti} = \left[\frac{P_{tot} M_w Q_g}{RT}\right] \int_{t=0}^{t=t_i} \left(\frac{y_{in}}{1-y_{in}} - \frac{y_{out}}{1-y_{out}}\right) dt \qquad \text{Eq 2.2}$$

where P_{tot} = 1 atm, y_{out} = concentration of the adsorbate in the outlet gas stream (mole fraction).

The minimum acceptable capture efficiency is set by emission permits and will vary by process. As an example, the emission requirement for isobutane for the packaging manufacturing industry is 98% destruction of organic gases in thermal oxidizers (*3*).

2.3.2. Materials Balance

2.3.2.1. Water

The amount of H_2O entering and leaving the GRS can be calculated from RH measurements at the inlet and outlet of the adsorption vessels, total gas flows of the system, and the amount of water recovered downstream of the vessels during desorption. The mass flow rate of water entering or leaving the system, $\dot{m}_{water}$, is found from Eq 2.3:

$$\dot{m}_{water} = Q_{tot} c_{water} \qquad \text{Eq 2.3}$$

where c_{water} is the concentration of water vapor in the gas phase (g/L) in the inlet or outlet gas stream:

$$c_{water} = \frac{M_w P_{water}}{RT} \qquad \text{Eq 2.4}$$

where P_{water} is the partial pressure of water in the gas phase (bar):

$$P_{water} = P_{water.sat}(RH) \qquad \text{Eq 2.5}$$

where *RH* is the relative humidity (fraction) and $P_{water,sat}$ is the saturation pressure of water in the gas phase (bar):

$$P_{water,sat} = 10^{\left(A - \frac{B}{T-C}\right)} \quad \text{Eq 2.6}$$

And where *A*, *B*, and *C* are Antoine equation constants and *T* is temperature (K). For these calculations *A* = 5.40221, *B* = 1838.675, and *C* = -31.373 (*79).*

The total mass water, m_{water}, that enters or leaves the adsorption vessels during a cycling experiment can be found from Eq 2.7. Note that this equation is applicable to both the inlet and outlet water vapor.

$$m_{water} = \sum_{i=0}^{i=end} \dot{m}_{water}\left(t_{i+1} - t_i\right) \quad \text{Eq 2.7}$$

2.3.2.2. Nitrogen

The amount of N_2 used during non-recirculation mode experiments was calculated from the set-point flow rates of the mass flow controllers that were used during the desorption cycle and total desorption cycle time (Eq 2.8). The total amount of N_2 used in each cycle was dependent on how long the ACFC took to cool from its set-point temperature to its temperature swing condition of 60°C. The amount of N_2 used was then normalized by the number of moles of isobutane recovered during the experiment.

$$M_{N_2} = Q_{N2,low}t_{low} + Q_{N2,high}t_{high} \quad \text{Eq 2.8}$$

where M_{N2} is the total mass of N_2 used during desorption, $Q_{N2,low}$ and $Q_{N2,high}$ are the low and high flow rate settings for N_2 during desorption, respectively, and t_{low} and t_{high} are the duration of the low and high N_2 flow rates during desorption, respectively.

2.3.3. Energy Usage

There are four major components in the total energy used by the experimental system. These are energy to heat the ACFC and adsorbed adsorbates, energy to compress the gas

stream after desorption, the energy to humidify the adsorption gas stream and dehumidify the desorption gas stream, and the energy to produce N_2 to inert the GRS during desorption. The energy to produce N_2 has been shown to be a significant portion (53.9%) of total energy usage in an industrial setting with the pilot scale VaPRRS unit (*71*). The energy to overcome the pressure drop in the system and the energy to cool the desorbed gas are not considered in this analysis because they were calculated to be less than 5% of the total energy used by the system (see Appendix).

2.3.3.1. Energy to Heat the ACFC

The energy required to heat the ACFC, adsorbate, carrier gas, and fittings during desorption, $E_{heating}$ is calculated using **Eq 2.9** (*42, 70, 77*).

$$E_{heating} = \sum_{i=1}^{t_{desorp}} I_{RMS} V_{RMS} \left(t_i - t_{i-1}\right) \qquad \text{Eq 2.9}$$

where I_{RMS} and V_{RMS} are the RMS current and voltage for the power supply to regenerate the ACFC, respectively, and t_{desorp} is the duration of the regeneration process.

2.3.3.2. Energy to Compress the Gas Stream

The energy required to compress the gas stream is determined directly from the electricity used by the compressor. The current consumed by the compressor was continuously monitored with an RMS AC current transducer (Omega OM9-31382AHD1). The voltage used is assumed to be a constant 120V. An equation analogous to **Eq 2.9** was used to determine the total energy used by the compressor during operation.

For the first through third GRS generations, only the heating and compression energy were analyzed. For the fourth generation GRS heating, compression, N_2 production, and water handling energies were all considered. The N_2 production and water handling energies were not considered in the first through third GRS generations because the systems were operating with dry adsorption air and the N_2 was considered an available utility. With the introduction of water

vapor and the ability to recirculate the adsorption gas that occurred with the fourth generation GRS, the N_2 production and water handling energies were recognized to be important components to consider.

2.3.3.3. Energy to Manage Water Vapor

For the fourth generation GRS, the energy required to manage water vapor, E_{water}, does need to be considered. E_{water} incorporates two terms: the energy required to humidify the adsorption gas (first term on the right hand side of **Eq 2.10**) and the energy to remove the water vapor from the desorbed gas stream by cooling and condensing the water vapor (second term on the right hand side of **Eq 2.10**).

$$E_{water} = m_{water,ads}\Delta h_{vap,25°C} + m_{water,des}\left(c_{p,water,vap}\Delta T_{(150-100°C)} + \Delta h_{vap,100°C} + c_{p,water,liq}\Delta T_{(100-20°C)}\right) \quad \text{Eq 2.10}$$

where $m_{water,ads}$ is the mass of water required to humidify the adsorption gas (Eq 2.7) and $m_{water,des}$ is the mass of water collected, c_p is the heat capacity, and $\Delta h_{vap,T}$ is the enthalpy of vaporization at T (Table 2.1).

Table 2.1 Thermal properties of water.

Quantity	Value (*14*)
$\Delta h_{vap,\ 25C}$	2440 kJ/g
$\Delta h_{vap,\ 100C}$	2260 kJ/g
$c_{p,water,vap}$	1.86 J/g-K
$c_{p,water,liq}$	4.187 J/g-K

2.3.3.4. Energy to Produce N_2

The energy to produce N_2, $E_{N2,Prod}$ is determined based on industry reports of the cost required to produce N_2 at an industrial scale (*80*). The energy and operation cost to produce N_2 at 99.5% purity ranges from \$0.03 to \$0.05 /sm^3 N_2 (standard m^3). A worst case scenario would

assume that this entire cost is energy cost and that the cost to produce energy is the lowest industrial cost in the U.S. ($0.0653/kWh in July 2014)(*81*). Using these pieces of information, the energy to produce N_2 at 99.5% purity at an industrial scale is 0.766 kWh/sm^3 N_2, or 2.7 kJ/sL N_2.

To determine the contribution of the energy to supply N_2 to the GRS, E_{N_2}, to the total energy used by the system, the normalized N_2 amount, M_{N2}/n_{iso} was multiplied by $E_{N2,Prod}$. For recycle experiments, the energy to produce N_2 was determined as described here and that value was then multiplied by the ratio of the average oxygen concentration downstream of the adsorption vessels to the atmospheric oxygen concentration (21%) to account for the reduction in N_2 required as a result of recirculation (**Eq 2.11**).

$$E_{N_2} = \frac{y_{O_2,GRS}}{y_{O_2,atm}} \left(\frac{M_{N2}}{n_{iso}} E_{N_2Prod} \right) \qquad \text{Eq 2.11}$$

where $y_{O2,GRS}$ is the average concentration of O_2 in the GRS during the cycling experiment, $y_{O2,atm}$ is the concentration of oxygen in the atmosphere (assumed to be 21%) and n_{iso} is the number of moles of isobutane recovered during the experiment.

2.3.3.5. 4th Generation GRS Total Energy

For the 4th generation GRS, the total energy used by the system (E_{sys}) is the sum of the electrothermal, compression, and N_2 production energy (**Eq 2.12**) for experiments with low relative humidity adsorption streams and includes the energy to cool and liquefy water for high relative humidity adsorption streams. The energy per liquid mol recovered (E_{tot}) was determined by normalizing the total energy used by that experiment to the total moles of liquid recovered during that experiment.

$$E_{sys} = E_{heating} + E_{compress} + E_{N_2} + E_{water} \qquad \text{Eq 2.12}$$

2.3.4. Effective Adsorption Capacity

To determine the effective adsorption capacity of the ACFC ($q_{effective}$), the total mass of adsorbate captured during operation (Eq 2.2) is divided by the number of adsorption cycles and the mass of the ACFC at steady-state operating conditions to determine the actual adsorption capacity (*82*). The maximum theoretical adsorption capacity of the ACFC ($q_{equilibrium}$) is determined with adsorption isotherms (*83*).

2.3.5. Mass Distribution of Adsorbate in the GRS

The mass distribution of adsorbate in the GRS was determined at the conclusion of each cycling experiment (i.e., adsorption, regeneration and cooling occurring multiple times over several hours). Three possible locations of the adsorbate were considered: liquid phase (M_{liq}), vapor phase (M_{vap}) in equilibrium with the liquid phase within the pressure vessel, and mass adsorbed to the ACFC ($M_{t,ads}$). The amount in the liquid phase was determined by measuring the volume of liquid recovered and multiplying it by the bulk liquid density (Table 1.3) of the adsorbate. The amount in the vapor phase was determined by considering the volume available for the vapor phase above the liquid phase in the pressure vessel and assuming that the adsorbate concentration in the volume was equivalent to the saturation partial pressure divided by the total pressure in the pressure vessel. The amount in the adsorbed phase was determined by difference (Eq 2.13) (*42*). The adsorbed phase includes adsorbate that is liquefied in the pores of the ACFC.

$$M_{t,ads} = M_{tot} - M_{liq} - M_{vap} \qquad \text{Eq 2.13}$$

where M_{tot} = total mass supplied to the system during the experiment.

2.4. Adsorption Characterization from Breakthrough Curves

2.4.1. Determination of ACFC Adsorption Capacity for Isobutane

The adsorption capacity of ACFC was determined with individual breakthrough curves and during automated adsorption/desorption cycling, without the recycle from the temperature

and pressure control module. For individual breakthrough curves, the ACFC was initially heated to 200°C in N_2 at ambient pressure for 10 min to desorb previously-adsorbed compounds. After cooling the ACFC, a feed gas was generated at 100 SLPM or 50 SLPM with an isobutane concentration of 2,000 ppm_v. The inlet gas concentration was stable before passing the gas through the vessels containing the ACFC. The isobutane concentration at the outlet of the vessel was monitored until it returned to 2,000 ppm_v to determine the ACFC's adsorption capacity.

The mass of isobutane adsorbed at any time, t_i, during adsorption is M_{ti} (Eq 2.2). Breakthrough is defined to occur when the isobutane concentration at the vessel's outlet reached 10% of the inlet concentration, corresponding to t_{10} and M_{t10}. The adsorption capacity of the ACFC is then determined by dividing M_{10} by the total ACFC mass (*82*).

2.4.2. Adsorption Properties from Breakthrough Curves

Breakthrough curves were also used to evaluate the throughput ratio (*TPR*), length of unused bed (*LUB*), and fractional *LUB* (*fLUB*). *TPR* characterizes the slope of the breakthrough curve (**Eq 2.14**). As TPR approaches unity, the time to develop the mass transfer zone becomes negligible compared to the adsorbent's saturation time. *LUB* is a measure of the unused length of bed at 5% breakthrough (**Eq 2.15**) and *fLUB* is the fractional unused length of bed at 5% breakthrough normalized to the total length of the bed (i.e., *LUB*/*L*) where *L* is length of adsorbent perpendicular to the adsorbate flow (*27*). For the characterizations performed here, the adsorbent depth (i.e., thickness of the annular cartridge) parallel to the gas flow is 1.5 cm.

$$TPR = \frac{t_5}{t_{50}} \qquad \text{Eq 2.14}$$

where t_5 = the time at which the breakthrough curve has reached 5% breakthrough and t_{50} = the time at which the breakthrough curve has reached 50% breakthrough.

$$LUB = 1 - \frac{M_{t_5}}{M_{t_{sat}}} \qquad \text{Eq 2.15}$$

where M_{t5} = mass of adsorbate adsorbed at time t_5, $M_{t,sat}$ = mass of adsorbate adsorbed at time t_{sat}, t_{sat} = time at which the breakthrough curve has reached 100% breakthrough.

As the value of fLUB approaches 0, the amount of ACFC that is being utilized during adsorption approaches 100%, which means that the ACFC is being used to its full potential. Achieving fLUB and TPR values less than 0.3 and greater than 0.7, respectively, are guidelines used to evaluate if the vessels were designed appropriately for the inlet gas stream (*73*).

2.5. Determination of Desorption and Post-Desorption Operating Conditions

2.5.1. Effect of Regeneration Temperature on Energy Efficiency

As previously mentioned, experiments were performed at several ACFC regeneration temperatures, with all other variables held constant (Table 2.2), to assess the effects of ACFC temperature on the performance metrics of interest. These experiments were conducted using the second generation GRS and in triplicate. The energy used by the GRS to capture and recover isobutane was determined based on the total isobutane captured rather than the amount of isobutane liquefied.

Table 2.2. Operating parameters for the bench-scale system.

System Component	Parameter	Value
Adsorption cycle	Air flow rate (SLPM)	40
	Isobutane relative pressure	6.7×10^{-4}
	Breakthrough condition (% of inlet concentration by volume) (condition at which the adsorption vessel is switched to the desorbing vessel)	5
Desorption cycle	N_2 low flow rate (SLPM)	0.5
	N_2 high flow rate (SLPM)	3.5
	Variac setting (%)	50
	ACFC temperature (^oC)	150, 175, 200
	Low N_2 flow heat time (min)	5
	High N_2 flow heat time (min)	2
	High N_2 flow without heat time (min)	1

Table 2.2 (cont.).

	ACFC temperature swing condition (^{o}C)	60
Compression/Cooling	Maximum pressure (psig / bar-gauge)	150 / 10.3
	Pressure vessel temperature (^{o}C)	< 0

2.5.2. Effect of Heating/Compression Time on Energy Requirements and Mass Distribution

Tests using varying heating and compression times were conducted using isobutane to determine what heating and compression times to use for all three adsorbates to be able to compare system performance across their relative pressures. All of the experiments used 40 SLPM air and 2,000 ppm_v isobutane ($P_i/P_{i,s} = 6.7x10^{-4}$) as the adsorbing gas and the total heating and compression time (Step 3 from section 2.2.3, above) varied from 2 – 7 min, with a total heating time (steps 2-4) of 3.5 – 8.5 min. The adsorption and desorption cycling was allowed to continue for 5-8 hours so that operational steady-state equilibrium conditions were reached. Each experiment was run in triplicate.

The effect of heating and compression time on the process performance was examined because a need to balance the amount of heating and compression that is used to recover the adsorbate and the amount of adsorbate recovered is expected. For example, supplying too little heat to the ACFC during regeneration could result in much of the adsorbate being left in the adsorbed phase leading to a reduction in the amount of adsorbate available for liquefaction. This is contrasted by operating the heating/compression module (step 3, above) for too long, which has diminishing returns, as there is less and less adsorbed compound to desorb and compress.

2.6. Gas Recovery System Performance: Controlled Adsorbate Relative Pressure

Once the duration of step 3 during the desorption process that resulted in the lowest energy per mole liquid recovered for isobutane ($P_i/P_{i,s} = 6.7x10^{-4}$) was determined, the GRS was tested with varying relative pressures of isobutane, n-butane, and R134A ranging from $8.3x10^{-5}$

to $3.4x10^{-3}$ (see Table 2.3). The duration of step 3 for all of these experiments was 4 min (total heating time in steps 2-4 was 5.5 min), which is justified in the results section 3.3. At a minimum, each experiment was conducted in duplicate and lasted for 5 hours to provide greater than 5 complete adsorption, regeneration, and cooling cycles to achieve steady-state conditions. The system was considered to be at steady state after the first two adsorption cycles were complete. The first two adsorption cycles were generally 10-50% longer than the average of the remaining adsorption cycles due to less adsorbate being recycled to the adsorbing vessel during regeneration and compression. The length of later adsorption cycles generally had a standard deviation of less than 5%. The data analysis was only conducted on adsorption/desorption cycles considered to be at steady state.

Table 2.3 Adsorbate relative pressures and carrier gas flow rates tested using the GRS.

Adsorbate	Relative Pressure in Adsorption Stream	Carrier Gas Flow Rate (SLPM)
R134A	$8.3x10^{-5}$	10
Isobutane	$6.7x10^{-4}$	40
Isobutane	$1.6x10^{-3}$	20
Isobutane	$3.4x10^{-3}$	10
n-butane	$6.7x10^{-4}$	50
n-butane	$3.4x10^{-3}$	15

2.7. Gas Recovery System Performance for Multicomponent Adsorption and Carrier Gas Recycling

The gas recovery system (3rd generation) was modified as described in section 2.2.4 to examine the effects of introducing water vapor into the adsorption gas stream and recycling the carrier gas during system operation. Experiments with isobutane (relative pressure $6.7x10^{-4}$) and 70-80% RH were conducted in the same manner described in section 2.6 prior to introducing the recycle of the carrier gas stream. Subsequently, the GRS was tested with

isobutane (relative pressure 6.7×10^{-4}) and 30% RH or 75% RH and carrier gas recycle. High and low RHs were chosen because they fall on the relatively flat portion of the type V isotherm for water on ACFC (Figure 1.5). The middle range of RHs was not tested because small perturbations in inlet relative humidity have a large effect on the adsorption capacity of ACFC for water vapor, which would make it difficult to control the system operation.

2.8. Modeling to Describe Isobutane Concentration During Desorption – MATLAB®

To better understand the best operating parameters for the post-desorption treatment system, the desorption cycle was modeled using energy and mass balances. Of particular interest was the adsorbate concentration generated during desorption, which directly affects the performance of the condensation apparatus. The higher this concentration, the easier it is to condense the desorbed adsorbate (see section 1.7).

2.8.1. Mass balance equation to determine amount of adsorbed adsorbate during desorption

To determine the concentration of adsorbate exiting the adsorption/desorption vessel during regeneration, a mass balance is required. There are three possible locations for adsorbate in the GRS during regeneration prior to entering the condensation system: in the ACFC, in the adsorption vessel, or in the gas flowing out of the adsorption vessel. **Eq 2.16** describes this time dependent process mathematically with the first term representing the total adsorbate adsorbed during an adsorption cycle and the terms to the right of the equal sign representing the three locations, respectively. In the equations that follow, certain parameters are well known either because they are directly measured or represent material properties. m_s, q_0, $M_{w,i}$, V, P_{tot}, R, T, and t are all well-known parameters. q, y_i, and Q_{tot} all result from the modeling calculations described below.

$$m_s q_0 = m_s q + M_{w,i} y_i \frac{VP_{tot}}{RT} + M_{w,i} y_i \frac{Q_{tot} P_{tot}}{RT} t \qquad \text{Eq 2.16}$$

The main variable of interest is the concentration of adsorbate exiting the adsorption vessel as a function of time, which will allow the GRS operation algorithm to be set to collect the most highly concentrated gas stream possible. In order to determine the concentration of adsorbate exiting the adsorption vessel, the mass of adsorbate leaving the adsorbed phase as a function of time must be determined. To find *q(t)*, the following equations were derived: the derivative with respect to t of **Eq 2.16**, was taken and the product rule for derivatives was implemented:

$$0 = m_s \frac{dq}{dt} + \frac{M_{w,i} P_{tot} V}{RT} \frac{dy_i}{dt} + \frac{M_{w,i} P_{tot}}{RT} \left(\frac{dy_i}{dt} Q_{tot} t + \frac{dQ_{tot}}{dt} y_i t + Q_{tot} y_i \right) \qquad \text{Eq 2.17}$$

Note that $Q_{tot} = \frac{Q_{N_2}}{1-y}$ for a binary system assuming N_2 and the adsorbate are the only two components. The chain rule was applied to obtain expressions in which the only required derivatives with respect to time were T_{ACFC} and q. dT_{ACFC}/dt can be determined from the GRS experimental results or modeled data and dq/dt is the variable of interest. Time derivatives in **Eq 2.18** and subsequent equations are represented with a dot over the variable of interest.

$$0 = m_s \dot{q} + \frac{PVM_{w,i}}{RT_{ACFC}} \left(\frac{dy}{dT_{ACFC}} \dot{T}_{ACFC} + \frac{dy}{dq} \dot{q} \right) +$$
$$\frac{m_s P Q_{N_2}}{RT_{ACFC}} \left[\left(\frac{dy}{dT_{ACFC}} \dot{T}_{ACFC} + \frac{dy}{dq} \dot{q} \right) \frac{t}{1-y} + \left(\frac{d\left(\frac{1}{1-y}\right)}{dT_{ACFC}} \dot{T}_{ACFC} + \frac{d\left(\frac{1}{1-y}\right)}{dq} \dot{q} \right) yt + \left(\frac{y}{1-y} \right) \right] \qquad \text{Eq 2.18}$$

Isolating the $\dot{q}$ terms and solving for $\dot{q}$:

$$\dot{q} = \frac{\left(-\frac{M_{w,i}PV}{RT_{ACFC}}\frac{dy}{dT_{ACFC}}\dot{T}_{ACFC} - \frac{M_{w,i}PQ_{N_2}}{RT_{ACFC}}\left[\left(\frac{1}{1-y}\right)t\frac{dy}{dT_{ACFC}}\dot{T}_{ACFC} + yt\frac{d\left(\frac{1}{1-y}\right)}{dT_{ACFC}}\dot{T}_{ACFC} + \frac{y}{1-y} \right] \right)}{\left(m_s + \frac{M_{w,i}PV}{RT_{ACFC}}\frac{dy}{dq} + \frac{M_{w,i}PQ_{N_2}}{RT_{ACFC}}\left[\left(\left(\frac{1}{1-y}\right)t\frac{dy}{dq} + yt\frac{d\left(\frac{1}{1-y}\right)}{dq} \right) \right] \right)} \quad \text{Eq 2.19}$$

As noted above, (the derivative of temperature with respect to time) can be determined from experimental data generated with the GRS. All other derivatives in the above equation can be determined using the Antoine (**Eq 1.7**) and DR Equations (**Eq 1.4**) (See Appendix).

2.8.2. Isobutane Concentration During Desorption from Experimental Temperature Data

To model the change in adsorbed-phase adsorbate with time, the temperature-time data from GRS experiments was imported into MATLAB (version 2013a). The temperature-time data was modeled with a cubic polynomial fit and then the ode45 function was used to estimate q as a function of time based on **Eq 2.19**. Ode45 is a built-in MATLAB function that uses a 4th and 5th order Runge-Kutta algorithm to solve ordinary differential equations (*84*). Once the amount of adsorbate still adsorbed as a function of time was determined, mass balances (**Eq 2.20**-**Eq 2.22**) were employed to determine the concentration of adsorbate exiting the adsorption vessel as a function of time, $y_i(t)$ (See Appendix).

$$y_i(t) = \frac{\text{mass of isobutane desorbed in time step}}{\text{total mass of gas in vessel in time step}} \quad \text{Eq 2.20}$$

where the subscript i represents the time step of interest.

$$y_i(t) = \frac{m_{ti} - \bar{m}_{t_i-1}}{m_{vessel,total}} \quad \text{Eq 2.21}$$

where $\bar{m}_{t_i-1}$ is the average mass of adsorbate that has desorbed from t_0 to t_{i-1}, and $m_{vessel,total}$ is the total mass of gas in the adsorption vessel, and m_{ti} is found from **Eq 2.22**:

$$m_{ti} = m_s q_{t=0} - m_s q_{ti} \qquad \text{Eq 2.22}$$

2.8.3. Isobutane Concentration During Desorption from Modeled Temperature Profiles

To explore the effects of different experimental scenarios (i.e., ACFC temperature during desorption and ACFC temperature ramp speed), temperature profiles were constructed with a linear ramp ranging from 50 to 300 s to the set point temperature. These temperature profiles were used as described above (section 2.8.2) to determine the outlet isobutane concentration during desorption as a function of time.

3. RESULTS AND DISCUSSION

3.1. Adsorption Isotherms Measurements and Modeling

Adsorption isotherms for isobutane, R134A, and dichloromethane were measured on a Cahn 2000 microbalance and the results were modeled with five isotherm models: Freundlich, Toth, Yaws, DR, and DQSAR. Figure 3.1 shows the results for isobutane on ACFC-15 on a linear plot and Figure 3.2 shows the same data on a semi-log scale to better illustrate the goodness of fit of the five models.

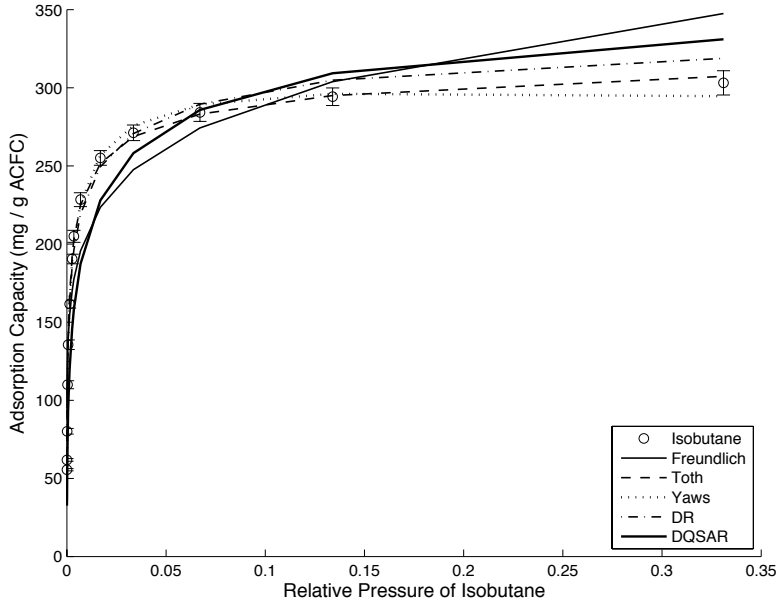

Figure 3.1 Room temperature adsorption isotherm of isobutane on ACFC-15 with the best fit of five isotherm models. Error bars represent +/- one standard deviation about the mean.

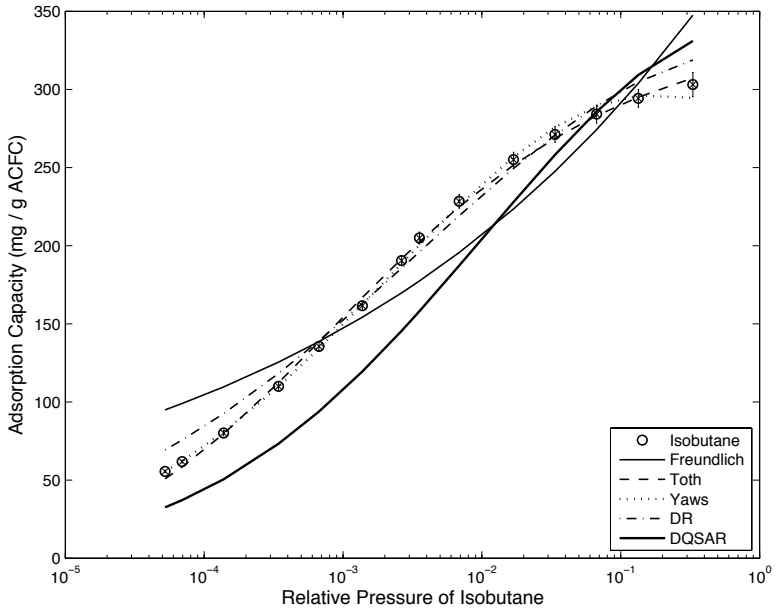

Figure 3.2 Room temperature adsorption isotherm of isobutane on ACFC-15 with the best fit of five isotherm models. Error bars represent +/- one standard deviation about the mean.

When compared to the adsorption isotherm for n-butane shown in Figure 1.4, it is clear that although n-butane has a higher boiling point than isobutane, at low relative pressures, ACFC-15 has a higher adsorption capacity for isobutane than n-butane. For example, at a relative pressure of 10^{-4}, the adsorption capacity of ACFC-15 for isobutane is 70 mg/g and for n-butane is 57 mg/g.

Figure 3.3 and Figure 3.4 show the results of the isotherm measurement and model fitting for R134A and DCM, respectively.

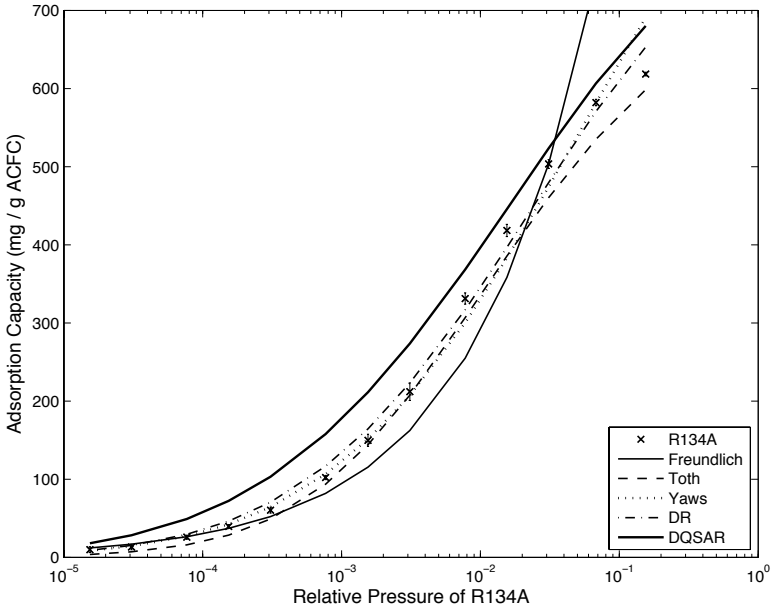

Figure 3.3 Room temperature adsorption isotherm of R134A on ACFC-15 with the best fit of five isotherm models. Error bars represent +/- one standard deviation about the mean.

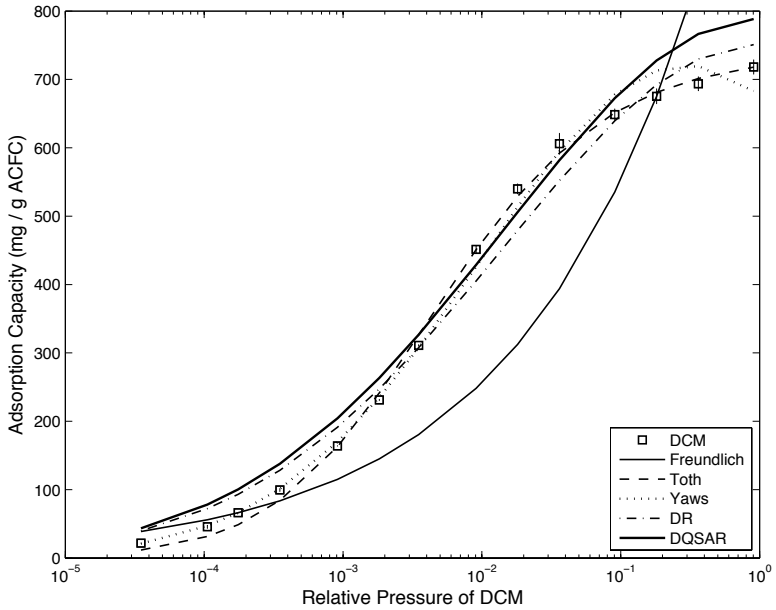

Figure 3.4 Room temperature adsorption isotherm of DCM on ACFC-15 with the best fit of five isotherm models. Error bars represent +/- one standard deviation about the mean.

The fitting parameters for each of the five isotherm models and the three adsorbate/adsorbent pairs are shown in Table 3.1. These fitting parameters can be input into the models to predict the adsorption capacity of ACFC-15 for each adsorbate. Both the Freundlich and Toth model results suggest that the isobutane-ACFC pair favors adsorption more strongly than desorption due to the high n and b values. As noted in section 1.3.4.1, n values approaching 10 indicate that a significant reduction in partial pressure is required to desorb the adsorbed compound. In the Toth equation, b represents the Langmuir affinity constant with higher values indicating a preference for adsorption.

Table 3.1 Fitting parameters for five isotherm models.

	Freundlich		**Toth**		
	k_f	n	q_s	b	t
	mg/g*kPa	[-]	mg/g	kPa^{-1}	[-]
Isobutane	176	6.75	341	57.8	0.37
R134A	115	2.03	756	0.56	0.51
DCM	311	2.99	740	9.00	0.64

	Yaws			**DR**		**DQSAR**
	A	B	C	$q_0=\rho_l W_0$	E	k
	[-]	[-]	[-]	mg/g	J/mol	$(J/mol)^2$
Isobutane	-0.43	0.66	-0.058	325	1.96E+04	3.97E-09
R134A	-1.91	1.07	-0.074	740	1.30E+04	5.00E-09
DCM	-0.85	1.04	-0.100	789	1.36E+04	4.53E-09

The goodness of fit of the models to the isotherm data is dependent on the adsorbate/adsorbent pair (Table 3.2). In general, the Toth, Yaws, and DR equations fit the data best. Similar to the findings of Ramirez, *et al.* the DQSAR equation does not provide a good prediction (Absolute Relative Difference, ARD > 20%) of the measured isotherm data for these compounds, which were all being tested above their boiling points (*50*). Additionally, the high

average ARD for the DQSAR prediction of the R134A isotherm might be attributable to the method by which the k parameter was calculated for R134A: k is calculated based on the first order molecular connectivity index, which requires the assignment of values to each of the atoms in the molecule of interest. In the literature, there is no value given for fluorine, so the value for chlorine was used as a surrogate. Of these isotherms, the DR equation is the most useful because it can be readily used to provide an estimate of the isosteric heat of adsorption if adsorption isotherms are measured at several temperatures.

Table 3.2 Average absolute relative difference (ARD) of the five isotherm models for isobutane, R134A, and DCM adsorption on ACFC-15.

	Average ARD (%)		
Isotherm Equation	**Isobutane**	**R134A**	**DCM**
Freundlich	19.25	21.62	29.96
Toth	2.15	18.66	9.08
Yaws	1.07	5.61	3.03
DR	6.97	9.54	19.98
DQSAR	20.1	50.42	23.4

3.1.1. Adsorbent pore volume

Table 3.3 shows the available pore volume for ACFC-15 based on isotherm measurements modeled using the DR equation. The average pore volume and standard deviation for ACFC-15 determined from this analysis (not including the N_2 data point) is 0.60 $cm^3/g \pm 0.037$ cm^3/g. This analysis assumes that the adsorbates are condensing in the pores of the adsorbent despite isobutane and R134A having boiling points more than 35°C below the test conditions of 24°C and 1 atm. This assumption is assumed to be justified based on the precision of the results and their agreement with the N_2 adsorption-determined pore volume of ACFC-15 (Table 1.2). This determination is also aligned with the findings of Yun, *et al.* who noted that the

volume of the micropores for a pellet activated carbon determined from the DR fitting of the isotherm data for several chlorinated organic solvents (1,1,1 trichloroethane T_b = 74°C and trichloroethylene T_b = 87°C) was analogous to the BET micropore volume of the adsorbate determined from N_2 adsorption (*85*). The ability to use adsorbates other than N_2 to determine the pore volume of adsorbents could be beneficial in the case where a surface analyzer that relies on N_2 adsorption at low pressures (10^{-3} atm) is not readily available.

Table 3.3 Available pore volume of ACFC-15 based on isotherm data from several adsorbates at 24°C and bulk density of the adsorbates.

Adsorbate	**Available Pore Volume (cm^3/g ACFC)**
N_2 (77 K)	0.66 (from *25*)
R134A	0.61
Isobutane	0.63
Dichloromethane	0.56

3.1.2. Isosteric Heat of Adsorption

The isotherms for isobutane and R134A on ACFC-15 were measured at four temperatures (Figure 3.5 and Figure 3.6, respectively) to determine ΔH_s. As expected, each of these isotherms follows Type I behavior and the adsorption capacity at a given relative pressure decreases with increasing temperature because adsorption is an exothermic process. The isosteric heat of adsorption varies with loading, which is consistent with other analyses (*66*). The isosteric heat of adsorption for isobutane ranges from 58 to 85 kJ/mol (Figure 3.7). The isosteric heat of adsorption for R134A ranges from 45 to 54 kJ/mol (Figure 3.8).

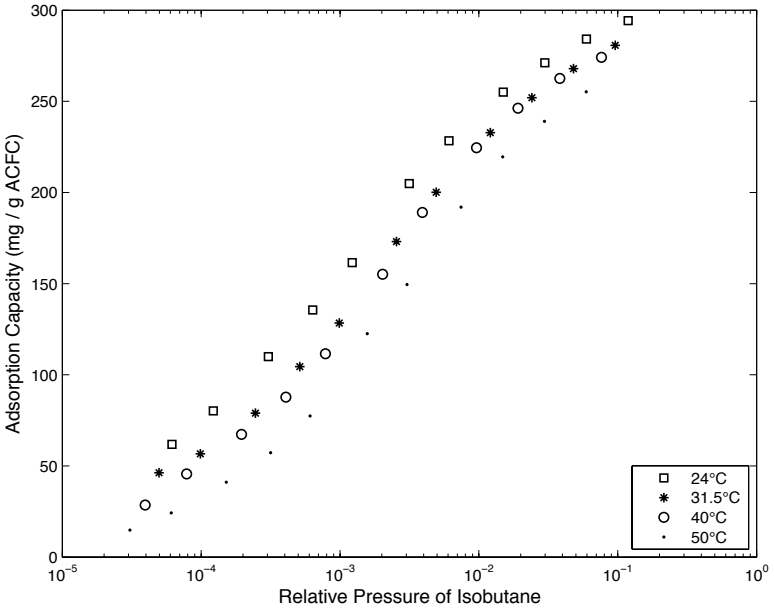

Figure 3.5 Adsorption capacity of ACFC-15 for isobutane for various temperatures.

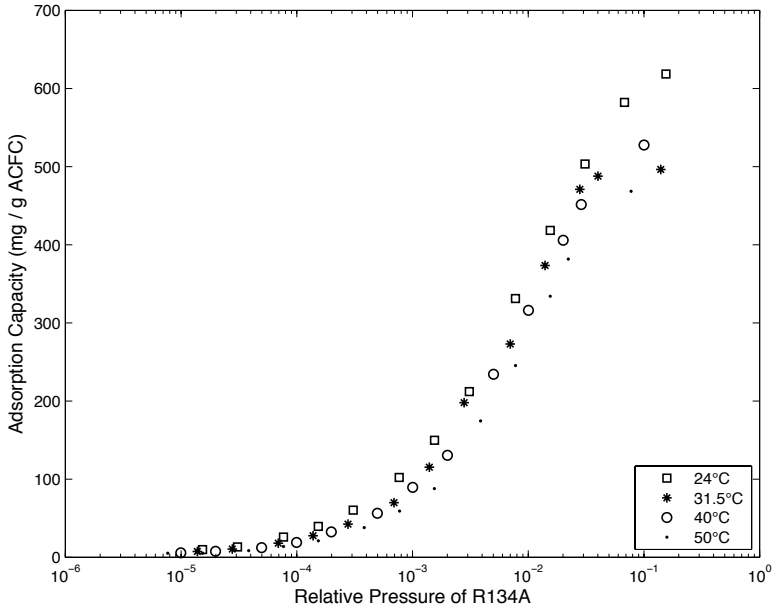

Figure 3.6 Adsorption capacity of ACFC-15 for R134A for various temperatures.

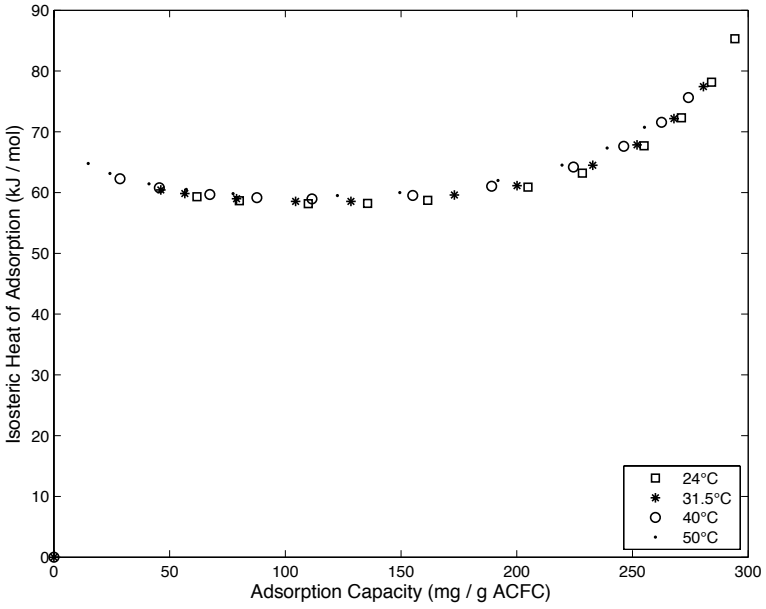

Figure 3.7 Isosteric heat of adsorption for isobutane on ACFC-15.

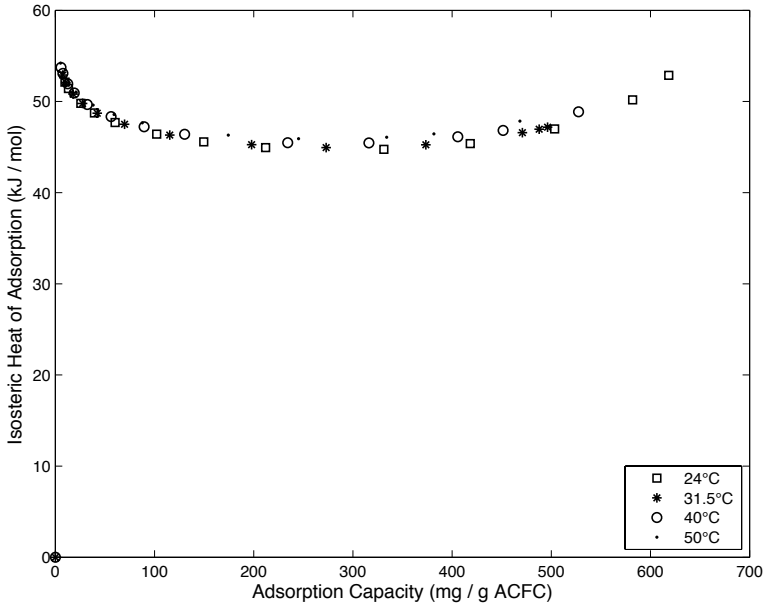

Figure 3.8 Isoteric heat of adsorption for R134A on ACFC-15.

The isosteric heats of adsorption determined for isobutane and R134A on ACFC-15 are similar to those provided by Ramirez, *et al.* for acetone and benzene on ACFC-20, which were determined to be 40-60 kJ/mol and 60-70 kJ/mol, respectively (*66*). The isosteric heat of adsorption can be used in models that describe the amount of adsorbate released and the minimum amount of energy required during desorption.

3.2. Adsorption Characterization from Breakthrough Curves

3.2.1. Adsorption Properties from Breakthrough Curves

Breakthrough curves (e.g., Figure 3.9) were generated for each vessel for an inlet carrier gas containing 2,000 ppm_v isobutane ($P_i/P_{i,s} = 6.7x10^{-4}$). The air and isobutane stream passed through the ACFC-15 at ambient temperature (22 to 24°C) and 1 atm. The average adsorption capacity calculated from six breakthrough curves was 94 mg isobutane / g ACFC with a standard deviation of 17 mg isobutane/g ACFC (*73*).

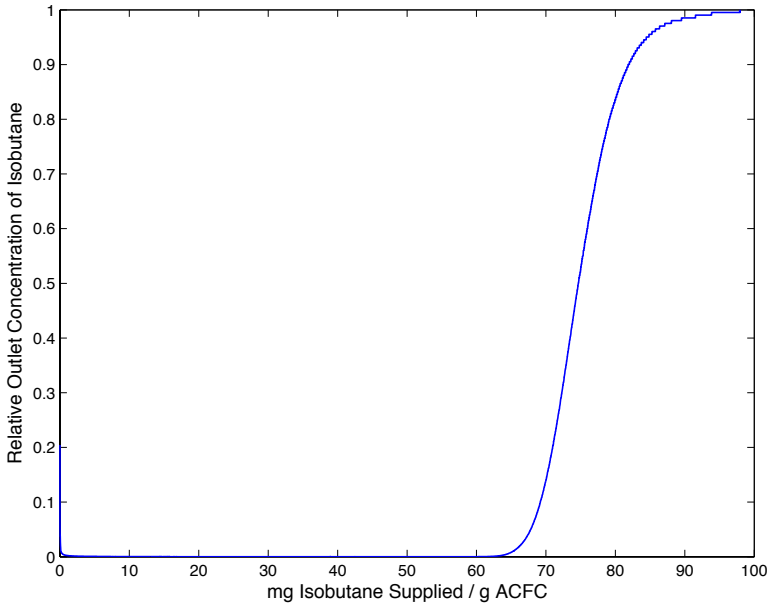

Figure 3.9. Typical breakthrough curve for isobutane on ACFC-15. The inlet gas was 100 SLPM air with 2,000 ppm_v isobutane in air, 22°C, and ambient pressure. The mass of ACFC was 183.3 g per vessel (*73*).

Comparing these results to the adsorption isotherms generated using the microbalance (Figure 3.1), it is clear that the GRS does not achieve the equilibrium adsorption capacity of ACFC for 2,000 ppm_v isobutane, which is 135 mg isobutane/g ACFC. This is likely due to several factors including the geometry of the ACFC cartridge not allowing 100% contact with the adsorbate gas stream and the GRS not reaching equilibrium during the breakthrough curve experiments. The other parameters of interest, average and standard deviation of TPR and fLUB values were 0.86 ± 0.03 and 0.29 ± 0.03, respectively, for the first generation GRS. These results are in the acceptable range of TPR values (> 0.7) and fLUB values (< 0.3) (*82*) indicating that the geometry of the system and adsorption gas flow rates were reasonable.

3.3. Determination of Desorption and Post-Desorption Operating Conditions

The success of the GRS depends on the energy efficiency of the process, which is in large part due to the effectiveness of the adsorbent regeneration and the adsorbate liquefaction. In trying to optimize the energy efficiency, tests were conducted to determine the most effective regeneration temperature and the best heating/compression time to minimize energy use while maximizing adsorbate liquefaction.

3.3.1. Effect of Regeneration Temperature on Energy Efficiency

Figure 3.10 shows an example of the operational results from one of the experiments described in section 2.5.1. This figure describes the concentration of isobutane exiting each of the vessels, the capture efficiency of isobutane as a function of time, and the ACFC temperatures obtained during operation at the conditions listed in Table 2.2. These experiments were performed for more than five hours to achieve steady-state operation. Additionally, the first adsorption cycle of each experiment is not included because it is not representative of steady-state conditions.

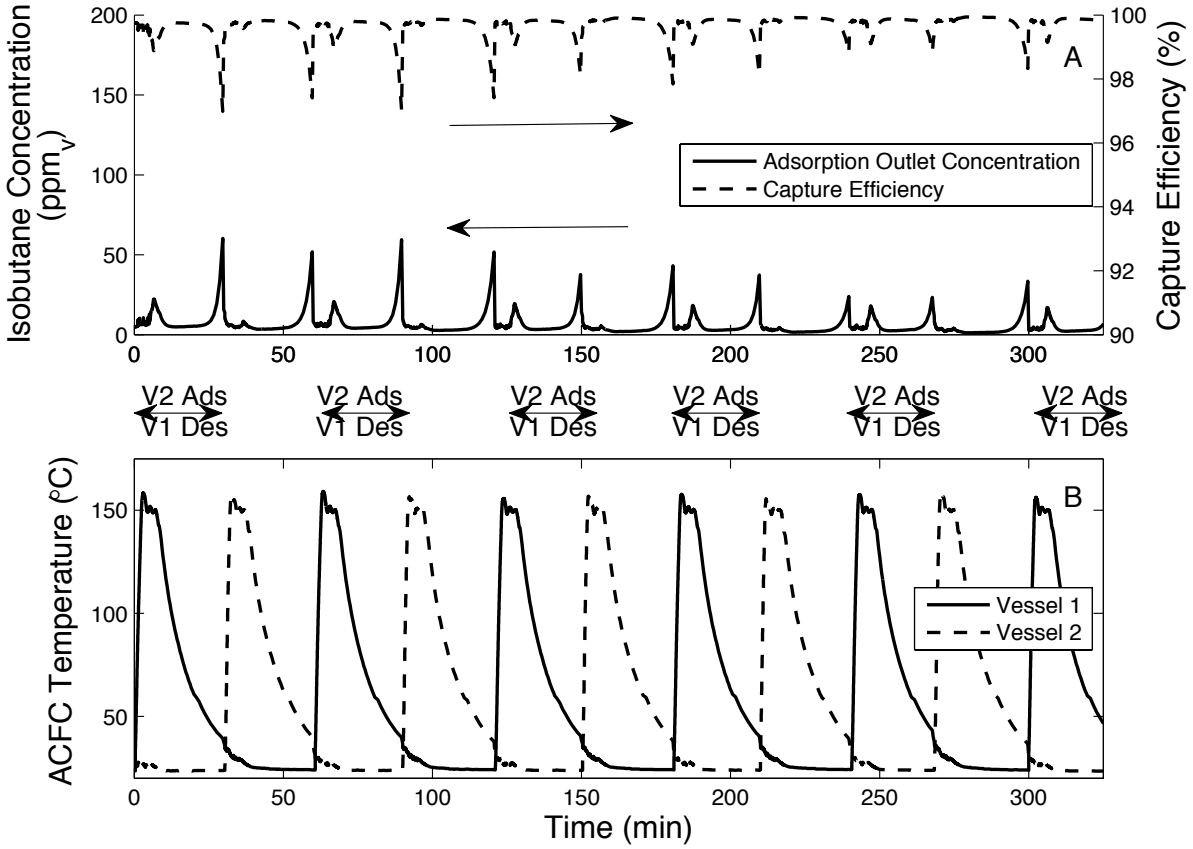

Figure 3.10 A: Outlet isobutane concentration (PID) during adsorption with capture efficiency **B**: ACFC temperature during desorption (Des) for a temperature set point of 150° C. Experimental conditions: 40 SLPM air; 2,000 ppm_v isobutane (*73*). Note that the y-axes for the top plot do not cover the entire range of possible values. The isobutane concentration could range from 0 to 2000 ppm_v and the capture efficiency could range from 0 to 100%.

Material balances based on the operating conditions from Table 2.2 with active cooling of the two vessels are included in Table 3.4. At each regeneration temperature tested, the system had an overall capture efficiency ≥ 99.4%. This capture efficiency is adequate for meeting air quality emission requirements for the packaging manufacturing industry, an example of which requires 98% destruction of organic gases in thermal oxidizers (*3*). Additionally, Table 3.4 shows that the average ACFC capacity for isobutane was 50 – 56 mg/g, which is 50-60% of the adsorption capacity determined with breakthrough curves shown in section 3.2.1. This

reduction in operating adsorption capacity is due to recycling isobutane that is emitted from the post-desorption control module during desorption cycles and incomplete regeneration of the ACFC during each cycle, leaving a "heel".

Table 3.4 Average material balance data for experiments described in Table 1 and exemplified in **Figure 3.10**. Results are from duplicate experiments at 150 and 175°C and triplicate experiments at 200°C.

ACFC Temp (°C)	Overall Capture Efficiency (%)	ACFC Adsorption Capacity (mg isobutane/g ACFC)
150	99.7	50.
175	99.6	54
200	99.4	56

Heating and compression energy consumption for GRS experiments conducted with various ACFC desorption temperatures is included in Table 3.5. Energy consumption values for VaPRRS is provided in Table 3.6 for comparative purposes. The heating energy for an ACFC temperature of 200°C reported in Table 3.5 is similar to values reported by Johnsen for select heating control schemes, which showed that the heating energy to desorb isobutane at 200°C ranged from 908-1237 kJ/mol (*10*).

Table 3.5 Average energy consumption per mol of isobutane captured for the experiments described in Table 2.2. (Duplicate experiments at 150 and 175°C and triplicate experiments at 200°C were conducted).

ACFC Temp (°C)	$E_{heating}$ (kJ/mol)	$E_{compressor}$ (kJ/mol)	E_{tot} (kJ/mol)
150	840	800	1640
175	990	730	1720
200	1,100	720	1820

Table 3.6 Energy requirements for capture and recovery of several organic compounds using VaPRRS (*42*).

Compound	Boiling Point (°C)	Relative Pressure (P/P_{sat})	Energy/mole recovered (kJ/mol)
Methyl propyl ketone	101	7.4×10^{-3}	375
Methyl ethyl ketone	79.6	2.2×10^{-3}	544
Hexane	69	1.5×10^{-3}	629
Acetone	56.5	2.1×10^{-3}	1,367
Dichloromethane	39.8	2.1×10^{-3}	4,698

The heating and compression energy consumption per mol of recovered isobutane (T_b = -11.7°C) is 1.2 to 4.8 times the energy consumption to recover organic vapors with boiling points greater than 55°C using the VaPRRS. Acetone with T_b = 56.5°C was considered the practical limit for efficient recovery using the VaPRRS, and the energy requirements for recovering dichloromethane (T_b = 39.8°C) warranted the proposal of system retrofits to improve the energy efficiency (*42*). The energy required to recover isobutane with the GRS is less than half that required by VaPPRS to recover dichloromethane, which suggests that the addition of the compression/cooling module in the GRS helps to overcome the issue of energy efficiency for recovery of low boiling point compounds experienced by VaPPRS. The increased energy consumption for isobutane compared to higher boiling point compounds (e.g., methyl ethyl ketone), as described above, is expected because of the compression/cooling module used by the GRS that is not part of the VaPRRS. The compression module is 40-50% of the total energy consumption. However, the values presented here represent the energy required to recover isobutane as a concentrated gas, not the energy required to liquefy the isobutane. In order for the GRS to remain competitive with the energy efficiency of VaPPRS, high liquefaction

efficiency is required. Section 3.3.2 reports the energy requirements to capture, recover, and liquefy isobutane using the GRS.

GRS cycling experiments with isobutane and a desorption temperature of 100°C were also conducted and showed that the ACFC did not regenerate sufficiently at that regeneration temperature. Based on the experiments conducted at regeneration temperatures ranging from 100 to 200°C, it was determined that 150°C provided a good balance between sufficient regeneration of the ACFC and minimizing energy use by the GRS. All subsequent experiments were conducted at 150°C as a result of this investigation.

3.3.2. Effect of Heating/Compression Time on Energy Requirements and Mass Distribution

The adsorbate concentration during adsorption follows a cyclic pattern similar to those reported in Figure 3.10 (*75*). The capture efficiency was greater than 99% for all experiments. Which again suggests that the GRS is an appropriate device for meeting air quality permitting requirements.

The total energy to recover liquid isobutane was determined for several heating/compression times. **Figure 3.11** shows the combined heating and compression energy per mole of liquid isobutane recovered for select heating and compression times (black triangles). It also shows the relative contribution of heating and compression to the total energy (bars). As expected, a minimum total energy used per mole liquid of isobutane recovered was observed. As is clear from **Figure 3.11**, at low heating/compression times, the standard deviations are quite high for the energy per mole liquid recovered (16-33% of the mean value), suggesting that the heating time was not sufficient to provide consistent regeneration of the ACFC. At higher heating and compression times the standard deviations are much smaller (3-8% of the mean value), suggesting that the system is operating consistently between experiments. Additionally, as the heating and compression time increases, the relative

contribution of the compressor's energy to the total energy also increases (from 44 to 63%). This is because the compressor's total energy use increases linearly with time, whereas the heating energy is highest during the early stages of heating in order to bring the ACFC from room temperature to 150°C and then drops off at longer heating times when the 150°C temperature is being maintained.

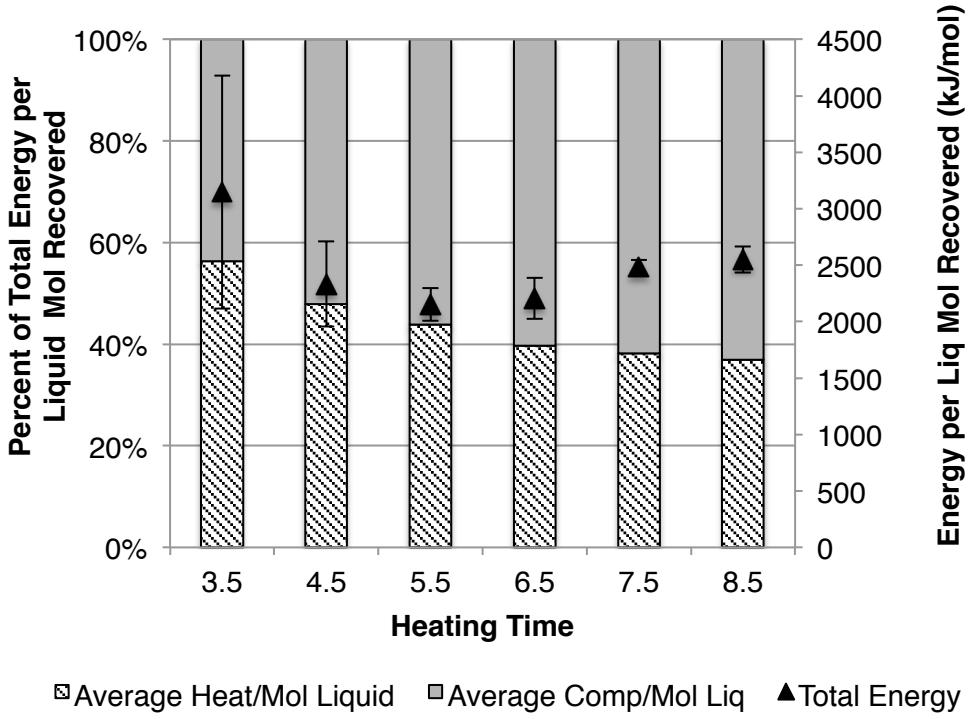

Figure 3.11 Heating and compression energy per mole liquid recovered (triangles) and the relative energy distribution between heating and compressor energy (bars) for cycling experiments with inlet isobutane at a relative pressure of 6.7×10^{-4}. Error bars represent +/- one standard deviation about the mean. Adapted with permission from (*86*). Copyright 2013 American Chemical Society.

3.3.2.1. Energy Cost and Emissions Estimates

The energy required to capture, recover, and liquefy a mole of isobutane can converted to a cost by comparing the cost of electricity to supply that energy to the cost to purchase the isobutane new, rather than attempting to recycle it. In Indiana, where the GRS would likely be installed, the average industrial electricity cost was $0.0634/kWh for 2012 (*87*). The cost to

purchase liquid isobutane on the market was $1.50/gallon ($0.40/liter) between 2012 and 2013 (*88*). Using 2152 kJ/mol, the energy per liquid mole recovered reported in **Figure 3.11** for a heating time of 5.5 minutes, the ratio of the cost of energy to recover the isobutane to the cost to purchase the isobutane was 0.88. This result suggests that the cost in energy to recover isobutane is 12% lower than the cost of purchasing isobutane new. This analysis is reasonably compelling, and it should be noted that isobutane costs are at near historic lows and industrial electricity costs for Indiana are at historic highs when considering the last two decades (*87*). Using values from 2007 when this research was initiated, the ratio of the energy cost to recover liquid isobutane to the purchase cost of liquid isobutane was 0.30, making the implementation of the GRS much more attractive from a financial standpoint. In addition, Johnsen, in his 2014 dissertation, determined that using an ACFC-ESA system to control isobutane emissions from packaging manufacturing would have an 11% yearly internal return on capital investment, indicating that the system would pay for itself within 10 years of operation (*10*). This analysis included capital and operating costs associated with ACFC-ESA, which strengthens the support for an ACFC-ESA system from a monetary standpoint.

The CO_2 emissions from implementing a GRS can be estimated based on the energy use of the GRS and the average CO_2 emissions from power plants. These emissions can be compared to the emissions of operating a thermal oxidizer with supplemental fuel to remove the isobutane. Using the result from **Figure 3.11** and the average CO_2 emissions from coal-fired power plants of 0.99 kg CO_2/kWh (*89*), the emissions per liquid mole of isobutane is 0.58 kg CO_2/mol isobutane. For the thermal oxidizer, 0.18 kg CO_2/mol isobutane is generated based on complete combustion stoichiometry (4 mol CO_2 generated per mol isobutane combused) and the supplemental fuel consumed by the thermal oxidizer represents less than 3% of the total CO_2 emissions from the oxidizer. This result suggests that implementing the GRS actually increases the CO_2 emissions related to controlling the emissions of isobutane. However, others have

shown with life cycle assessments that the global warming impacts of using ACFC-ESA is lower than using a thermal oxidizer system for a variety of electricity sources (*10*).

3.3.3. Effect of Heating/Compression Time on Mass Distribution

The effect of heating time on adsorbate mass distribution for isobutane can be seen in Figure 3.12. An increase in total heating time leads to an increase in the fraction of isobutane in the liquid phase and a decrease in the fraction of isobutane in the adsorbed phase. This is as expected since a higher heating time allows more isobutane to desorb from the ACFC, however there are diminishing returns on the reduction of mass in the adsorbed phase and the increase of mass in the liquid phase with every added minute of heating time, suggesting that heating time (i.e., energy input) and liquid recovery must be balanced for the most efficient operation of the GRS. The fraction of mass in the liquid phase at the end of each experiment ranged from 47.5 to 87%. These values are acceptable when compared to data from previous work. Dombrowski, *et al.*, reported fractional liquid recoveries of higher boiling point compounds between 11-81% for the VaPRRS, which did not include a post-desorption pressure and temperature control system and did not recycle desorbed adsorbate back to the adsorbing vessel (*42*). Ramirez, *et al.* reported a fractional liquid recovery of 90.6% for MEK in a bench-scale ACFC-ESA system that did not include a post-desorption pressure and temperature control system, but did include desorbed gas recycle (*90*).

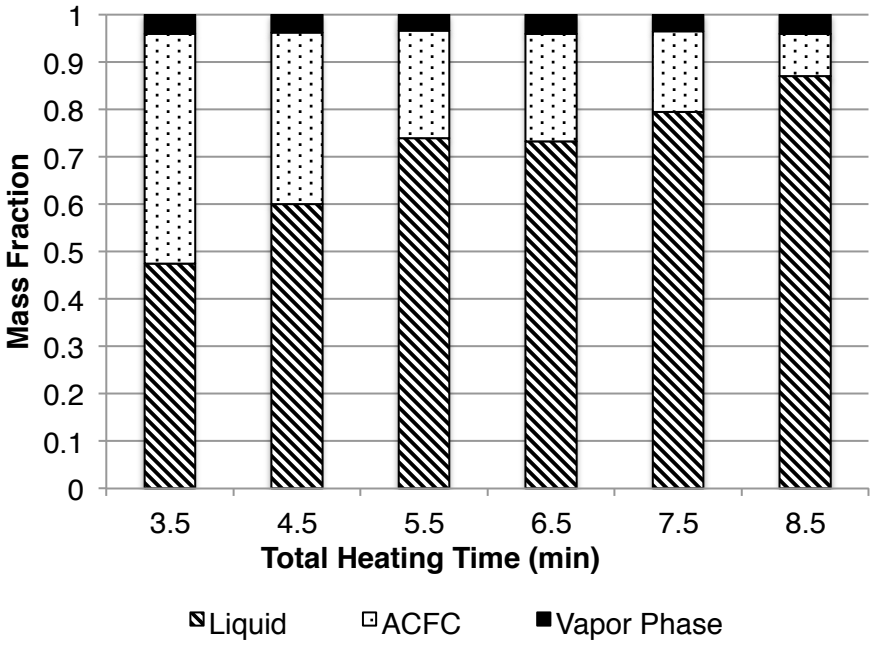

Figure 3.12 Mass distribution of isobutane as a function of heating time averaged over the duration of each experiment (> 5 regeneration cycles) Adapted with permission from (*86*). Copyright 2013 American Chemical Society.

Using the results from the isobutane screening experiments, subsequent experiments were conducted at varying relative pressures using a heating and compression time (step 3) of 4 min (total heating time in steps 2-4 was 5.5 min). This heating and compression time resulted in the lowest energy per mole liquid recovered for experiments with isobutane at a relative pressure of 6.7×10^{-4} and also had less than 25% of isobutane remaining in the ACFC during the experiment, which is reasonable compared to the 15-30% of adsorbate remaining in the vessel as was found by Dombrowski, *et al*. (*42*).

3.4. Modeling Results – MATLAB

Modeled results predicting the adsorbate concentration during desorption were generated using time and ACFC temperature data from representative GRS experiments. **Figure 3.13** shows the temperature of the ACFC during desorption for a cycling experiment on the GRS and the corresponding modeled isobutane concentration during desorption. This particular experiment had a total of 5.5 min of heating with the first 5 of those minutes having

low flow (0.5 SLPM) N_2 through the system and the last 0.5 min having high flow (3.5 SLPM) N_2, which can be seen in the concentration data at t = 300 s where a steep drop in the outlet isobutane concentration occurs.

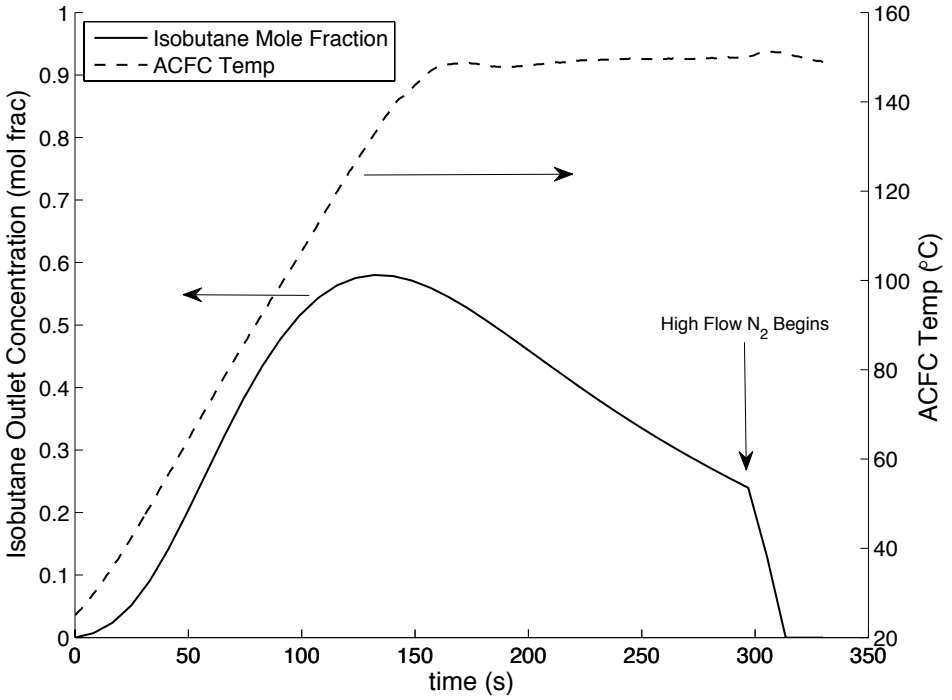

Figure 3.13 Isobutane concentration as a function of time as predicted by a MATLAB model. Based on adsorption of 2000 ppm_v ($P_i/P_{i,s} = 6.7x10^{-4}$) isobutane. The ACFC temperature generated during a GRS experiment that was used in the model is also included.

The same temperature profile was used to examine the effect of increasing the inlet concentration (relative pressure) of isobutane on the desorption concentration profile (**Figure 3.14**). Using equivalent temperature profiles for different inlet isobutane concentrations is not a perfect representation of reality due to the higher adsorption capacities experienced for higher inlet concentrations and thus different heating profiles due to the additional heat required for the heat of adsorption of isobutane. However the model shows that when more adsorbate is

adsorbed to the ACFC, the adsorbate desorbs from the ACFC more quickly and with a higher peak concentration.

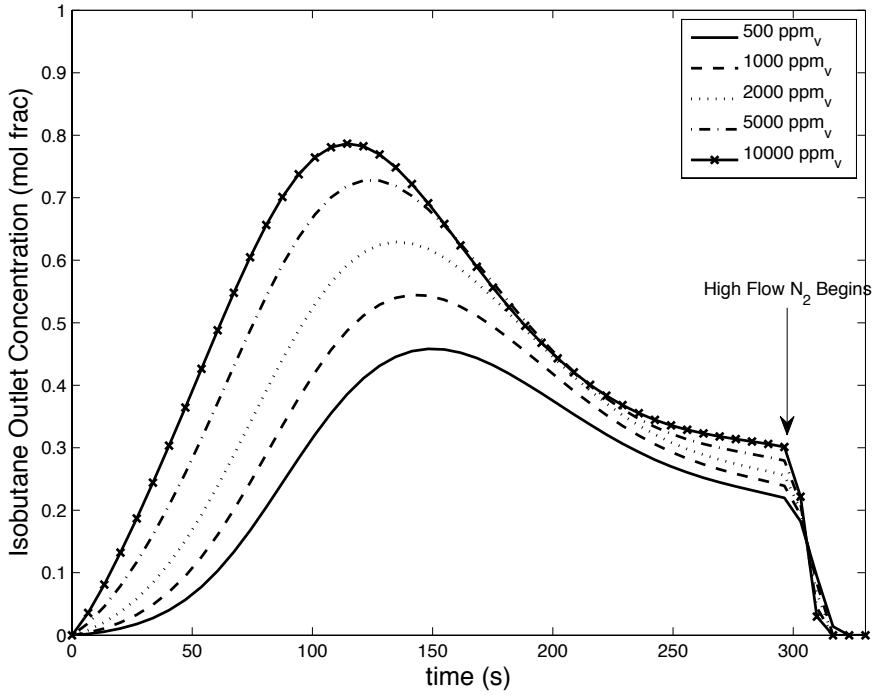

Figure 3.14 Modeled isobutane concentration during desorption for select inlet concentrations of isobutane. Each model result is based on the ACFC temperature profile shown in **Figure 3.13** which has a linear increase in temperature from 25 - 150°C over 150 s (50°C/min).

The effect of changing the amount of time it takes the ACFC to heat from room temperature to its set point temperature was examined with a final ACFC temperature of 150°C (Figure 3.15). The modeled results indicate that the faster the ACFC reaches its set point temperature, the more highly concentrated the desorption gas stream is. However, the temperature ramp speed for the GRS is constrained by the amount of current the system can handle. The best ramp time achievable with the GRS is 150 seconds to reach 150°C.

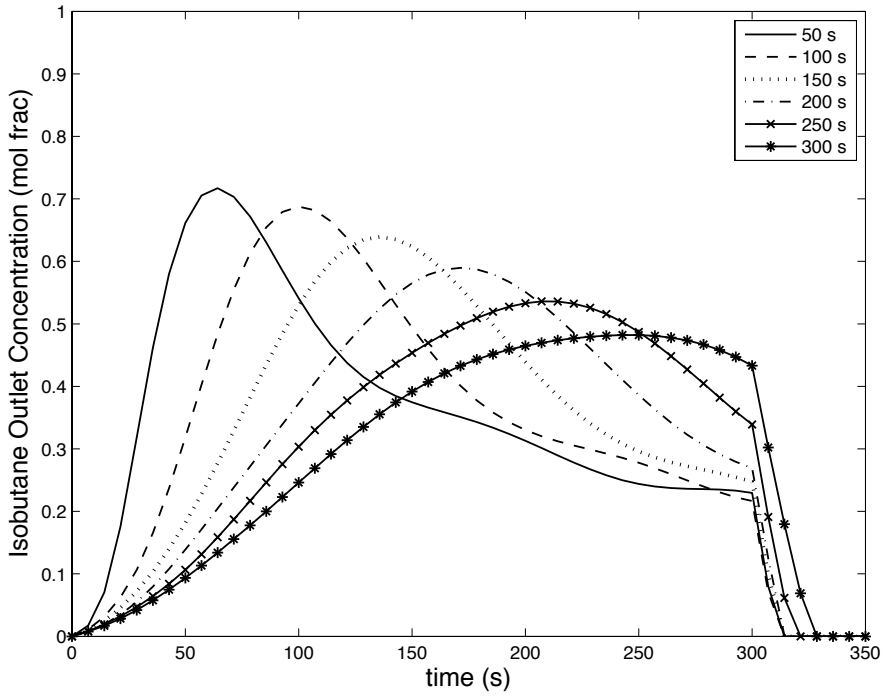

Figure 3.15 Modeled isobutane concentration during desorption for different ACFC temperature ramp times. Each model result assumed an inlet isobutane concentration of 2000 ppm_v and a final ACFC temperature of 150°C.

Finally, the effect of changing the set point temperature while maintaining the ramp speed is shown in Figure 3.16. This result indicates that as the set point temperature increases, the outlet isobutane concentration also increases, but begins to plateau at 150°C. This result is consistent with experimental results that showed little difference in the energy performance of the GRS when the ACFC set point temperature ranged from 150-200°C (Table 3.5).

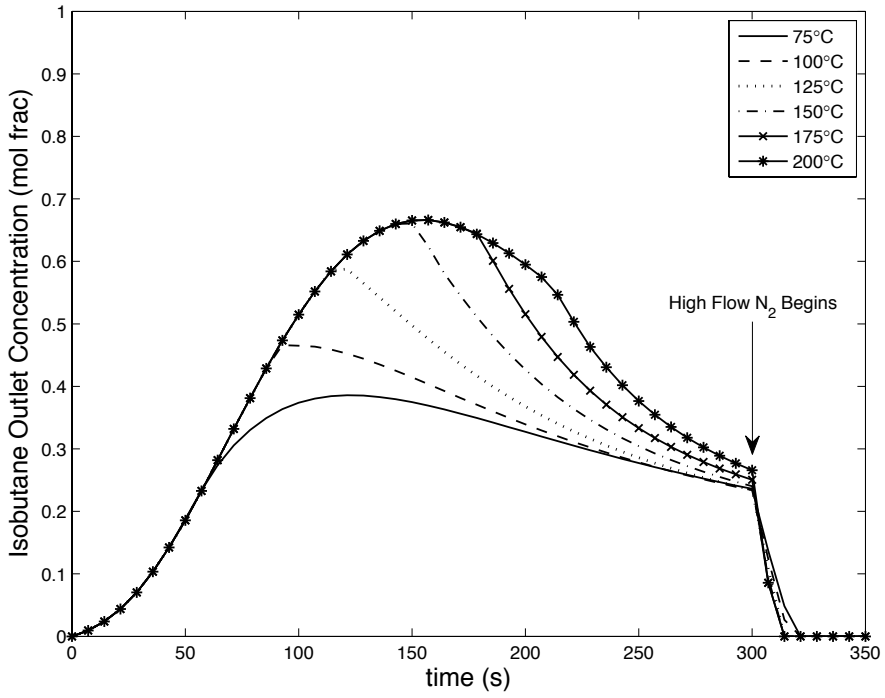

Figure 3.16 Modeled isobutane concentration during desorption for different ACFC final temperatures. Each model result assumed an inlet isobutane concentration of 2000 ppm_v and a temperature ramp speed of 50 °C per min.

These modeled results can help explain some of the results seen in section 3.3.2 examining the effect of heating/compression time on the energy required to capture and liquefy isobutane. Many attempts were made to generate measured data to compare to the modeled results. The PID and FID that had been used for previous concentration measurements were considered, but the PID's concentration range is two orders of magnitude too small for the expected desorption concentrations. Additionally, the FID was previously shown to have a large lag time, which would affect its reliability when comparing measured to modeled data (*91*). A gas chromatograph (GC) was also considered as a tool for measuring desorption concentration as a function of time, but a functioning GC was not available. While it was not possible to directly compare these modeled results to the GRS operational results due to lack of access to an appropriate concentration measurement device, the trends seen in both the modeled

isobutane concentration data and the GRS energy usage data are consistent with one another. For example, examining the first 120 seconds of data in **Figure 3.14** and Figure 3.15 indicates that small perturbations in inlet concentration or ACFC temperature could have a large effect on the concentration of isobutane desorbed. For example, increasing the isobutane adsorption concentration from 5000 to 10,000 ppm_v results in a 10% increase in the peak isobutane concentration during desorption. If this trend were accurate, a decrease in the energy to capture, recover, and liquefy isobutane would be expected when the inlet isobutane concentration increased due to the resulting higher concentration in the desorption stream. Experimental results did show a 35% reduction in energy to capture, recover, and liquefy isobutane under experimental conditions similar to those modeled (Figure 3.19). It is also clear that if the ACFC were only heated for 120 s, much of the isobutane would be left adsorbed on the ACFC because heating would stop just as the peak desorption concentration is achieved. From an energy standpoint, this could result in the high standard deviations and the higher energy required to recover isobutane shown in **Figure 3.11** for low heating times. The shape of the curve in **Figure 3.14** also provides insight in to why longer heating times also result in higher energy requirements: as the ACFC heats for more than 2-3 min, the amount of isobutane being desorbed decreases, so more energy is being consumed (primarily via the compressor), but not much isobutane is being liquefied.

Similar models were constructed for R134A (Figure 3.17) and n-butane (Figure 3.18). It is clear from the figures that both R134A and n-butane achieve lower maximum concentrations than n-butane. This is in part due to the lower adsorption capacity of ACFC for the relative pressures of R134A and n-butane shown here compared to the adsorption capacity of ACFC for isobutane at a relative pressure of 6.7×10^{-4}, as shown in **Figure 3.13**. However, the reduced desorption concentrations are also a function of the characteristic adsorption energy of the adsorbate and how the vapor pressure of the adsorbate changes with temperature.

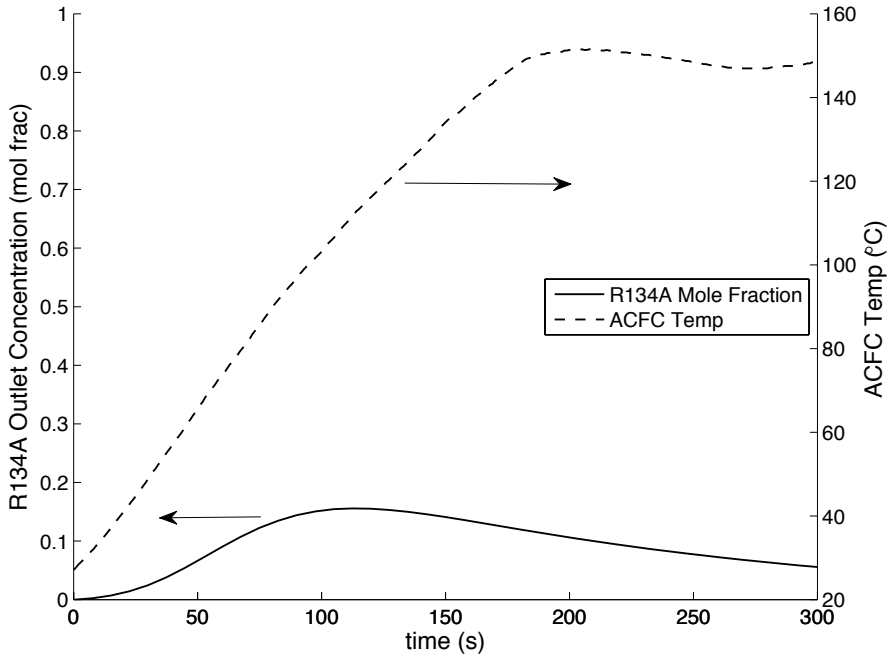

Figure 3.17 R134A concentration as a function of time as predicted by a MATLAB model. Based on adsorption of 500 ppm_v ($P_i/P_{i,s} = 8.3x10^{-5}$) R134A. The ACFC temperature generated during a GRS experiment that was used in the model is also included.

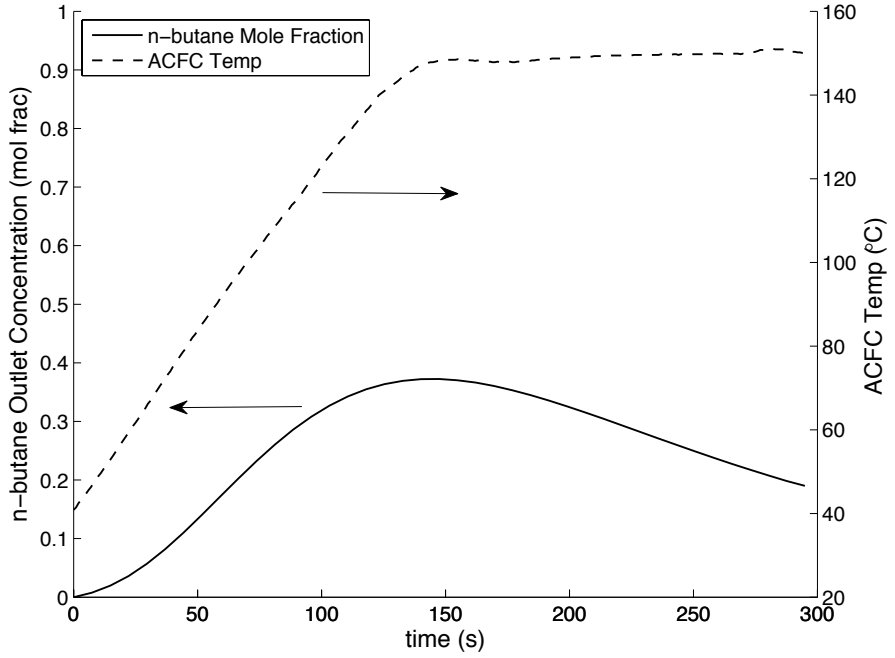

Figure 3.18 n-butane concentration as a function of time as predicted by a MATLAB model. Based on adsorption of 1324 ppm_v ($P_i/P_{i,s} = 6.7x10^{-4}$) n-butane. The ACFC temperature generated during a GRS experiment that was used in the model is also included.

There are several areas for improvement in these models. First, the models do not take into account the high concentration (15% by volume) adsorbate that is recycled to the adsorption vessel during the desorption process, which accounts for approximately 15% of the total adsorbate supplied to the adsorption vessel during a given cycle. Including this additional adsorbate would likely increase the slope of the desorption curves and the peak concentrations achieved during desorption. In addition, direct comparison of the modeled results to measured desorption concentrations would improve the credence of the models.

3.5. Effect of Adsorbate Relative Pressure on Energy Requirements

The effect of adsorbate relative pressure on the energy required to recover liquefied organic gas is shown in Figure 3.19. The standard deviations for the GRS data points were less than 7% of the mean for all experiments. The energy to recover the organic compound in liquid form increases drastically as the relative pressure decreases. This is expected due to the reduction in adsorption capacity associated with reduction in relative pressure of the adsorbate. For example, R134A ($P_i/P_{i,s} = 8.3x10^{-5}$) had an effective adsorption capacity of 5 mg/g ACFC, whereas isobutane at the highest relative pressure ($P_i/P_{i,s} = 3.4x10^{-3}$) had an effective adsorption capacity of 78.5 mg/g ACFC. Since the total amount of energy input per cycle is essentially equivalent for all GRS experiments (338 ± 16 kJ/cycle) with the same heating/compression time, the less adsorbate captured per cycle, the higher the energy required to recover that adsorbate. A power law was chosen to model this data because previous researchers had used such a relationship and the power law models the data well ($R^2 > 0.99$) (*42*). The plateau observed at high relative pressures is the result of there being a minimum energy required to heat the ACFC to desorb the adsorbed compounds. While the number of moles of adsorbed compound could increase with higher relative pressures and thus reduce the energy per mole liquefied, this

increase would be limited by the pore volume of the adsorbate. However, for this research, the power law is a useful descriptor for the data.

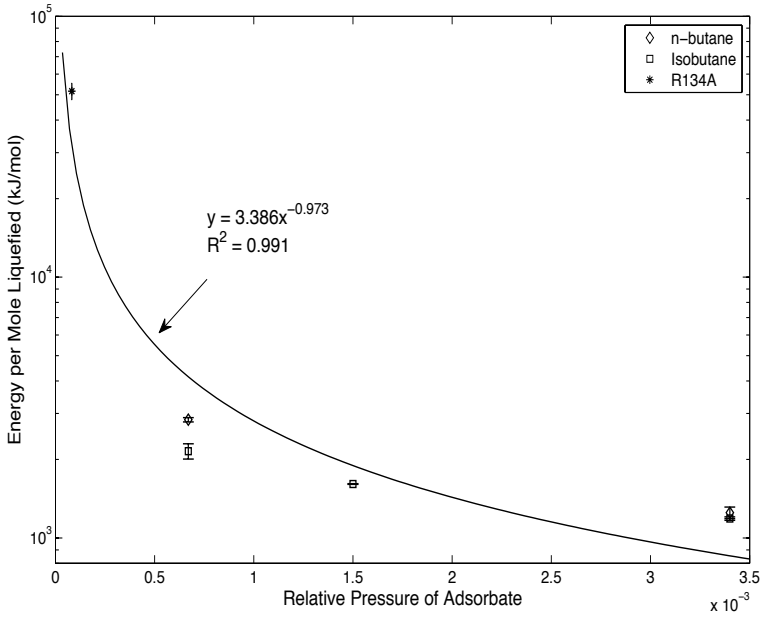

Figure 3.19 Average heating and compression energy per mole liquid recovered as a function of relative pressure for the GRS operating with three different adsorbates (*86*). Error bars represent +/- one standard deviation about the mean. The power law fit is $y = 3.386x^{-0.973}$, $R^2 = 0.991$. Adapted with permission from (*86*). Copyright 2013 American Chemical Society.

Because the relative pressure of the adsorbate is an important variable in the energy requirements of the GRS and the effective ACFC adsorption capacity is related to the relative pressure via the equilibrium adsorption capacity, the effective adsorption capacity was compared to the theoretical equilibrium capacity of the ACFC to better relate the operating conditions of the GRS to its performance. Figure 3.20 compares the average ACFC capacity for each of the three adsorbates during cycling experiments ($q_{effective}$) to the equilibrium capacity determined using the Dubinin Raduskevich (DR) fit of the adsorption isotherms ($q_{equilibrium}$) or data from previous work (*92*). From this it is clear that the effective adsorption capacity for each

of the adsorbates is, on average, 36% lower than the equilibrium capacity. This is likely due to three causes: the ACFC in the adsorption vessels is not being used to its full capacity due to the nature of the geometry and configuration of the ACFC cartridges, the ACFC is not allowed to come to equilibrium with the adsorbate because breakthrough is considered to be 5% of the inlet adsorbate concentration, and the $q_{equilibrium}$ value does not take into account the high concentration adsorbate that is recycled to the adsorption vessel during regeneration, which reduces the amount of adsorbent available for the low concentration gas stream.

This result suggests that one cannot rely on equilibrium adsorption isotherms to design ACFC-ESA systems and it is critical to run bench and pilot studies with representative adsorbates prior to designing a full-scale system. However, the linear fit of the data in Figure 3.20 shows that a reasonable estimate of the effective adsorption capacity during operation of the bench scale GRS would be 36% of the equilibrium adsorption capacity predicted by adsorption isotherms.

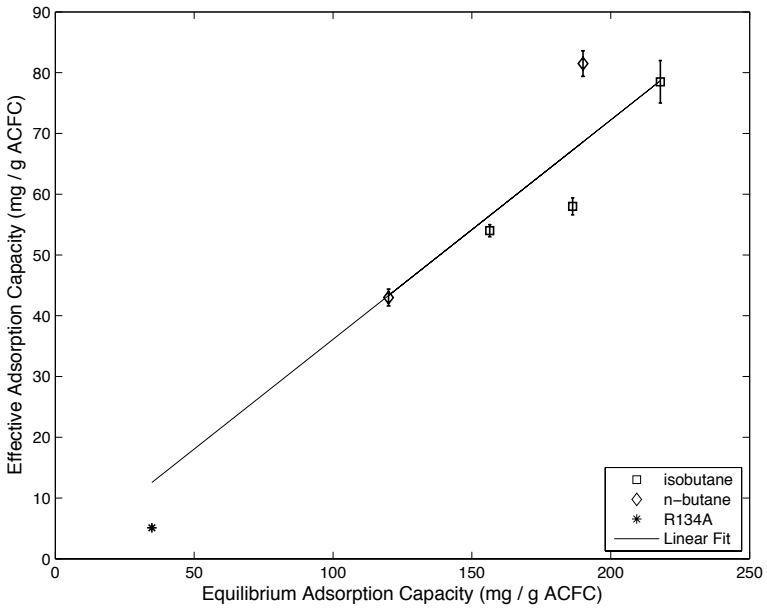

Figure 3.20 Effective adsorption capacity during GRS cycling experiments compared to the equilibrium adsorption capacity determined from isotherm

experiments. Error bars represent +/- one standard deviation about the mean. The linear fit equation is $y = 0.3611x$; $R^2 = 0.92$. Adapted with permission from (*86*). Copyright 2013 American Chemical Society.

Combining Figure 3.19 and Figure 3.20 leads to Figure 3.21. The high R^2 values for the power law fit of the data shown in Figure 3.21 indicates that using either the equilibrium adsorption capacity or the effective adsorption capacity of a given adsorbate to predict the amount of energy that would be required to capture, recover, and liquefy that adsorbate would be possible.

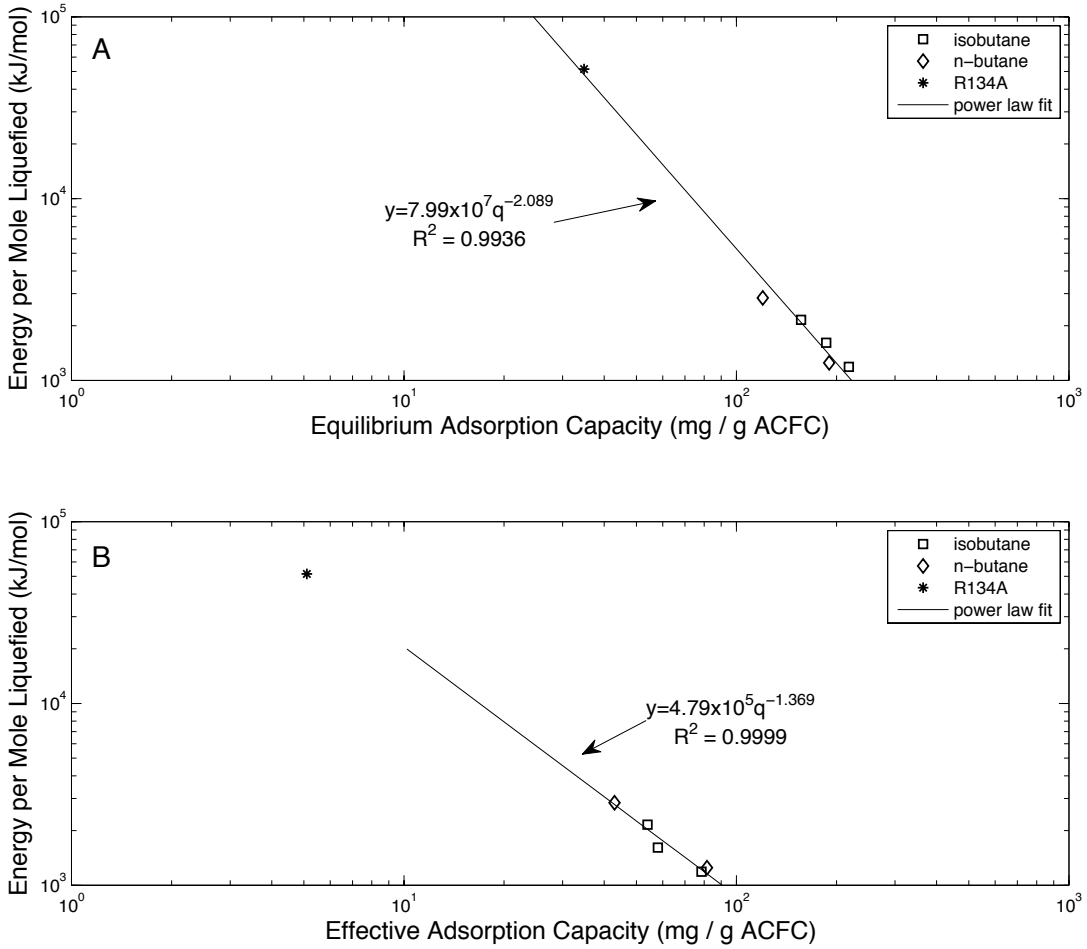

Figure 3.21 Heating and compression energy per mole liquid of adsorbate as a function of the equilibrium (A) or effective (B) adsorption capacities.

3.6. Performance of the GRS with Multicomponent Adsorption and Carrier Gas Recirculation

For all experiments conducted with multi-component adsorption gas streams, the capture efficiency for isobutane was greater than 99%. The following energy use results include the energy to heat the ACFC, the energy to compress the desorption gas stream, the energy to handle water vapor, and the energy to supply N_2 to the GRS, as discussed in section 2.3.3. The energies reported for 5% RH experiments without carrier gas recycling are the same as those

reported for the 5.5 min heating time in **Figure 3.11** with the addition of the energies to handle water vapor and supply N_2.

3.6.1. Multicomponent Adsorption

Prior to implementing carrier gas recirculation, the GRS was tested with a non-recycled carrier gas of air, isobutane (relative pressure $6.7x10^{-4}$), and water vapor (RH 30-80%) as described in section 2.7. As expected, introducing water vapor to the carrier gas stream increased the energy required to recover liquid isobutane (Figure 3.22 and Figure 3.23). A 24% increase in the GRS energy use was observed when increasing the carrier gas RH from 5% to 24% (2910 kJ/mol to 3620 kJ/mol), and this difference is statistically significant at the 95% confidence level. Similarly, when the RH was increased to 80% the energy usage also increased to 5750 kJ/mol.

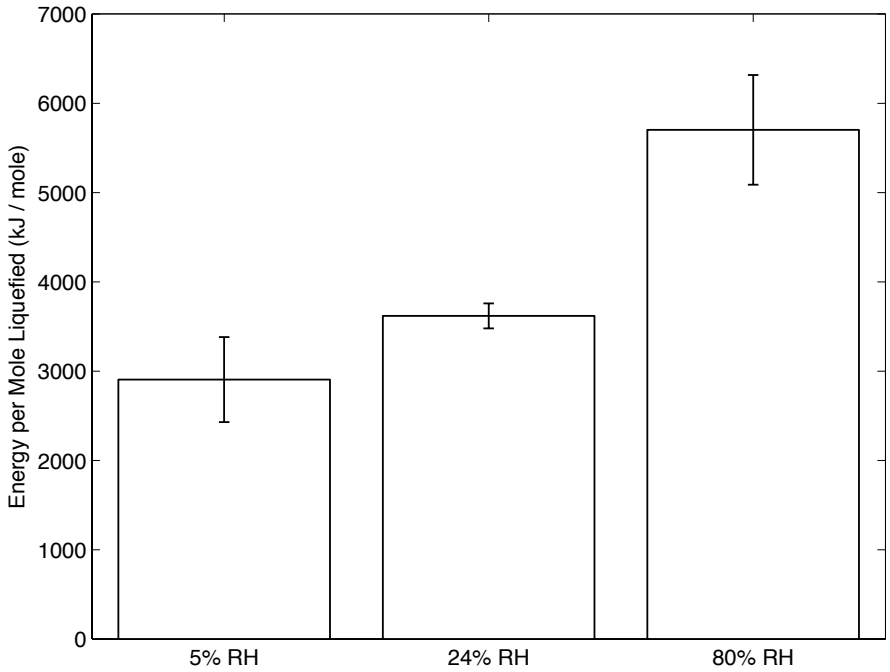

Figure 3.22 Energy required to capture, recover, and liquefy isobutane with select amounts of water vapor present in the adsorption gas stream for the GRS in non-reciruclation mode. Energy values include ACFC heating, desorption gas compression, N_2 production, and water vapor production/removal. Error bars represent the 95% confidence interval.

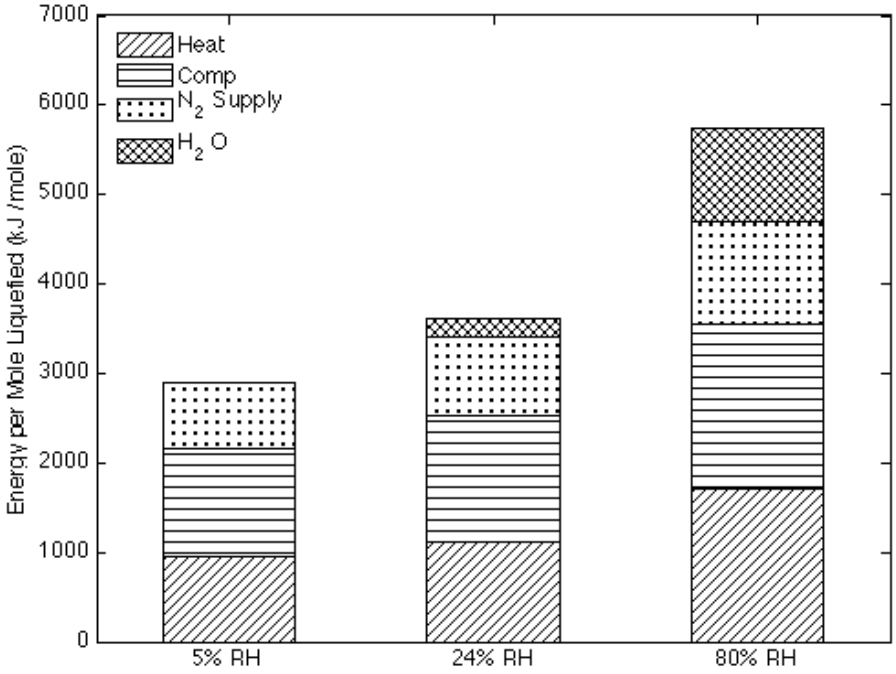

Figure 3.23 Energy required to capture, recover, and liquefy isobutane with select amounts of water vapor present in the adsorption gas stream for the GRS in non-recirculation mode with specific energy uses denoted.

This result is not surprising considering the adsorption behavior of water vapor on ACFC (Figure 1.5) and how water vapor interacts with competitive non-polar adsorbates (Figure 1.2), which both show very low water adsorption on ACFC when the inlet RH is less than 40%. At higher relative humidities, when the adsorption of water vapor on the ACFC is significant (300 mg H_2O /g ACFC), the energy required to recover liquid isobutane increases significantly. As shown in Figure 3.22, when the inlet RH was 80%, the energy required to recover a mole of liquid isobutane nearly doubled from 2910 kJ/mol to 5750 kJ/mol. This reflects the decrease in the ACFC's effective capacity for isobutane during high RH experiments and the increased energy required to supply the water vapor. The ACFC's effective capacity for isobutane in the presence of high RH decreases by 38% compared to 5% RH conditions (33.5 mg/g ACFC compared to 54 mg/g ACFC). If the reduction in isobutane capacity were the only thing

contributing to the increase in energy usage, one would expect the energy used by the GRS to increase by 1880 kJ/mol liquefied based on the power law data fit in Figure 3.21B. This leaves 960 kJ/mol liquefied unaccounted for. The energy required to supply water to the adsorption gas, heat and vaporize the water that adsorbed to the ACFC, and condense the desorbed water to prevent it from contaminating the recovered isobutane averaged 1040 kJ/mol liquefied for the experiments with 80% RH in the inlet gas stream for the non-recirculation experiments. This energy effectively accounts for the entirety of the energy increase noted.

Figure 3.23 highlights another major contributor to the energy required to capture, recover, and liquefy isobutane: the energy required to supply N_2 to the GRS. Based on the calculations described in section 2.3.3.4, the energy to supply N_2 is approximately 25% of the total energy used by the GRS. This value is congruent with results from Rood, *et al*. who determined that N_2 accounted for 25% of total operating costs for an ACFC-ESA system that used ancillary cooling to recover organic vapors (*93*). In contrast, this fraction is low compared to the results found by Ramirez, *et al*. who examined the energy use of a pilot-scale VaPRRS and found that the compressor that supplied air to a N_2-producing membrane accounted for greater than 50% of the total energy used by the system and was three times the electrothermal regeneration energy (*71*). However, the energy efficiency of the pressurized membrane system used in the pilot scale VaPRRS is unknown.

In addition to the energy used by supplying N_2 to the GRS, the continuous supply of N_2 was found by D.L. Johnsen to contribute to the environmental impacts of the GRS. For example, using N_2 in the GRS represented nearly 20% of the GRS's eutrophication and carcinogenic impact (*10*). This N_2 energy requirement and environmental impact combined with the large fraction of the energy that is due to humidification of the adsorption gas stream highlights an important opportunity to reduce the energy used and environmental impact caused by the GRS

to capture, recover, and liquefy isobutane. To take advantage of this opportunity, carrier gas recirculation was implemented as described in section 2.2.4.

3.6.2. Multicomponent Adsorption Coupled with Carrier Gas Recirculation

The GRS was modified to operate by recycling the adsorption carrier gas through the system. Prior to implementing carrier gas recycling, the GRS required 40 SLPM of air from a compressed air system to operate. Once carrier gas recycling was implemented, the GRS only required 2.65 SLPM of air from a compressed air system (less than 7% of the non-recycling system's requirement). Over half of the supplied air was required due to the flow needs of the oxygen sensor and the FID, so the dependence on compressed air could be further reduced to less than 0.8 SLPM with careful pressure control and gas recirculation from the instrumentation.

3.6.2.1. Mass Balance Effects of Carrier Gas Recycling

One of the goals of implementing carrier gas recycling was to reduce the amount of water and N_2 needed to operate the GRS. Based on the cycling experiments conducted, the required N_2 was reduced by 25% by implementing carrier gas recirculation, whereas the required H_2O for high relative humidity experiments was reduced by greater than 60%.

Based on the gas flows in the GRS in recycle mode (2.65 SLPM makeup air being supplied and an average N_2 flow of 0.92 SLPM over the course of the entire cycling experiment), the lowest steady-state O_2 concentration that could be achieved is 15% by volume. In these experiments, the average O_2 concentration in the GRS for a carrier gas recycling experiment was 16% by volume, which is within 7% of the lowest achievable O_2 concentration based on the flowrates of N_2 noted above.

The effectiveness of the carrier gas recirculation in terms of maintaining the water vapor concentration in the carrier gas is a function of the RH in the adsorption gas stream (Figure 3.24). Experiments showed that at low relative humidities the inlet and outlet RH of the adsorption vessels in the GRS are nearly identical (A). At higher relative humidities, some water

vapor is adsorbed to the ACFC, resulting in lower RH in the adsorption vessel outlet gas than in the inlet (B). The data in Figure 3.24 also shows the repetitive, cyclical nature of the GRS operation with consistent switching between the two adsorption vessels (V1 and V2).

Despite some water vapor adsorbing to the ACFC at high relative humidities, even at 75% RH in the inlet adsorption stream, greater than 60% by mass of the supplied water vapor is retained in the carrier gas while passing through the adsorption vessel. The remainder of the water was not lost; it was condensed into the chilled water trap during desorption as described in section 2.2.4. The ability to retain water vapor in the carrier gas could potentially be improved by heating the ACFC during adsorption to lower the RH of the adsorption gas stream, and consequently lowering the adsorption capacity of ACFC for water vapor. However, this technique has drawbacks including lowering the adsorption capacity of the ACFC for the target adsorbate and increasing the overall energy used by the system. This strategy will be discussed in more detail in the next section.

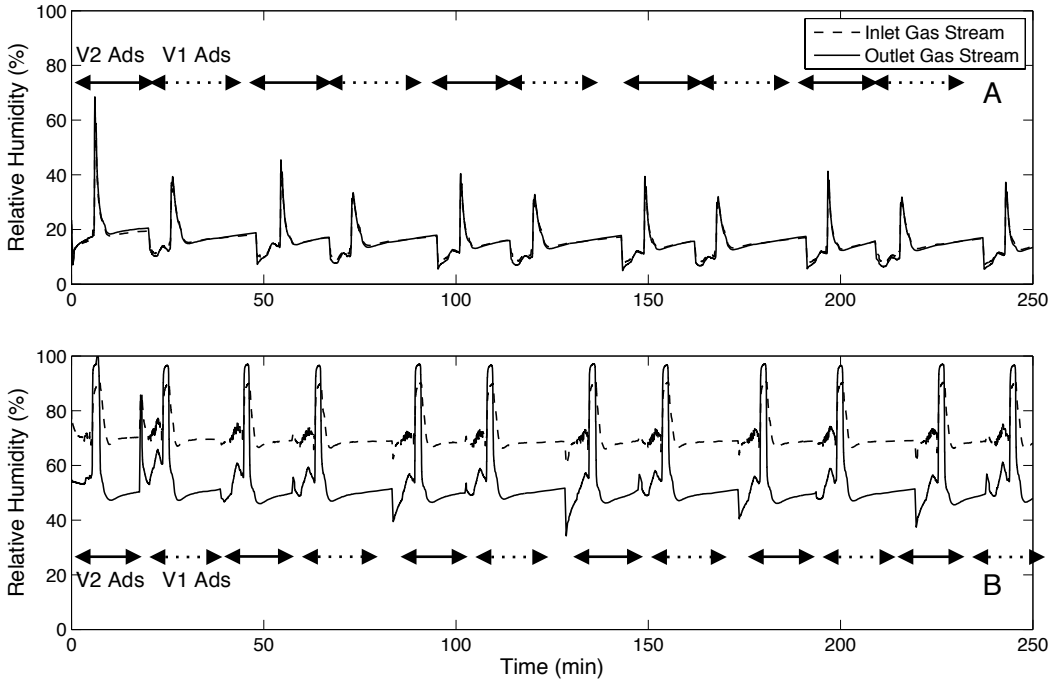

Figure 3.24 Inlet and outlet relative humidities for the GRS with carrier gas recycle. A. represents low inlet RH (20%) and B. represents high inlet RH (70%). Arrows indicate the duration of vessels 1 and 2 adsorption cycles. Spikes in the RH occur when the desorption gas stream, which is saturated with water vapor during high RH experiments, is recycled to the adsorption vessel.

3.6.2.2. Methods to Improve O_2 Reduction during Carrier Gas Recycling

The following thought-experiment provides a means to achieve one of the overall goals of carrier gas recycling, which is to reduce the amount of N_2 needed to operate the GRS continuously while maintaining an safe oxygen concentration ($< 6\%$ by volume, which is 50% of the LOC). To reduce the average O_2 concentration in the system to 6% by volume, the ratio of makeup air flow rate to N_2 flow rate would have to be decreased from 2.88 to 0.4. This 86% reduction in relative N_2 flow rate would also make the ACFC-ESA system more attractive from an environmental standpoint when compared to thermal oxidation or using GAC (*10*). Lowering the makeup air flow rate would allow subsequent lowering of the N_2 flow rate as long as the ratio to achieve the appropriate oxygen level is maintained. While this was not possible with the GRS in the configuration discussed here due to the high volume requirements of the oxygen sensor

and the FID, in a larger scale system in which the operational monitoring equipment would require a smaller fraction of the carrier gas flow rate to operate, or in a system that does not require the use of monitoring equipment (*94*), this reduction in makeup air and subsequent reduction in N_2 requirement could be achieved. For example, in a pilot scale system, such as that described by Ramirez, *et al.* with an adsorption carrier gas flow rate of 1700 SLPM (*71*), the flow rate of makeup air could be kept the same as for the bench scale GRS (2.65 SLPM), but the N_2 flow rate would increase by a factor of 40, resulting in a makeup air flow rate to N_2 ratio of 0.07, which would effectively remove the need to supply N_2 to the system once steady state was achieved. Alternatively, N_2 could be supplied to the GRS in place of makeup air to maintain the system pressure. In this case, the ratio of makeup air flow rate to N_2 flow rate would be 0 and would allow for steady state operation well below the LOC.

3.6.2.3. Energy Requirements for Carrier Gas Recycling

Figure 3.25 shows how relative humidity and carrier gas recycling affect the energy used by the GRS to capture, recover, and liquefy isobutane. At low relative humidities, operating the GRS with carrier gas recycle led to a 2.5% decrease in the total energy used per mole liquid of isobutane recovered. Under ideal operating conditions, a 25% decrease in the total energy would have been observed due to the elimination of the continuous supply of N_2. The difference between the observed and ideal energy reduction is the result of the high makeup air flow rate relative to the N_2 flow rate required to maintain the gas pressure in the GRS, which was discussed in the previous section.

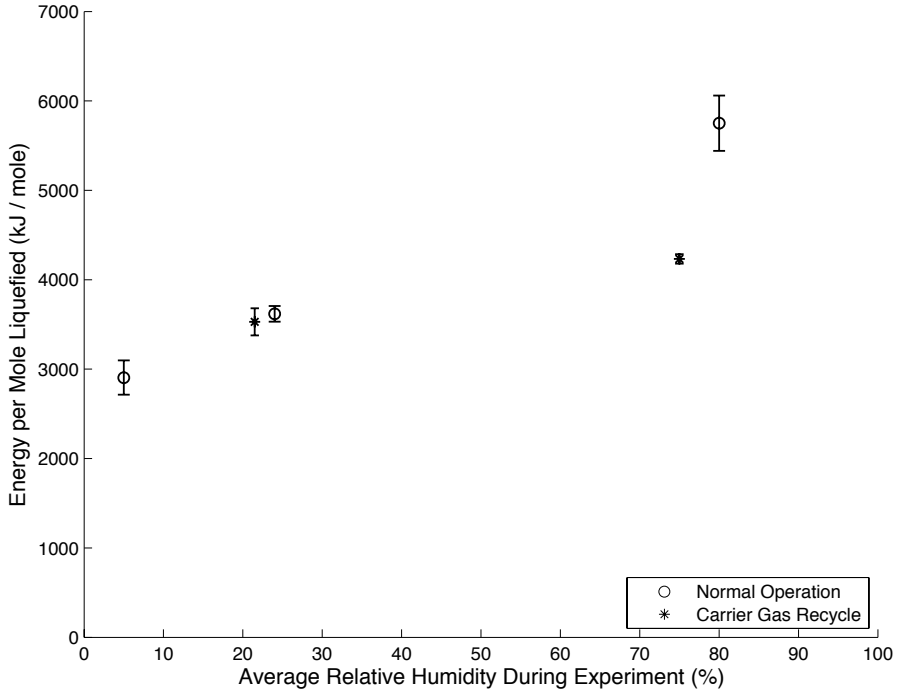

Figure 3.25 Energy consumed by the GRS per mole liquid of isobutane recovered. Energy values include ACFC heating, desorption gas compression, N_2 production, and water vapor production/removal. Error bars represent the standard deviation of the data.

In contrast, at higher relative humidities, operating with carrier gas recycle provided a significant energy benefit to the system: the energy consumed by the GRS in recycle mode was 74% of the energy consumed in non-recycle mode (4230 kJ/mol liquefied compared to 5750 kJ/mol liquefied) and this result was statistically significant at the 95% confidence level. Figure 3.26 shows the energy breakdown of the different energy users for the GRS operating a high RH in recycle and non-recycle (normal) mode. Recall that the energy to supply water vapor to the system is included because the industrial process of interest requires a humid gas stream to operate. Each of the energies shown in Figure 3.26 are normalized by the moles of isobutane liquefied downstream of the adsorption vessel. Based on the data shown in Figure 3.26, the GRS operating in recycle mode under idealized conditions would use 62% of the energy used

by the GRS in normal operation (assuming the energy required to supply N_2 and H_2O could be eliminated completely).

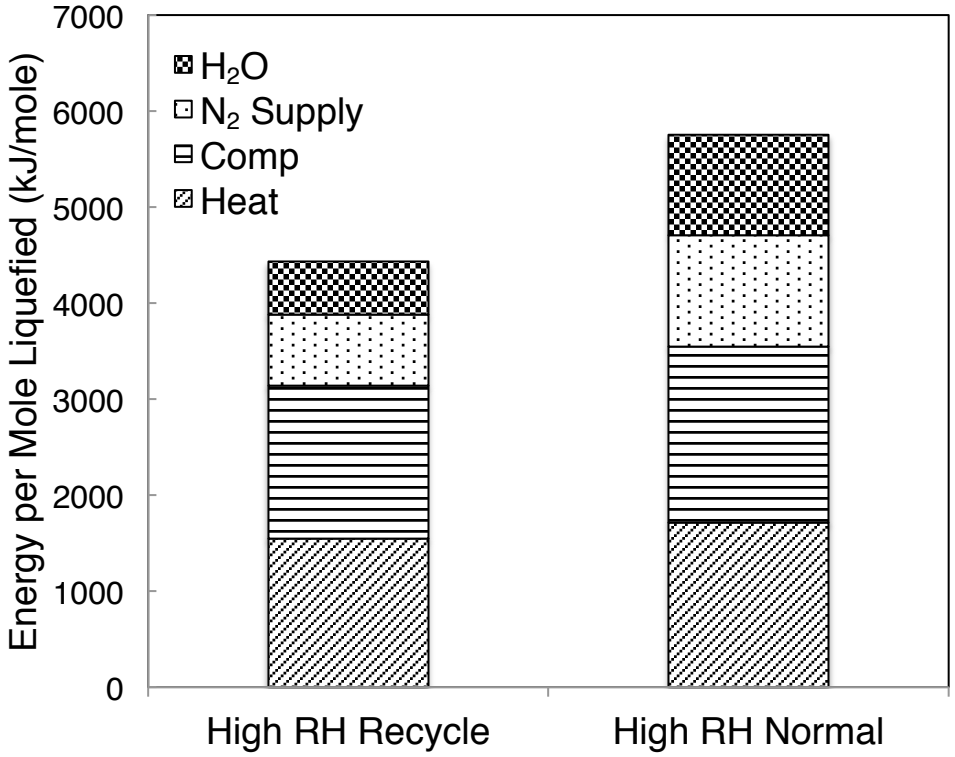

Figure 3.26 Energy required to capture, recover, and liquefy isobutane for the GRS operating at high relative humidity with specific energy uses denoted.

As is clear from the above figure, the energy usage in every category decreases in recycle operation compared to normal operation. Some of the difference observed could be the result of small differences in the RH in the inlet adsorption stream (75% RH vs 80% RH for recycle vs non-recycle). This could have affected the extent of the competitive adsorption of isobutane with water vapor. Although experiments were conducted at RH greater than 70% to operate on the flat part of the water adsorption isotherm found at high RH (Figure 1.5), the experimental results shown in Figure 1.2 suggest that water vapor and organic compound adsorption capacity are both highly dependent on RH when RH is greater than 45%. The adsorption capacities for isobutane for the normal operation and carrier gas recycle operation at

high RH were 33.5 mg/g ACFC and 35.7 mg/g ACFC, respectively. This difference in adsorption capacity of isobutane will affect each of the energy categories because the reported energies are normalized per mole liquid recovered, so the less isobutane that is captured per cycle, the higher the energy per mole liquid recovered. Using the power law determined with data shown in Figure 3.21, the predicted heat and compressor energy usage for the measured adsorption capacities indicate that the heat and compression energy in recycle operation (RH = 75%) should be 10% less than the energy in normal operation (RH = 80%).

In addition to the difference in effective adsorption capacity, there was also a difference in the fraction of isobutane that was liquefied. This, again, will have an affect on the energy reported in Figure 3.26 due to the nature of normalizing the energy consumed to the amount of liquid isobutane recovered. On average, 84% of the captured isobutane was liquefied during the recycle experiments, whereas only 78% of the supplied isobutane was liquefied during non-recycle experiments. This component contributes another 8% to the reduction in energy use when considering recycle operation compared to normal operation. The remaining difference in energy usage between normal and recycle operation is due to the reduction in the amount of water vapor and N_2 that need to be supplied to the adsorption gas stream in recycle mode compared to normal operation. As discussed above, more than 60% of the water vapor (by mass) is maintained in the carrier gas when the carrier gas is recycled. This reduces the energy consumed by humidifying the air by greater than 60% and accounts for 40% of the total energy difference between the recycle and non-recycle GRS operation modes.

The energy benefit from recycling the carrier gas could be further improved if the fraction of water vapor recycled were increased. As noted in the previous section, one strategy would be to heat the ACFC during adsorption to reduce the effective RH during the adsorption cycle, and therefore reduce the adsorption capacity of the ACFC for water vapor. However, there is a fine balance that must be achieved when using this technique because while increasing the ACFC

temperature during adsorption decreases the ACFC's adsorption capacity for water vapor, it also decreases the ACFC's adsorption capacity for the adsorbate of interest (isobutane).

For example, in order to reduce the RH from 80% at 25°C to below 40%, the ACFC temperature during adsorption would have to be increased to 40°C. Based on the adsorption isotherms reported in section 3.1 and the results shown in Figure 3.20, this temperature increase would result in an 18% reduction in the effective isobutane adsorption capacity (49 to 40 mg isobutane / g ACFC). This reduction in effective adsorption capacity corresponds to a 32% increase in heating and compression energy from 2325 kJ/mol liquefied to 3070 kJ/mol liquefied based on Figure 3.21B. Considering that the energy benefit from operating at low RH compared to high RH while recycling the carrier gas is only 20%, heating the ACFC to reduce the RH in the adsorption gas stream does not make sense from an energy use standpoint when recycling the carrier gas. However, if the system is operated without carrier gas recycling, heating the ACFC to reduce the RH is more favorable because the energy benefit from operating at low RH compared to high RH is 40% (3620 kJ/mol liquefied compared to 5750 kJ/mol liquefied for low and high RH experiments, respectively).

3.6.2.4. Advantages of Carrier Gas Recirculation

The major advantage of carrier gas recirculation is that it minimizes the need for conditioning of the inlet gas during manufacturing operations and therefore reduces the energy used to capture and recover low concentration organic gases. The energy reduction from operating in recycle mode compared to normal mode ranged from 2.5 to 26%. As discussed in the previous sections, there are operational modifications that could be made to improve the energy benefits of carrier gas recycle including reducing the dependence on make up air with instrumentation modifications, supplying N_2 instead of air to maintain system pressure control, and heating the adsorption vessels to reduce water vapor loss. If some or all of these techniques were implemented, the GRS operating in recycle mode under ideal conditions has

the potential to reduce the total energy used by the system by 38% for high RH conditions and 25% for low RH conditions.

3.7. System Operation Improvement Strategies

As discussed in previous sections, improving the GRS performance is critical to improving the economics of the system. Improvement strategies implemented in this research included physical as well as operational changes. Physical changes that were made included reducing the adsorption vessel volume, increasing the amount of ACFC in the vessel, and reducing the volume of the post-desorption plumbing and pressure vessel. Operational changes resulted from systematic exploration of the effect of certain parameters on the performance of the system such as ACFC temperature and heating and compression times during desorption. The primary focus of this research was on isobutane, so while other adsorbates were tested and the performance of the GRS for those adsorbates was determined, that performance was not optimized for each of those adsorbates as it was for isobutane. A similar, parametric approach to that used with isobutane could be taken to optimize the GRS performance for any adsorbate of interest.

3.7.1. Optimization with Multi-Component Gas Streams

While the VaPRRS was previously shown to be able to capture a mixture of toluene and methyl isobutyl ketone, no ACFC-ESA system has ever been optimized for mutli-component gas streams (*95*). Optimizing the GRS performance for multiple adsorbates is necessarily more complex than optimizing its performance for a single component. For instance, consider a carrier gas with both isobutane and water vapor (Sec 3.6): while raising the ACFC temperature during adsorption may increase the amount of water vapor that is recycled, it would also likely decrease the adsorption capacity of the system for isobutane. In such cases, the goals related to each individual component must be balanced with the other performance goals. Again, a parametric approach could be useful such that certain parameters are held constant while

others are varied and the GRS performance is quantified. While optimization of the system during multi-component operation was not part of this research, it is an obvious extension of this work that would be worth pursuing.

4. Summary and Conclusions

4.1. Research Summary

This research had three major objectives surrounding the development and characterization of a bench-scale adsorption system that combines an activated carbon fiber cloth (ACFC) adsorbent, electrothermal swing adsorption (ACFC-ESA) and post-desorption treatment for capturing and recovering low boiling point organic compounds. These three objectives were achieved as described in the preceding sections.

4.1.1. Develop and Test a Bench-Scale ACFC-ESA System with Post-desorption Treatment

An ACFC-ESA system with post-desorption treatment was developed to capture low boiling point organic compounds and recover them as liquids. The bench-scale system was tested with isobutane as a model compound and characterized with mass and energy balances which showed that isobutane was captured with greater than 99% capture efficiency and required heating and compression energies of 2100 – 3150 kJ/mol of liquid isobutane recovered. This is a significant advancement over previous technology because it expanded the range of compounds that can be captured and recovered with ACFC-ESA from those with boiling points between 50-100°C to those with boiling points below 40°C.

4.1.2. Evaluate and Characterize ACFC-ESA System with Post-desorption Treatment

The second objective of the proposed work was to evaluate the bench-scale ACFC-ESA system with post-desorption treatment using mass and energy balances for several organic compounds that span a range of boiling points and have different functional groups. The compounds of interest in addition to isobutane were n-butane, R134A, and dichloromethane, which have boiling points that span 50°C. Extensive testing with n-butane and R134A was done, however DCM was experienced to be too chemically aggressive for safe and reliable testing with the GRS. Results showed that, in addition to isobutane, n-butane and R134A could both be

captured and recovered as liquids by the GRS with relative pressures ranging from $8.3x10^{-5}$ to $3.4x10^{-3}$. The heating and compression energy to achieve liquid recovery ranged from 10^3 – $5x10^5$ kJ/mol liquefied.

Models to describe the concentration of adsorbate generated during desorption were also developed. These models used adsorption isotherms measured as part of this research and helped explain experimental data that showed how the energy required to capture and liquefy isobutane was a function of ACFC temperature and ACFC heating time. This contribution is important to more fully evaluate the general applicability of this new technology and benchmark its performance with existing technologies.

4.1.3. Conduct Multicomponent Adsorption with Carrier Gas Recirculation for Improved System Sustainability

The final objective of this work was to use the bench-scale ACFC-ESA system to capture isobutane from a carrier gas with relative humidities ranging from 5-80% while maintaining the water vapor concentration of the carrier gas and reducing the O_2 concentration in the carrier gas. These results showed that the GRS operated with greater than 99% capture efficiency for isobutane in low and high humidity carrier gases. In addition, 100% of the water vapor was maintained in the carrier gas for low humidity carrier gases and 60% of the water vapor by mass was maintained in high humidity carrier gases, which will significantly reduce the amount of humidification necessary in an industrial setting. Finally, the steady state oxygen concentration in the GRS was lowered from 19.5% to 16% by implementing carrier gas recirculation, which will reduce the need for N_2 to safely operate the GRS. With changes to the instrumentation or scale of the system, the steady state oxygen concentration could be further reduced. These factors combined resulted in significantly less energy use by the GRS in recycle mode compared to normal operation (4230 and 5750 kJ/mol, respectively). This new ability to recycle the carrier gas stream represents an improvement in system sustainability and a reduction in operating

costs because it reduces the need for re-humidification, reduces the N_2 demand of the system, and significantly reduces the energy required by the system.

4.2. Recommendations for Future Research

There are several avenues for expansion of this research, which fall into two main categories: improving understanding of adsorption/desorption behavior of adsorbates on the GRS and improving GRS performance. In the former category, models developed in this and other research could be modified to include the adsorption of water vapor and other secondary adsorbates on ACFC to better predict performance under realistic operating conditions. While this has been done for organic vapors (*28*) it has not been done for organic gases, such as those explored in this research. In addition, the models could be modified to take into account carrier gas recirculation and/or desorption gas recirculation to more accurately represent the GRS. This would involve modifying the concentration of organic gas in the modeled adsorption gas based on the concentration of organic gas during desorption and in the pressure vessel.

In the latter category, as noted above, performance optimization would be an obvious next step for the GRS, especially with respect to multi-component operation. This could take place via parametric testing of select variables that are known to affect GRS performance (e.g., heating and compression time). The GRS performance could be also improved through examination of ways to increase the effective adsorption capacity of the GRS, such as draining the liquid isobutane collected during operation to minimize the amount of desorbed gas that gets recycled back to adsorption and improving the desorption gas collection algorithm to ensure capture of the most highly concentrated gas stream possible. The ACFC or the entire GRS could also be heated to reduce the competitive adsorption with water vapor experienced at high relative humidities. In addition, the heating algorithm could be modified to allow for a faster increase in ACFC temperature, which was shown in the modeling results reported here to result in higher isobutane concentrations during regeneration. Furthermore, exploration of the GRS's

physical parameters, such as location of adsorption vessel inlets and outlets and the ratio of ACFC cartridge volume to adsorption vessel volume could enhance the performance of the GRS. Finally, as noted in the results and discussion, reducing the ratio of makeup air to N_2 flow could greatly improve the energy and material costs related to N_2. This could be achieved by scaling up the GRS or modifying or eliminating the gas monitoring equipment or, in another scenario, replacing the air in the carrier gas with N_2 at the start of the experiment to remove oxygen from the system entirely.

With increased understanding of system performance and improvements of that performance, the GRS and the ACFC-ESA technology will become more attractive and relevant to industries faced with increasing emissions standards and pressure to reduce costs.

APPENDIX A

A.1 Nomenclature

Variable	Definition
${}^1X^v$	first-order molecular connectivity index
A	Yaws correlation constant
a	amount of water adsorbed at corresponding P_i/P_{is}
A_{cond}	Surface area for conduction
A_{conv}	Surface area for convection
A_{rad}	Surface area for radiation
a_0	DS-4 fitting parameter
A_1	Antoine correlation constant
A_2	Antoine correlation constant
A_3	Antoine correlation constant
A_4	Antoine correlation constant
A_5	Antoine correlation constant
α	thermal coefficient limiting adsorption
b	Langmuir affinity constant
B	Yaws correlation constant
C	Yaws correlation constant
c	DS-4 fitting parameter (eq. 1.8)
c	concentration in the gas phase (ppm_v)
c_p	heat capacity
c_{pf}	heat capacity of fittings

c_{pg}	heat capacity of carrier gas
c_{pl}	heat capacity of liquid adsorbate
c_{ps}	heat capacity of adsorbent
c_{pv}	heat capacity of gaseous adsorbate
ΔH_s	isosteric heat of adsorption
$\Delta h_{vap,T}$	enthalpy of vaporization at temperature T
E	characteristic adsorption energy of the adsorbate
$E_{compress}$	energy required for compression of the desorbed gas
$E_{heating}$	energy required for electrothermal regeneration
E_{sys}	total energy used by the system
ε	emissivity of ACFC
h	convective heat transfer coefficient
I_{RMS}	root mean square current
k	DQSAR parameter that depends only on the adsorbate
k	conductive heat transfer coefficient
$k_{DS\text{-}4}$	DS-4 correlation constant
k_f	Freundlich correlation constant
k_{QHR}	QHR correlation constant
L	length of conduction
LUB	length of unused bed
m_l	condensate mass in control volume
M_{liq}	mass of liquid adsorbate collected
m_s	mass of adsorbent

$M_{t,ads}$	mass of adsorbate adsorbed when $t_i = t_{ads}$
M_{ti}	mass of adsorbate desorbed at time t_i
m_{ti-1}	average mass of adsorbate that has desorbed from t_0 to t_{i-1}
M_{tot}	total mass supplied to the system during the experiment
M_{vap}	mass of adsorbate in the vapor phase of the system
$m_{vessel,total}$	total mass of gas in the adsorption vessel
M_w	molecular weight
m_f	mass of fittings
$m_{water,ads}$	mass of water in the adsorption gas stream
$m_{water,des}$	mass of water desorbed
n	Freundlich correlation constant
P	atmospheric pressure
P_c	critical pressure
P_{50}	isotherm constant defined when $q = q_{50}$ (the amount adsorbed when the outlet concentration is 50% of the inlet adsorbate concentration during a breakthrough curve)
P_i	partial pressure of the adsorbate
P_{is}	saturation partial pressure of the adsorbate
P_{tot}	total pressure in the vessel
q	amount of adsorbate adsorbed on the adsorbent
Q_g	flow rate of carrier gas
Q_{N2}	flow rate of N2 during desorption
$Q_{N2,low}$	low flow rate of N2 during desorption (0.5 SLPM)
$Q_{N2,high}$	high flow rate of N2 during desorption (0.5 SLPM)

$q_{t=0}$	amount of adsorbate adsorbed at the start of desorption
Q_{tot}	total gas flow rate during desorption
$\dot{q}$	dq/dt
q_0	limiting adsorption capacity
q_s	amount of adsorbate adsorbed on the adsorbent at saturation
R	ideal gas constant
ρ	density of the adsorbed material (assumed to be bulk liquid density)
ρ_g	density of carrier gas
ρ_b	gas density at the boiling temperature
ρ_c	gas density at the critical temperature
ρ_l	density of liquid adsorbate
σ	Stefan-Boltzmann constant
t	fitting parameter (eq. 1.2)
t	time
t_{ads}	duration of the adsorption cycle
t_{desorp}	duration of the regeneration process
t_{low}	total desorption time when low flow rate (0.5 SLPM) N_2 was flowing
t_{high}	total desorption time when high flow rate (3.5 SLPM) N_2 was flowing
t_i	time at which the adsorption outlet concentration during a breakthrough curve has reached i% of the inlet concentration
T	absolute temperature

$\dot{T}_{ACFC}$	dT_{ACFC}/dt
T_∞	ambient temperature
T_b	boiling temperature
T_c	critical temperature
TPR	throughput ratio
V	volume of the vessel
VP_A	Wagner correlation constant
VP_B	Wagner correlation constant
VP_C	Wagner correlation constant
VP_D	Wagner correlation constant
V_{RMS}	root mean square voltage
W	volume of adsorbate per mass of adsorbent
W_0	limiting micropore volume
x	$1-T/T_c$
y_i	mole fraction of component i
$y_i(t)$	mass of isobutane desorbed in time step / total mass of gas in vessel in time step
y_{in}	concentration of the adsorbate in the inlet gas stream (mole fraction)
y_{out}	concentration of the adsorbate in the outlet gas stream (mole fraction)

A.2 Cooling Energy Analysis

The energy required for cooling the desorption gas stream can be calculated using one of several methods. The first method is to consider the total power consumed by the cryogenic cooler that is used to chill the glycol/water mixture surrounding the pressure vessel (actual

conditions for bench-scale). The second method is to consider the total energy required to maintain the glycol/water mixture at a given temperature including heat lost to the ambient atmosphere and the cooling requirement to cool and condense the N_2/adsorbate desorption gas stream (100% efficiency for cooling with 16 L glycol/water bath). The third method is to consider only the cooling requirement to chill and condense the N_2/adsorbate desorption gas stream for an adiabatic device. However, analysis of the cooling energy determined using the third method above showed that the cooling component of the total energy when considering experiments with the first through third generation GRS is 1-3% of the total energy requirement (20 kJ/mol compared to 700-1200 kJ/mol for heating (*75*).

A.3 Energy Required to Overcome Pressure Drop

Assuming:

1. Gas velocity into and out of the GRS is constant
2. There is no enthalpy change between the inlet and outlet of the GRS
3. Gas density is constant

$$Power = Q(\Delta P)$$

where ΔP is the pressure drop across the ACFC cartridge, which was measured to be 7 inH_2O when the flow rate through the GRS was 50 SLPM. Converting the pressure drop to Pa and the flow rate to sm^3/s, one can determine the power required to overcome the pressure drop.

$$Power = 8.33x10^{-4}\frac{sm^3}{s}1742Pa = 1.16\frac{J}{s}$$

Multiplying by the total time for an experiment and dividing by the total adsorbate liquefied during the experiment, one can obtain the total energy required to overcome the pressure drop per mole liquid recovered. For example, during an experiment conducted on May

3, 2012, the experiment ran for 347 min and 53.4 g of isobutane was liquefied. This is equivalent to 26.3 kJ/mol liquefied being used to overcome the pressure drop through the ACFC cartridges. The total energy used by the heating and compression systems for this experiment was 2,000 kJ/mol liquefied. The energy to overcome the pressure drop is less than 2% of the total energy used by the system.

A.4 Calculation of derivatives of interest for modeling the desorption process.

From equation 2.11 in section 2.8.1

$$\dot{q} = \frac{\left(-\frac{M_{w,i}PV}{RT}\right)\frac{dy}{dT_{ACFC}}\dot{T}_{ACFC} - \frac{M_{w,i}PQ_{N_2}}{RT}\left[\left(\frac{1}{1-y}\right)t\frac{dy}{dT_{ACFC}}\dot{T}_{ACFC} + yt\frac{d\left(\frac{1}{1-y}\right)}{dT_{ACFC}}\dot{T}_{ACFC} + \frac{y}{1-y}\right]}{\left(m_s + \frac{M_{w,i}PV}{RT}\frac{dy}{dq} + \frac{M_{w,i}PQ_{N_2}}{RT}\left(\left(\frac{1}{1-y}\right)t\frac{dy}{dq} + yt\frac{d\left(\frac{1}{1-y}\right)}{dq}\right)\right)}$$

The time derivatives of the temperature can be found from experimental data or from artificially created data (used to test different scenarios). All other derivatives must be derived from the DR and Antoine Equations (below). In particular, the following derivatives are required (note that T has replaced T_{ACFC} for simplicity):

$$\frac{dy}{dT}, \frac{d\left(\frac{1}{1-y}\right)}{dT}, \frac{dy}{dq}, \text{ and}$$

The DR Equation is:

$$W = W_0 \exp\left(-\left(\frac{RT\ln\left(\frac{P_{is}}{P_i}\right)}{E}\right)^2\right)$$

and W and W_0 can be replaced by q and q_0 knowing the following relationships:

$$q = \rho_L W$$
$$q_0 = \rho_L W_0$$

to give:

$$q = q_0 \exp\left(-\left(\frac{RT \ln\left(\frac{P_{is}}{P_i} \right)}{E} \right)^2 \right)$$

The Antoine Equation is:

$$P_{is} = \exp\left(A_1 + \frac{A_2}{T} + A_3 \ln(T) + A_4 T^{A_5} \right)$$

Rearrange the DR equation to solve for $\frac{P_{is}}{P_i}$

$$\frac{P_{is}}{P_i} = \exp\left(\frac{E}{RT} \sqrt{-\ln\left(\frac{q}{q_0} \right)} \right)$$

According to Dalton's Law:

$$y = \frac{P_i}{P_{tot}}$$

To obtain an expression for y, divide the Antoine equation by the rearranged DR equation and P_{tot}:

$$y = \frac{\exp\left(A_1 + \frac{A_2}{T} + A_3 \ln(T) + A_4 T^{A_5} \right)}{P_{tot} \exp\left(\frac{E}{RT} \sqrt{-\ln\left(\frac{q}{q_0} \right)} \right)} = \frac{\exp\left(A_1 + \frac{A_2}{T} + A_3 \ln(T) + A_4 T^{A_5} - \frac{E}{RT} \sqrt{-\ln\left(\frac{q}{q_0} \right)} \right)}{P_{tot}}$$

from this equation, the derivatives of y with respect to T and q can be determined.

Recalling the exponential rule for derivatives:

$$\frac{de^u}{dx} = e^u \frac{du}{dx}$$

$$\frac{dy}{dT} = \frac{\exp\left(A_1 + \frac{A_2}{T} + A_3 \ln(T) + A_4 T^{A_5} - \frac{E}{RT} \sqrt{-\ln\left(\frac{q}{q_0} \right)} \right)}{P_{tot}} \left(-\frac{A_2}{T^2} + \frac{A_3}{T} + A_4 A_5 T^{A_5 - 1} - \frac{E}{RT^2} \sqrt{-\ln\left(\frac{q}{q_0} \right)} \right)$$

$$\frac{dy}{dq} = \frac{\exp\left(A_1 + \frac{A_2}{T} + A_3 \ln(T) + A_4 T^{A_5} - \frac{E}{RT} \sqrt{-\ln\left(\frac{q}{q_0} \right)} \right)}{P_{tot}} \left(\frac{E}{2RTq \sqrt{-\ln\left(\frac{q}{q_0} \right)}} \right)$$

Use the equation for y to solve for $\frac{1}{1-y}$

$$\frac{1}{1-y} = \frac{1}{1 - \frac{P_{tot}}{\exp\left(A_1 + \frac{A_2}{T} + A_3 \ln(T) + A_4 T^{A_5} - \frac{E}{RT} \sqrt{-\ln\left(\frac{q}{q_0} \right)} \right)}}$$

Use the symbolic method in MATLAB (v. 2013a) to determine $\frac{d\left(\frac{1}{1-y}\right)}{dT}$ and $\frac{d\left(\frac{1}{1-y}\right)}{dq}$

$$\frac{d\left(\frac{1}{1-y}\right)}{dT} = \frac{-P_{tot}\exp\left(\frac{E\sqrt{-\log\left(\frac{q}{q_0}\right)}}{RT} - \frac{A_2}{T} - A_3\log(T) - A_4T^{A_5} - A_1\right)\left(\frac{A_3}{T} - \frac{A_2}{T^2} + A_4A_5T^{(A_5-1)} + \frac{E\sqrt{-\log\left(\frac{q}{q_0}\right)}}{RT^2}\right)}{\left(P_{tot}\exp\left(\frac{E\sqrt{-\log\left(\frac{q}{q_0}\right)}}{RT} - \frac{A_2}{T} - A_3\log(T) - A_4T^{A_5} - A_1\right) - 1\right)^2}$$

$$\frac{d\left(\frac{1}{1-y}\right)}{dq} = \frac{-P_{tot}\exp\left(\frac{E\sqrt{-\log\left(\frac{q}{q_0}\right)}}{RT} - \frac{A_2}{T} - A_3\log\left(T\right) - A_4T^{A_5} - A_1\right)}{2RTq\left(\sqrt{-\log\left(\frac{q}{q_0}\right)}\right)\left(P_{tot}\exp\left(\frac{E\sqrt{-\log\left(\frac{q}{q_0}\right)}}{RT} - \frac{A_2}{T} - A_3\log\left(T\right) - A_4T^{A_5} - A_1\right) - 1\right)^2}$$

A.5 MATLAB® Code

```
%This code is written to determine the rate of desorption of isobutane from
%ACFC-15 during electrothermal regeneration using a combination of mass and
%energy balances.

clear all
close all
clc

%Define the temperature profile we wish to determine the results for.
 %Read in temperature data from excel 1st column is time (seconds) 2nd column
   %is temp (K).

  TimeTemp = xlsread('042413_Iso_TempData.xls');

   Time = TimeTemp (:,1);
   Temp = TimeTemp(:,2);

%-------------------------------------------------------------------------
%Find fitting parameters for temperature data with a polynomial of defined
%order
PolyOrder = 3;
FittingParams = polyfit(Time, Temp, PolyOrder);


%General parameters
P = 1; %pressure in atm
Ptot = P*101325; %total system pressure in Pascals
Rconst1 = 0.08206; %L-mol/atm-K gas constant
Rconst2 = 8.31; %J/mol-K gas constant
T0 = 293; %K initial temperature in the system ~20C
Tinf = T0; %temperature far away from vessel (room temp)
t_init = Time(1); %intial time
t_final = Time(length(Time)); % seconds final time for analysis (4 minutes)
TimeSpan = [t_init, t_final]; %defines the time span for analysis
Boltzmann = 5.67 * 10^(-8); %W/m^2-K^4 Boltzmann constant

%-------------------------------------------------------------------------

V_vessel = 1.436; %L - volume of adsorber see pp 289 of lab notebook #2



%-------------------------------------------------------------------------
%Purge Gas parameters
QN2 = 0.5; %SLPM- flow of nitrogen during regeneration
LowFlowN2Time = 300; %Time in seconds that low flow N2 + heating is occurring
QN2_high = 3.5; %SLPM - high flow N2 flow rate
```

```
MW_N2 = 28; %g/mol


%------------------------------------------------------------------------
%Isobutane parameters
MW_iso = 58.12; %g/mol molecular weight of isobutane
rho_l_iso = 0.598; %g/cm^3 density of the liquid phase at 20C (source: Perry's p2-31)

W0 = 0.543; %cm^3/g ACFC; DR parameter for isobutane on ACFC-15 determined with
isotherms

q0 = W0*rho_l_iso; %g iso/g ACFC; DR parameter found by multiplying W0 by rhoL

E = 19575; %J/mol; DR parameter for isobutane on ACFC-15 determined with isotherms

Ci = 2000; %inlet concentration of isobutane in ppmv

Piso = Ci/10^6 * 101325; %partial pressure of isobutane in Pascals

reduc = 0.36; %Reduction in adsorption capacity between real system and isotherm model.
Based on experiments with GRS

q0mod = reduc*q0;%Reduces the q0 value by the reduction multiplier

%Antoine Constants for Isobutane: Ps = exp(A1+A2/T+A3lnT+A4T^A5) gives pressure in Pa if T
is in K:
   A1 = 100.18;
   A2 = -4814.9;
   A3 = -13.541;
   A4 = 0.0201;
   A5 = 1;

%Antoine equation
Pis = exp(A1+A2/T0 + A3*log(T0) + A4*(T0)^A5);

qiso_0 = q0mod*exp(-(Rconst2*T0*log(Pis/Piso)/E)^2); %Determine the initial amount of
isobutane adsorbed based on the DR equation

%------------------------------------------------------------------------
%ACFC parameters

m_ACFC = 115; %g of ACFC per vessel

%Determine the adsorbed amount at the given time and loading

ADS_AMOUNT = @(t, q) AdsorbedAmount(t, q, A1, A2, A3, A4, A5, Rconst1, Rconst2,...
   MW_iso, Ptot, V_vessel, QN2, m_ACFC, q0mod, E, FittingParams, PolyOrder);

options = odeset(odeset('RelTol', 1e-4, 'AbsTol', 1E-5));
```

```
%use an ODE solver and provides a matrix of time and q using the function AdsorbedAmount
[TimeOut,qCalc] = ode45 (ADS_AMOUNT, TimeSpan, qiso_0, options);

%Set up variables for results
Y = zeros(1, length(TimeOut));
m = zeros(1, length(TimeOut));
Q = zeros(1, length(TimeOut));
MassLeaving=zeros(1,length(TimeOut));
Yavg = zeros(1, length(TimeOut));
index = find(TimeOut > LowFlowN2Time); %Find the indices of the TimeOut...
   %matrix where the values of TimeOut are greater than the LowFlowN2 Time

for i = 1 : length(TimeOut)

   %This if statement determines if we're in the low or high flow N2 range.
   %If in the low flow, the total amount of N2 through the system is
   %simply the low flow rate times the total time. If we're in the high
   %flow rate, the total N2 through the system is the amount that flowed
   %through during low flow plus however much has flowed during high flow
   %so far.
   if i < index(1)
      QN2_used = QN2;
      Q(i) = (QN2_used/60) * (TimeOut(i)); %total vol of N2 that has left the vessel
   else
      QN2_used = QN2_high;
      Q(i) = Q(index(1)-1) + (QN2_used/60)*(TimeOut(i)-LowFlowN2Time);

   end

   Z = MW_iso * P / (Rconst1 * T0);

   m(i) = m_ACFC*(qCalc(i) - qCalc(1)); %mass of isobutane that has left the ACFC at time i


   if i ==1
         Yavg(i) = 0;

   else
         Yavg(i) = mean(Y(1:(i-1))); %calculates the average concentration of isobutane that has
left the vessel with the nitrogen


   end


   Y(i) = (- m(i) - (Z*Yavg(i)/(1-Yavg(i)))*(Q(i)))/(Z*V_vessel);

   %Contrain results to be between zero and 1
```

```
    if Y(i)>1
        Y(i)=0.99;
    else if Y(i)<0
            Y(i)=0;
        else Y(i)=Y(i);
        end
    end

    %outlet isobutane concentration = mass that has left the ACFC - average
    %amount that has left the vessel (comes from mass balance)
    %knowing yiso+ yN2 = 1; iso_generated = totalmolesout * yiso,out
%
end


%Finds T of cloth given the time based on an earlier fitting of the T vs t
%data
T = zeros(1,length(TimeOut));

for j = 1:length(TimeOut)

    for i = 1:length(FittingParams)

        T(j) = T(j) + FittingParams(i)*TimeOut(j)^(PolyOrder-i+1);


    end
end

TempC = Temp - 273.15;


%%Plotting data generated

plot(TimeOut, Y, 'k','LineWidth',1.1)


hold on
xlabel('time (seconds)', 'fontsize', 14)
ylabel('Isobutane Outlet Concentration (mol frac)', 'fontsize',14)
%title('Isobutane Concentration with Time')
axis([0 TimeOut(length(TimeOut)) 0 1])



figure(2)
[ax, h1, h2]=plotyy(TimeOut,Y, Time, TempC); %plots isobutane concentration out and temp on
same plot
hold on
```

```
legend('Isobutane Mole Fraction', 'ACFC Temp','Location','NorthWest')
xlabel('time (s)', 'fontsize', 14)

axes(ax(1)); ylabel('Isobutane Outlet Concentration (mol frac)', 'fontsize',14,'color','black');
axes(ax(2)); ylabel('ACFC Temp (\circC)','fontsize',14);
box(ax(1),'off')
set(h1,'LineWidth',1.1,'LineStyle','-','color','black');
set(h2,'LineWidth',1.1, 'LineStyle','--','color','black');
set(ax(1),'ylim',[0 1], 'YTick', linspace(0,1,11),'ycolor','k','fontsize',12)
set(ax(2),'ylim',[20 160],'YTick', linspace(20,160,8),'ycolor','k','fontsize',12)
```

```
function dqdt = AdsorbedAmount(t, q, A1, A2, A3, A4, A5, Rconst1, Rconst2,...
    MWads, Ptot, V_vessel, QN2, m_ACFC, q0, E, FittingParams, PolyOrder)

%differential equation to determine q as a function of T, which will be fed
%in to the MATLAB function ode45
%dq/dt = (-PVMw/RT * dy/dT*dT/dt - WPMwy/RT)/(PVmw/RT *dy/dq - ms)
%T values must be in kelvin, Ptot in Pa

T0 = 293;
T_N2 = 298;

Ptot_atm = Ptot/101325; %converts pressure in Pa to atm

T = 0; %initialize the temperature T as 0 before calculating

%Finds T of cloth in K given the time based on an earlier fitting of the T vs t
%data
for i = 1:length(FittingParams)

    T = T + FittingParams(i)*t^(PolyOrder-i+1);

end


R = Rconst2;


Pis = exp(A1+A2/T+A3*log(T)+A4*T^(A5)); % saturated isobutane pressure (Pa) at T

Pads = Pis/(exp((-log(q/q0))^(0.5)*E/(R*T))); %Partial pressure of adsorbate given q and T (Pa)

Y = Pads/Ptot;
```

```
%Calls function DeltaYDeltaTemp,DeltaYDeltaq, and DeltaTDeltat
%to determine the change in gas phase concentration with temperature, the
%change in gas phase concentration with adsorbed amount, and the change
%ACFC temperature with time.


dYdT = DeltaYDeltaTemp(A1, A2, A3, A4, A5, T, R, Ptot, E, q0, q);

dYdq = DeltaYDeltaq(A1, A2, A3, A4, A5, T, R, E, q0, Ptot, q);

dTdt = DeltaTDeltat(FittingParams, PolyOrder, T, t);

dYinvdT = DeltaYInverseDeltaT(A1, A2, A3, A4, A5, T, R, Ptot, E, q0, q);

dYinvdq = DeltaYInverseDeltaq(A1, A2, A3, A4, A5, T, R, Ptot, E, q0, q);


Z1 = Ptot_atm*MWads/(Rconst1*T); %defines a common constant
Z2 = Ptot_atm*MWads/(Rconst1*T_N2);



dqdt = (-Z1*V_vessel*dYdT*dTdt - Z2*QN2*((1/(1-Y))*t*dYdT*dTdt + Y*t*dYinvdT*dTdt+Y/(1-
Y)))...
    /(m_ACFC + Z1*V_vessel*dYdq + Z2*QN2*((1/(1-Y))*t*dYdq + Y*t*dYinvdq));
```

```
function dYdT = DeltaYDeltaTemp(A1, A2, A3, A4, A5, T, R, Ptot, E, q0, q)
%This function determines the change in gas phase mole fraction of isobutane as a funciton
%of temperature assuming that the DR and Antoine equations are applicable.
%A1 through A5 are Antoine constants, T is the temp in K, R is the gas
%constant in J/mol-K, Ptot is the total system pressure in Pascals
%E is the adsorption energy term from the DR equation
%q0 is the max adsorptionc capacity from the DR equation in g / gACFC and q
%is the adsorption capacity at T = T from the DR equation g / gACFC

dYdT = (exp(A1 + A2/T + A3*log(T) + A4*T^A5 - (E*(-log(q/q0))^(1/2)) / (R*T))     * (A3/T -
A2/T^2 + A4*A5*T^(A5 - 1) + (E*(-log(q/q0))^(1/2))/(R*T^2)))/Ptot;
```

```
function dYdq = DeltaYDeltaq(A1, A2, A3, A4, A5, T, R, E, q0, Ptot, q)
%This function determines the change in gas phase concentration as a funciton
%of adsorbed mass assuming that the DR and Antoine equations are applicable.
%A1 through A5 are Antoine constants, T is the temp in K, R is the gas
%constant in J/mol-K, E is the adsorption energy term from the DR equation
%and q0 is the max adsorptionc capacity from the DR equation in g / gACFC
```

```
%%The equation below was found using MATLAB symbolic function

dYdq = (E*exp(-(E*(-log(q/q0))^(1/2))/(R*T))*exp(A1 + A2/T + ...
    A3*log(T) + A4*T^A5))/(2*Ptot*R*T*q*(-log(q/q0))^(1/2));
```

```
function dTdt = DeltaTDeltat(FittingParams,order, T, t)
%this function cacluates dTdt given the fitting parameters for the data of
%temp versus time, the order of the fitting equation, and the temperature
%(K)

if t == 0
    dTdt = 0;
else

DiffCoeff = zeros(1,length(FittingParams-1));

dTdt = 0;
for i = 1 : length(FittingParams-1)

    DiffCoeff(i) = (order-i+1)*FittingParams(i);

    dTdt = dTdt + DiffCoeff(i)*t^(order-i);

end
end
```

```
function dYinvdT = DeltaYInverseDeltaT(A1, A2, A3, A4, A5, T, R, Ptot, E, q0, q)

%This function determines the change in the function 1/(1-y) as a function
%of T assuming that the DR and Antoine equations are applicable.
%A1 through A5 are Antoine constants, T is the temp in K, R is the gas
%constant in J/mol-K, E is the adsorption energy term from the DR equation
%and q0 is the max adsorption capacity from the DR equation in g / gACFC


dYinvdT = -(Ptot*exp((E*(-log(q/q0))^(1/2))/(R*T) - A2/T - A3*log(T) -...
A4 * T ^ A5 - A1)*(A3/T - A2/T^2 + A4*A5*T^(A5 - 1) +... (E*(log(q/q0))^(1/2)) /(R*T^2)))/
(Ptot*exp((E*(-log(q/q0))^(1/2))/ ...
(R*T) - A2/T - A3*log(T) - A4*T^A5 - A1) - 1)^2;
```

```
function dYinvdq = DeltaYInverseDeltaq(A1, A2, A3, A4, A5, T, R, Ptot, E, q0, q)

%This function determines the change in the function 1/(1-y) as a function
```

```
%of adsorbed mass assuming that the DR and Antoine equations are applicable.
%A1 through A5 are Antoine constants, T is the temp in K, R is the gas
%constant in J/mol-K, E is the adsorption energy term from the DR equation
%and q0 is the max adsorption capacity from the DR equation in g / gACFC

dYinvdq = -(Ptot*exp((E*(-log(q/q0))^(1/2))/(R*T) - A2/T - A3*log(T)...
    - A4*T^A5 - A1)*(A3/T - A2/T^2 + A4*A5*T^(A5 - 1) + ...
    (E*(-log(q/q0))^(1/2))/(R*T^2)))/(Ptot*exp((E*(-log(q/q0))^(1/2))/...
    (R*T) - A2/T - A3*log(T) - A4*T^A5 - A1) - 1)^2;
```

REFERENCES

1 NCDC: Greenhouse Gases. http://www.ncdc.noaa.gov/oa/climate/gases.html#carbonmonoxide (Accessed Mar 23, 2011).

2 EPA. TRI Chemicals, TRI Program, EPA. http://www.epa.gov/tri/trichemicals/index.htm (Accessed Mar 23, 2011).

3 Indiana Department of Environmental Management. Title V Operating Permit: Pregis Innovative Packaging, Plymouth Indiana. **2007**. T099-17908-00028.

4 EPA. *Inventory of US Greenhouse Gas Emissions and Sinks: 1990-2012*; EPA430-R-14-001; U.S. Environmental Protection Agency, Office of Atmospheric Programs, Washington, D.C., April, 2014.

5 Requirements for Preparation, Adoption, and Submittal of Implementation Plans. *Code of Federal Regulations*, Part 51, Title 60, 2005.

6 EPA. Polystyrene. *Compilation of Air Pollutant Emission Factors*, *Volume 1: Stationary Point and Area Sources,* AP-42, Fifth Edition; U.S. Environmental Protection Agency, Office of Air Quality Planning and Standards, Research Triangle Park, North Carolina, January, 1995.

7 U.S. Resin production and sales 2012 vs. 2011. American Chemistry Council. April 2013.

8 EPA. *Control of VOC Emissions From Polystyrene Foam Manufacturing.* U.S. Environmental Protection Agency, Office of Air Quality Planning and Standards, EPA-450/3-90-020. Research Triangle Park, North Carolina, 1990.

9 Cooper, D. C.; Alley, F. C. *Air Pollution Control: A Design Approach*. 3rd ed.; Waveland Press, Inc.: Prospect Heights, IL, 2002; pp 323, 393.

10 Johnsen, D.L. Monitoring and Control of Electrothermal Swing Adsorption Based on Electrical Properties of the Adsorbent. Ph.D. Dissertation, University of Illinois, Urbana-Champaign, **2014.**

11 Khan, F. I.; Goshal, A.K. Removal of volatile organic compounds from polluted air. *Journal of Loss Prevention in the Process Industries*. **2000**, *13*, 527-545.

12 Hunter, P. and Oyama, S.T. (2000) Control of Volatile Organic Compound Emissions: Conventional and Emerging Technologies. John Wiley & Sons, New York.

13 Altwicker, E. R.; Canter, L. W.; Cha, S. S.; Chuang, K. T.; Liu, D. H. F.; Ramachandran, G.; Raufer, R. K.; Reist, P. C.; Sanger, A. R.; Turk, A.; Wagner, C. P. Air Pollution. In *Environmental Engineers' Handbook*; Liu, D. H. F.; Liptak, B. G., Eds.; CRC Press: 1999.

14 Perry, R. H.; Green, D.W. *Perry's Chemical Engineers' Handbook*, 7th ed.; McGraw Hill: New York, 1997.

15 Noll, K. E. *Fundamentals of Air Quality Systems*; American Academy of Environmental Engineers: 1999.

16 Parmar, G.; Rao, N. Emerging control technologies for volatile organic compounds. *Critical Reviews in Environ. Sci. Technol.* **2009,** *39* (1), 41-78.

17 DeNevers, N. *Air Pollution Control Engineering*; McGraw Hill: New York, 1995.

18 Khan, F. I.; Ghoshal, A. K. Removal of Volatile Organic Compounds from polluted air. *Journal of Loss Prevention in the Process Industries.* **2000,** *13* (6), 527-545.

19 Jiang, X.; Ding, J.; Kumar, A. Polyurethane-poly(vinylidene fluoride) (PU-PVDF) thin film composite membranes for gas separation. *J. Membr. Sci.* **2008,** *323* (2), 371-378.

20 Baker, R. W.; Wijmans, J. G. *Membrane Separation of Organic Vapors From Gas Streams*; CRC Press: Boca Raton, 1994.

21 Deng, S.; Sourirajan, A.; Matsuura, T.; Farnand, B. Study of volatile hydrocarbon emission control by an aromatic poly(ether imide) membrane. *Ind. Eng. Chem. Res.* **1995,** *34* (12), 4494-4500.

22 Ribeiro, C. P.; Lage, P. L. C.; Borges, C. P. A combined gas-stripping vapour permeation process for aroma recovery. *J. Membr. Sci.* **2004,** *238* (1-2), 9-19.

23 Yang, Y.T. *Adsorbents: Fundamentals and Applications;* John Wiley & Sons: Hoboken, NJ, 2003; pp 3.

24 Noll, K.E., Gounaris, V., Hou, W. *Adsorption Technology for Air and Water Pollution Control;* Lewis Publishers, Inc: Chelsea, MI, 1992; pp 2-7.

25 Lo, S. Characterization of the Chemical, Physical, Thermal, and Electrical Properties of a Series of Activated Carbon Fiber Cloths. University of Illinois, Urbana, IL, 2002.

26 Yu, F. D.; Luo, L.A.; Grevillot, G. Adsorption Isotherms of VOCs onto Activated Carbon Monolith: Experimental Measurements and Correlation with Different Models. *J. of Chem. Eng. Data*. **2002,** *47* (3), 467-473.

27 Ruthven, D. M., *Principles of Adsorption and Adsorption Processes*; Wiley: New York, 1984; pp 270-271.

28 Cal, M.P.; Larson, S.M.; Rood, M.J. Experimental and modeled results describing the adsorption of acetone and benzene onto activated carbon fibers. *Environmental Progress.* **1994**, *13* (1), 26-30.

29 Lordgooei, M.; Carmichael, K. R.; Kelly, T. W.; Rood, M. J.; Larson, S. M. Activated carbon cloth adsorption-cryogenic system to recover toxic volatile organic compounds. *Gas Sep. Purif.* **1996**, *10* (2), 123-130.

30 Subrenat, A.; Le Cloirec, P. Thermal behavior of activated carbon cloths heated by Joule effect. *J. Environ. Eng.* **2003**, *129* (12), 1077-1084.

31 Petkovska, M.; Tondeur, D.; Grevillot, G.; Granger, J.; Mitrović, M. Temperature-swing gas separation with electrothermal desorption step. *Sep. Sci. and Technol.* **1991**, *26* (3), 425–444.

32 Baudu, M.; LeCloirec, P.; Martin, G. Thermal regeneration by Joule effect of activated carbon for air treatment. *Environ. Technol.* **1992**, *13* (5), 423–435.

33 Foster, K. L.; Fuerman, R. G.; Economy, J.; Larson, S. M.; Rood, M. J. Adsorption characteristics of trace volatile organic compounds in gas streams onto activated carbon fibers. *Chem. Mater.* **1992**, *4* (5), 1068-1073.

34 Physical properties of gases, safety, MSDS, enthalpy, material compatibility, gas liquid equilibrium, density, viscosity, flammability, transport properties. http://encyclopedia.airliquide.com/encyclopedia.asp. (accessed April 17, 2011).

35 Dichloromethane - Solvent Center, Sigma Aldrich. http://www.sigmaaldrich.com/chemistry/solvents/dichloromethane-center.html. (Accessed August 6, 2014).

36 Miyamoto, H.; Koshi, T.; Uematsu, M. *J. Chem. Thermodynamics.* **2008**, *40*, 1222–1225.

37 Younglove, B.A. and Ely, J.F. Thermophysical Properties of Fluids. II. Methane, Ethane, Propane, Isobutane, and Normal Butane. *J. Phys. Chem. Ref. Data.* **1967**, *16*(4). 577-798.

38 1,1,1,2-tetrafluoroethane | R134A | ChemSpider. http://www.chemspider.com/Chemical-Structure.12577.html. Accessed August 7, 2014.

39 Mao, Z.; Sinnott, S.B. Separation of organic molecular mixtures in carbon nanotubes and bundles: molecular dynamics simulations. *J. Phys. Chem. B.* **2001**, *105*, 6916-6924.

40 Silvestre-Albero, J.; Wahby, A.; Sepulveda-Escribano, A.; Martinez-Escandell, M.; Kaneko, K.; Rodriguez-Reinoso, F. Ultrahigh CO_2 adsorption capacity on carbon molecular sieves at room temperature. *Chem. Commun.*, **2011**, *47*. Supplemental Material.

41 Nirmalakhandan, N.N.; Speece, R.E. Prediction of activated carbon adsorption capacities for organic vapors using quantitative structure-activity relationship methods. *Environ. Sci. Technol.* **1993,** *27* (8), 1512-1516.

42 Dombrowski, K. D.; Lehmann, C. M. B.; Sullivan, P. D.; Ramirez, D.; Rood, M. J.; Hay, K. J. Organic vapor recovery and energy efficiency during electric regeneration of an activated carbon fiber cloth adsorber. *J. of Environ. Eng.* **2004,** *130* (3), 268-275.

43 Do, D.D.; Do, H.D. Surface diffusion of hydrocarbons in activated carbon: comparison between constant molar flow, differential permeation and differential adsorption bed methods. *Adsorption*. **2001**, *7*(3), 189-209.

44 Qi, N.; Appel, W.S.; LeVan, M.D. Adsorption Dynamics of Organic Compounds and Water Vapor in Activated Carbon Beds. *Ind. Eng. Chem. Res.* **2006**, *45*, 2303-2314.

45 Cal, M. P.; Rood, M. J.; Larson, S. M., Gas phase adsorption of volatile organic compounds and water vapor on activated carbon cloth. *Energy & Fuels.* **1997,** *11* (2), 311-315.

46 Cal, M. P.; Rood, M. J.; Larson, S. M. Removal of VOCs from humidified gas streams using activated carbon cloth. *Gas Separation & Purification.* **1996,** *10* (2), 117-121.

47 Russell, B. P.; LeVan, M. D. Coadsorption of organic compounds and water vapor on BPL activated carbon .3. Ethane, propane, and mixing rules. *Ind. Eng. Chem. Res.* **1997,** *36* (6), 2380-2389.

48 Sullivan, P.D., Stone, B. R., Hashisho, Z., Rood, M. J. Water adsorption with hysteresis effect onto microporous activated carbon fabrics. *Adsorption*. **2007**, *13*, 173-189.

49 Brunauer, S.; Deming, L.S. On a theory of the van der Waals adsorption of gases. *J. Am. Chem. Soc*. **1940**, *62*(7),1635-1888.

50 Ramirez, D.; Sullivan, P.; Rood, M.; Hay, K. Equilibrium adsorption of phenol-, tire-, and coal-derived activated carbons for organic vapors. *J. Environ. Eng.* **2004,** *130* (3), 231-241.

51 Ramirez, D. Capture and Recovery of Organic Vapors with an Electrothermal-Swing Adsorption System. Ph.D. Dissertation, University of Illinois, Urbana-Champaign, **2005**.

52 Do, D.D. *Adsorption Analysis: Equilibria and Kinetics*; Imperial College Press: London, 1998; pp 51.

53 EPA. GAC Isotherm. Drinking Water Treatability Database. http://iaspub.epa.gov/tdb/pages/treatment/treatmentOverview.do?treatmentProcessId=-979193564. Accessed 15July2014.

54 Walton, K.S., Cavalcante, C.L., LeVan, M.D. Adsorption if Light Alkanes on Coconut Nanoporous Activated Carbon. *Brazilian J. of Chem. Eng*. **2006**, *23*(4), 555-561.

55 Yaws, C.L., Bu, L., Nijhawan, S. *Pollution Engineering.* **1995,** *27*(2), 34-37.

56 Yaws, C.L., Bu, L., Nijhawan, S. Equation Calculates Activated Carbon's Capacity for Adsorbing Pollutants. *Oil & Gas J.* **1995,** *93*(7).

57 Dubinin, M. M. Fundamentals of the Theory of Adsorption in Micropores of Carbon Adsorbents: Characteristics of Their Adsorption Properties and Microporous Structures. *Carbon.* **1989,** *27*(37), 457-467.

58 Nirmalakhandan, N.N., Speece, R.E. Prediction of activated carbon adsorption capacities for organic vapors using quantitative structure-activity relationship methods. *Environ. Sci. Technol*. **1993,** *27* (8), pp. 1512-1516.

59 Prakash, J.; Nirmalakhandan, N.; Speece, R. E. Prediction of Activated Carbon Adsorption-Isotherms for Organic Vapors. *Environ. Sci. Technol.* **1994,** *28* (8), 1403-1409.

60 Qi, S. Y.; Hay, K. J.; Rood, M. J. Isotherm equation for water vapor adsorption onto activated carbon. *J. Environ. Eng.* **1998,** *124* (11), 1130-1134.

61 Hashisho, Z.; Emamipour, H.; Rood, M. J.; Hay, K. J.; Kim, B. J.; Thurston, D. Concomitant adsorption and desorption of organic vapor in dry and humid air streams using microwave and direct electrothermal swing adsorption. *Environ. Sci. Technol.* **2008,** *42* (24), 9317-9322.

62 Qi, S. Y.; Hay, K. J.; Rood, M. J.; Cal, M. P. Equilibrium and heat of adsorption for water vapor and activated carbon. *J. Environ. Eng. A.* **2000,** *126* (3), 267-271.

63 Chakraborty, A.; Saha, B. B.; Koyama, S.; Ng, K. C. On the thermodynamic modeling of the isosteric heat of adsorption and comparison with experiments. *Appl. Phys. Lett.* **2006,** *89* (17), 3.

64 Sircar, S. Recent developments in macroscopic measurement of multicomponent gas adsorption equilibria, kinetics, and heats. *Ind. Eng. Chem. Res.* **2007,** *46* (10), 2917-2927.

65 Sircar, S.; Mohr, R.; Ristic, C.; Rao, M. B. Isosteric heat of adsorption: Theory and experiment. *J. Phys. Chem. B.* **1999,** *103* (31), 6539-6546.

66 Ramirez, D.; Qi, S. Y.; Rood, M. J. Equilibrium and heat of adsorption for organic vapors and activated carbons. *Environ. Sci. Technol.* **2005,** *39* (15), 5864-5871.

67 Hashisho, Z.; Rood, M.J.; Botich, L. Microwave swing adsorption to capture and recover vapors from air streams with activated carbon fiber cloth. *Environ. Sci. Technol.* **2005,** *39* (17), 6851-6859.

68 Petkovska, M., and Mitrovic, M. Microscopic modeling of electrothermal desorption. *Chem. Eng. J. & Biochem. Eng. J.* **1994,** *53* (3), 157-165.

69 Sullivan, P. D.; Rood, M. J.; Dombrowski, K. D.; Hay, K. J. Capture of organic vapors using adsorption and electrothermal regeneration. *J. Environ. Eng.* **2004,** *130* (3), 258-267.

70 Sullivan, P. D.; Rood, M. J.; Grevillot, G.; Wander, J. D.; Hay, K. J. Activated carbon fiber cloth electrothermal swing adsorption system. *Environ. Sci. Technol.* **2004,** *38* (18), 4865-4877.

71 Ramirez, D. Vidal, E. X., Rood, M. J., Hay, K. J. Pilot-scale electrothermal-swing adsorption system for the capture and recovery of vapor emissions from a painting facility, 98th Annual Meeting of the Air & Waste Management Association, Minneapolis, MN, **2005**, No. 1295, pp. 14.

72 Emamipour, H.; Hashisho, Z.; Cevallos, D.; Rood, M.; Thurston, D.; Hay, K.; Kim, B.; Sullivan, P. Steady-state and dynamic desorption of organic vapor from activated carbon with electrothermal swing adsorption. *Environ. Sci. Technol.* **2007,** *41* (14), 5063-5069.

73 Mallouk, K. E.; Johnsen, D. L.; Rood, M. J. Capture and Recovery of Isobutane by Electrothermal Swing Adsorption with Post-Desorption Liquefaction. *Environ. Sci. Technol.* **2010,** *44* (18), 7070-7075.

74 Aeropres 17 (A-17), Chemical Information. Aeropres Corp. 2009.

75 Mallouk, K.E.; Rood, M.J. Energy Efficiency during Capture and Recovery of Organic Gases with Activated Carbon Fiber Cloth, Electrothermal Swing Adsorption, and Post-Desorption Treatment. *Proceedings of the Air & Waste Management Assoc. Annual Conference & Exhibition*. Orlando, FL. **2011**. Paper No. 53.

76 Carrico, C. M., M. J. Rood, and J. A. Ogren. Aerosol light scattering properties at Cape Grim, Tasmania, during the First Aerosol Characterization Experiment (ACE 1), *J. Geophys. Res*. **1998**, *103*(D13), 16565–16574.

77 Johnsen, D.J., Mallouk, K.E., Rood, M.J. Control of Electrothermal Heating During Regeneration of Activated Carbon Fiber Cloth. *Environ. Sci. Technol*. **2011**, *45* (2), 738-743.

78 Niknaddaf, S., Atkinson, J.D., Shariaty, P., Jahandar-Lashaki, M., Hashisho, Z., Philips, J.H., Anderson, J.E., and Nichols, M. Heel Formation during Volatile Organic Compound Desorption from Activated Carbon Fiber Cloth Using Resistive Heating. *Carbon*. **2016**, *96*, 131-138.

79 Bridgeman, O.C., Aldrich, E.W., Vapor Pressure Tables for Water, *J. Heat Transfer*, 1964, 86, 2, 279-286.

80 Nitrogen Generators: Advanced Gas Technologies. http://adgastech.com/Products/Industrial-Gas-Generators/Nitrogen-Generators/. Accessed 20Sep2014.

81 EIA Electricity Data. http://www.eia.gov/electricity/monthly/epm_table_grapher.cfm?t=epmt_5_6_a. Accessed 20Sep2014.

82 Sullivan, P. D.; Rood, M. J.; Hay, K. J.; Qi, S., Adsorption and electrothermal desorption of hazardous organic vapors. *J. Environ. Eng*. **2001,** *127* (3), 217-223.

83 Mallouk, K.E.; Rood, M.J. Characterization of Adsorption of Select Organic Gases on Activated Carbon Fiber Cloth. *Proceedings of the Air & Waste Management Assoc. Annual Conference & Exhibition*. San Antonio, TX. **2012**. Paper No. 65.

84 ode45: Solve nonstiff differential equations; medium order method. http://www.mathworks.com/help/matlab/ref/ode45.html. Accessed 01Dec2014.

85 Yun, J.H.; Choi, D.K. *Ind. Eng. Chem. Res.* **1998,** *37*. 1422-1427.

86 Mallouk, K.E., Rood, M.J. Performance of an Electrothermal Swing Adsorption System. *Environ. Sci. Tech.* **2013,** *47*, 7373-7379.

87 U.S. Energy Information Administration. Indiana Electricity Profile 2012. http://www.eia.gov/electricity/state/indiana/. Accessed 18May2015.

88 US Energy Information Administration. Natural gas liquids prices trend down since the start of 2012. http://www.eia.gov/todayinenergy/detail.cfm?id=12291. Accessed 18May2015.

89 US Energy Information Administration. How much carbon dioxide is produced per kilowatthour when generating electricity with fossil fuels? http://www.eia.gov/tools/faqs/faq.cfm?id=74&t=11. Accessed 18May2015.

90 Ramirez, D., Emamipour, H., Vidal, E.X., Rood, M.J., Hay, K.J. Capture and Recovery of Methyl Ethyl Ketone with Electrothermal Swing Adsorption Systems, *J. Environ. Eng.* **2011,** 137 (9), 826-832.

91 Mallouk, K.E. Capture and Recovery of Isobutane with Activated Carbon Fiber Cloth and Electrothermal Desorption. Master's Thesis, University of Illinois, Urbana-Champaign, 2009.

92 Foster, K. L.; Fuerman, R. G.; Economy, J.; Larson, S. M.; Rood, M. J., Adsorption Characteristics of Trace Volatile Organic Compounds in Gas Streams onto Activated Carbon Fibers. *Chem Mater*. **1992,** *4* (5), 1068-1073.

93 Rood, M.J. *et al*. Removal and recovery of organic vapor emissions by carbon fiber adsorber-cryogenic condenser, Construction Engineering Research Lab, **1999**, Champaign, Ill., 39.

94 Johnsen, D.L.; Zhang, Z.; Emamipour, H.; Yan, Z.; Rood, M.J. Effect of isobutane adsorption on the electrical resistivity of activated carbon fiber cloth with select physical and chemical properties. *Carbon*. **2014**, *76.* 435-445.

95 Dombrowski, K. Electrothermal regeneration of activated carbon fiber cloth with adsorbed volatile organic compounds. MS thesis, University of Illinois, Urbana, Ill., 2001.